

**DOCTORAL THESIS**

# Synergistic Mechanisms and Toxicity Profiles of Silver and Copper Nanoparticles for the Development of Novel Antimicrobial Materials

Grigory Vasiliev

TALLINN UNIVERSITY OF TECHNOLOGY  
DOCTORAL THESIS  
28/2023

**Synergistic Mechanisms and Toxicity  
Profiles of Silver and Copper  
Nanoparticles for the Development of  
Novel Antimicrobial Materials**

GRIGORY VASILIEV



TALLINN UNIVERSITY OF TECHNOLOGY  
School of Science  
Department of Chemistry and Biotechnology, Tallinn, Estonia

NATIONAL INSTITUTE OF CHEMICAL PHYSICS AND BIOPHYSICS  
Laboratory of Environmental Toxicology, Tallinn, Estonia

The dissertation was accepted for the defence of the degree of Doctor of Philosophy in gene technology on 30/06/2023

**Supervisor:** Dr. Olesja Bondarenko, Senior Research Scientist  
Laboratory of Environmental Toxicology  
National Institute of Chemical Physics and Biophysics  
Tallinn, Estonia

**Opponents:** Prof. Vilma Petrikaite  
Preclinical Research Center  
Lithuanian University of Health Sciences  
Kaunas, Lithuania

Dr. Kai Kunnis-Beres  
Landscaping Division  
Tallinn Urban Environment and Public Works Department  
Tallinn, Estonia

**Defence of the thesis:** 25/08/2023, Tallinn

**Declaration:**

Hereby I declare that this doctoral thesis, my original investigation and achievement, submitted for the doctoral degree at Tallinn University of Technology has not been submitted for doctoral or equivalent academic degree.

Grigory Vasiliev

-----  
signature



European Union  
European Regional  
Development Fund



Investing  
in your future

Copyright: Grigory Vasiliev, 2023  
ISSN 2585-6898 (publication)  
ISBN 978-9916-80-010-2 (publication)  
ISSN 2585-6901 (PDF)  
ISBN 978-9916-80-011-9 (PDF)  
Printed by Koopia Niini & Rauam

TALLINNA TEHNIKAÜLIKOOL  
DOKTORITÖÖ  
28/2023

**Vase ja hõbeda nanoosakeste sünergilise  
koosmõju mehhanismid ja rakendamine  
uute antimikroobsete materjalide  
arendamiseks**

GRIGORY VASILIEV





# Contents

List of publications .....	6
Author's contribution to the publications .....	7
Author's other publications: .....	8
Introduction .....	9
Abbreviations .....	10
1 Literature review .....	11
1.1 NPs as antimicrobial agents .....	11
1.1.1 Antimicrobial properties of Ag NPs .....	12
1.1.2 Antimicrobial properties of Cu and CuO NPs .....	13
1.1.3 Antimicrobial synergy effect between Ag and Cu components .....	14
1.1.4 Antimicrobial properties of filter materials with NPs .....	15
2 Aims of the study .....	17
3 Materials and methods .....	18
3.1 Bacterial cells .....	18
3.2 Mammalian cells .....	18
3.3 Methods .....	19
3.3.1 Characterization of NPs and materials .....	20
3.3.2 Tests with bacteria .....	20
3.3.3 Tests with human cells .....	21
4 Results and discussion .....	23
4.1 Physico-chemical characteristics of NPs .....	23
4.2 Antibacterial properties of CuO ja Ag NP with different functionalization .....	24
4.3 Comparison of antibacterial properties and toxicity for human cells using different functionalization in CuO NPs .....	25
4.4 Mechanisms of toxicity of CuO NPs with different functionalization .....	27
4.5 Antibacterial synergy between Cu and Ag components .....	28
4.6 Mechanisms of antibacterial synergy .....	31
4.7 Antiviral properties of CuO and Ag NPs .....	33
4.8 Characterization of produced filter materials .....	34
4.8.1 Antibacterial properties of filter materials .....	35
4.8.2 Antiviral properties of filter materials .....	36
5 Conclusions .....	39
References .....	40
Abstract .....	47
Lühikokkuvõte .....	48
Appendix 1 .....	49
Appendix 2 .....	65
Appendix 3 .....	83
Curriculum vitae .....	104
Elulookirjeldus .....	105

## List of publications

### MAIN PUBLICATIONS

- I Kubo, A.-L., **Vasiliev, G.**, Vija, H., Krishtal, J., Tõugu, V., Visnapuu, M., Kisand, V., Kahru, A., & Bondarenko, O. M. (2020). Surface carboxylation or PEGylation decreases CuO nanoparticles' cytotoxicity to human cells in vitro without compromising their antibacterial properties. *Archives of Toxicology*, 94(5), 1561–1573. <https://doi.org/10.1007/s00204-020-02720-7>
- II **Vasiliev, G.**, Kubo, A.-L., Vija, H., Kahru, A., Bondar, D., Karpichev, Y., & Bondarenko, O. (2023). Synergistic antibacterial effect of copper and silver nanoparticles and their mechanism of action. *Scientific Reports*, 13(1), 9202. <https://doi.org/10.1038/s41598-023-36460-2>
- III Kubo, A. L., Rausalu, K., Savest, N., Žusinaite, E., **Vasiliev, G.**, Viirsalu, M., Plamus, T., Krumme, A., Merits, A., & Bondarenko, O. (2022). Antibacterial and Antiviral Effects of Ag, Cu and Zn Metals, Respective Nanoparticles and Filter Materials Thereof against Coronavirus SARS-CoV-2 and Influenza A Virus. *Pharmaceutics*, 14(12). <https://doi.org/10.3390/pharmaceutics14122549>

## **Author's contribution to the publications**

- I Participated in planning, conducted and analysed all experiments with mammalian cells and participated in writing.
- II Conceptualization, Data curation, analysis, Investigation, Methodology, Visualization, Writing draft, revision, responses to reviewers.
- III Participated in planning, performed and analysed all antibacterial experiments, participated in writing.



## Author's other Publications:

Vanags, M., Mežule, L., Spule, A., Kostjukovs, J., Šmits, K., Tamm, A., Juhna, T., Vihodceva, S., Käämbre, T., Baumanė, L., Začs, D., **Vasiliev, G.**, Turks, M., Mierina, I., Sherrell, P. C., Šutka, A., Rapid Catalytic Water Disinfection from Earth Abundant Ca<sub>2</sub>Fe<sub>2</sub>O<sub>5</sub> Brownmillerite. *Adv. Sustainable Syst.* 2021, 5, 2100130. <https://doi.org/10.1002/adsu.202100130>

Heinlaan, M., Kasemets, K., Aruoja, V., Blinova, I., Bondarenko, O., Lukjanova, A., Khosrovyan, A., Kurvet, I., Pullerits, M., Sihtmäe, M., **Vasiliev, G.**, Vija, H., & Kahru, A. (2020). Hazard evaluation of polystyrene nanoplastic with nine bioassays did not show particle-specific acute toxicity. *The Science of the total environment*, 707, 136073. <https://doi.org/10.1016/j.scitotenv.2019.136073>

## Introduction

In the escalating battle against microbial pathogens, nanoparticles (NPs) have emerged as potent weapons, exhibiting significant antibacterial and antiviral properties. Recent advancements in nanotechnology have facilitated the manipulation of NPs, such as metal-based NPs, including copper (Cu), silver (Ag), and zinc (Zn), offering exciting possibilities for novel antimicrobial applications. These novel applications can be developed, if we understand the efficacy and safety of nanoparticles and underlying mechanisms.

The main objective of this PhD thesis was to characterize antimicrobial effects and safety of differently functionalized metal-based NPs, determine their mechanism of action and to develop new antimicrobial materials. More specifically, the aims were:

- 1) To compare the toxicity and mechanisms of differently functionalized Cu and Ag NPs to bacteria, viruses and mammalian cells *in vitro*;
- 2) To understand the antimicrobial mechanism of action (synergy) of Cu and Ag NPs combinations; and
- 3) To develop and characterize new nanoparticle-based antibacterial and antiviral materials.

In the first part of the PhD thesis, we characterized the toxicity and mechanisms of differently functionalized Cu, Ag, and Zn NPs to bacteria, viruses, and mammalian cells *in vitro*. Despite the widespread interest in NPs-mediated antimicrobial strategies, a comprehensive understanding of their toxicological profile across different cells and microbes is still lacking. This knowledge gap hinders the development of safer and more efficient antimicrobial applications. Thus, we strived to dissect the intricate interplay between NPs functionalization and its impact on toxicity, which could provide pivotal insights for the design of more effective and safer antimicrobial agents.

The second part of this PhD thesis dissected the antimicrobial mechanism of action (synergy) of Cu and Ag NPs combinations. Both Cu and Ag have been recognized for their antibacterial properties since ancient times. However, their combined antimicrobial effect remained a relatively unexplored. Unraveling this synergistic action allowed to enhance the antimicrobial potency of NPs-based solutions, leading to more efficient way for combating persistent bacterial infections, such as those encountered in wound treatment.

In the final part of this PhD thesis, we developed and characterized new NPs-based antibacterial and antiviral materials. The rapid spread of pathogens such as SARS-CoV-2 and Influenza A underscores the urgency for innovative antimicrobial materials. Leveraging the antiviral properties of Cu, Ag, and Zn NPs, we designed novel filter materials capable of mitigating transmission of bacteria and viruses. This research significantly contributes to the design of advanced antimicrobial materials, textiles and surfaces, particularly crucial in healthcare settings.

Taken together, this PhD thesis helps to improve NPs-mediated antimicrobial strategies, contributing into understanding of toxicological profile of metal-based NPs, elucidation of their synergistic action and the development of novel antimicrobial materials. Through this research, we aim not only to advance the current understanding of NPs-based antimicrobial strategies but also pave the way for revolutionary applications in the fight against microbial pathogens.

## Abbreviations

1-NPN	N-Phenyl-naphthalen-1-amine
AAS	Atomic absorption spectroscopy
AgNO <sub>3</sub>	Silver nitrate
cAg	Coated silver nanoparticles
BL	Bioluminescence
CA	Cellulose acetate
Cu	Copper
CuO	Copper oxide
CuO-COOH	CuO functionalized with carboxyl groups
CuO-NH <sub>2</sub>	CuO functionalized with amino groups
CuO-PEG	CuO functionalized with polyethylene glycol
CuSO <sub>4</sub>	Copper sulfate
EC <sub>50</sub>	Half maximal effective concentration
H <sub>2</sub> DCFA-DA	2',7'-dichlorodihydrofluorescein diacetate
HIV	Human immunodeficiency virus
IC <sub>50</sub>	Half maximal inhibitory concentration
K(AbS)	Coefficient of antibacterial synergy
LB agar	Luria-Bertani agar
LPS	Lipopolysaccharides
MBC	Minimal bactericidal concentration
NA	Not applicable
ND	Not determined
NPs	Nanoparticles
OD <sub>620</sub>	Optical density at 620nm
PBS	Phosphate-Buffered Saline
ppm	Parts-per-million
ROS	Reactive oxygen species
RPMI CCM	Roswell Park Memorial Institute cell culture media
SARS-CoV-2	Severe acute respiratory syndrome-related coronavirus 2
TGEV	Transmissible gastroenteritis virus
Zn	Zinc
ZnO	Zinc oxide

# 1 Literature review

Nanoparticles (NPs), particles with at least one dimension below 100 nanometers in size, have become a focal point of research across various scientific domains due to their unique properties (O. Bondarenko et al., 2013). In the field of antimicrobial research, nanoparticles offer novel avenues for combating the increasing issue of antibiotic resistance, courtesy of their exceptional physicochemical properties and potent antimicrobial activities.

The **size** of nanoparticles directly influences their interaction with microbial cells. Smaller nanoparticles have a greater surface area to volume ratio, which allows enhanced contact with bacteria and viruses, leading to a more potent antimicrobial effect (Huang et al., 2017).

The **functionalization** of nanoparticles is another critical factor that can modulate their antimicrobial activity. Different ligands used in functionalization can change the NP's surface charge, stability, dispersibility, and biocompatibility. For instance, functionalization can enhance the affinity of nanoparticles for microbial cells, facilitating their action (Sanità et al., 2020).

Antibiotic resistance is growing public problem because it poses a threat to the effective treatment of bacterial infections, which can lead to increased morbidity and mortality rates in populations (Huemer et al., 2020). The overuse of antibiotics can accelerate the development and spread of antibiotic-resistant bacteria, making it more difficult to treat common infections and increasing the risk of outbreaks (Abushaheen et al., 2020). Antibiotic resistance also has significant environmental impact, as antibiotics and antibiotic-resistant bacteria can enter the environment through wastewater and agriculture, contributing to the spread of resistance genes and potentially impacting ecosystems (S. Y. D. Zhou et al., 2022). The economic costs of antibiotic resistance are also significant, as it can result in longer hospital stays, increased healthcare costs, and lost productivity due to illness (Murray et al., 2022).

A lot of different metal-based NPs like titan, cobalt, aluminium, iron and others have been tested for antibacterial properties. But Ag and CuO nanoparticles have shown to be especially effective in this regard due to their superior properties against microbes as bacteria, protozoa (Aruoja et al., 2015), fungi (Suppi et al., 2015) or viruses. That why silver and copper NPs have been chosen as antimicrobial agents in this PhD thesis.

## 1.1 NPs as antimicrobial agents

Development of new antimicrobial methods is one of the priorities of World Health Organization (Theuretzbacher et al., 2020). That is why the investigation of antimicrobials based on metal NPs is important for population and environment. It represents a promising way for solving the problem of antibiotic resistance. Metal NPs have demonstrated potent antimicrobial properties against a wide range of pathogens including multi-resistant bacteria (Mishra et al., 2022), viruses (Alavi et al., 2022), and fungi (O. Bondarenko et al., 2013). Also, it is uncommon for bacteria to develop resistance to metal-based NPs compared to traditional antibiotics as they have a different mode of action than traditional antibiotics (Wang et al., 2017). This broad-spectrum activity makes them potentially useful for treating a variety of infections. Overall, the development of new antimicrobials based on metal NPs has the potential to address the growing problem of antimicrobial resistance and provide new options for treating

infections (O. Bondarenko et al., 2013). Also, metal-based NPs have been shown to have activity against certain viruses by damaging the virus's outer membrane or interfering with its ability to replicate (Luceri et al., 2023).

### 1.1.1 Antimicrobial properties of Ag NPs

#### 1.1.1.1 Antibacterial properties of Ag NPs

One of the oldest well-known antibacterial metals is Ag. Ag NPs have demonstrated potent antibacterial properties, making them a promising alternative to traditional antibiotics (O. Bondarenko et al., 2013). Antibacterial mechanisms of Ag NPs have been extensively researched. There are multiple mechanisms of action for Ag NPs against bacteria described in the literature. One of the main antibacterial mechanisms of Ag NP is the **disruption of the bacterial cell membrane**. This can cause leakage of intracellular components, leading to cellular damage and death. Ag NPs bind to lipopolysaccharides (LPS) of the Gram-negative outer membrane and distract it (O. M. Bondarenko et al., 2018). Main mechanism of Ag NP toxicity is the release of Ag ions. **Ag ions** from Ag NPs affect bacterial inner membrane, increasing proton leakage; it leads to destabilization of electron transport chain and decreasing of ATP synthesis (Holt & Bard, 2005). Especially the positively charged NPs interact with the negatively charged bacterial membrane more efficiently, leading to changes in the membrane permeability and potential (Kubo et al., 2018). In addition to disrupting membranes, Ag ions inactivate proteins by binding to S groups. Another antibacterial mechanism of Ag NPs is their ability to bind to bacterial DNA, interfering with replication and transcription processes (Adeyemi et al., 2020). Also, NPs can **induce oxidative stress** within the bacteria, leading to the production of reactive oxygen species (ROS) and damage to intracellular structures, proteins and lipids (Adeyemi et al., 2020). Even though bacteria encounter a considerable barrier to developing resistance against silver, certain bacterial processes can still potentially lead to the evolution of silver-resistant strains (McNeilly et al., 2021).

#### 1.1.1.2 Antiviral properties of Ag NPs

Ag NPs have been studied for their potential effectiveness against viruses. The potential antiviral effect of Ag NPs is due to their ability of the physical interaction of Ag NPs with the viral membrane (Luceri et al., 2023). Several studies have shown that Ag NPs can be effective against a range of viruses, including influenza (Park et al., 2018), HIV (Elechiguerra et al., 2005), (Lara et al., 2010), herpes simplex virus (Baram-Pinto et al., 2009), respiratory syncytial virus (Yang et al., 2016), hepatitis B (Lu et al., 2008) and C (Shady et al., 2020) viruses and others.

The mechanism by which Ag NPs exert their antiviral effects is not fully understood, but most of the studies showed that Ag NP interact with viral membrane proteins and disrupting the viral binding to mammalian cells (Park et al., 2018), (Elechiguerra et al., 2005), (Baram-Pinto et al., 2009). Also, the inactivation and damaging of viral membrane proteins (for example, influenza hemagglutinin and neuraminidase (Park et al., 2018)) and inner proteins (as hepatitis C helicase and protease (Shady et al., 2020)) have been shown. Additionally, Ag NPs have been shown to have immunomodulatory effects against virus (Orłowski et al., 2018), partially through upregulation of TGF- $\beta$  (Zhang et al., 2017) which may enhance the host's immune response to viral infections.

In case of coronavirus SARS-CoV-2, *in vitro* studies have shown that Ag NPs with a diameter of about 10 nm effectively inhibited extracellular SARS-CoV-2 at concentrations of 1 to 10 ppm. A luciferase-based pseudovirus entry assay showed that they strongly

inhibited the viral entry step by lowering the integrity of the virus (Jeremiah et al., 2020). While Ag NPs have shown promise as antiviral agents, it is important to note that their effectiveness may vary depending on the type of virus and the specific properties of the Ag NPs used (Luceri et al., 2023), (He et al., 2022). Further research is needed to determine the optimal conditions for using Ag NPs as antiviral agents and to fully understand their mechanism of action.

It is also important to consider the potential toxicity of Ag NPs, as they may have adverse effects on human health and the environment (Ivask et al., 2014). Therefore, any potential use of Ag NPs as antiviral agents should be carefully evaluated for safety and efficacy.

### **1.1.1.3 Toxicity of Ag NPs to mammalian cells and environmental organisms**

Studies have suggested that the toxicity of NPs is influenced by several factors, including their size, shape, surface charge, and concentration (Heinlaan et al., 2008). For example, the number of atoms on a NPs surface rises as NP size decreases, increasing its specific surface area and, consequently, its reactivity (Delay & Frimmel, 2012). Moreover, the use of biocompatible coatings, such as polyethylene glycol, can enhance the safety of NPs (Jenkins et al., 2016).

The toxicity of Ag NPs to mammalian cells has been a topic of concern among researchers and medical professionals (Ferdous & Nemmar, 2020). While Ag NPs have been shown to possess potent antimicrobial properties, their potential adverse effects on human health cannot be ignored.

Multilaboratory evaluation of Ag NP toxicity with different mammalian cells have shown that Ag NPs are toxic for mammalian cells almost in the same concentration as for pathogenic bacterial cells (O. M. Bondarenko et al., 2016). In the same report the most susceptible organisms to Ag NPs were water flea *Daphnia magna* and microalgae *Raphidocelis subcapitata*. It showed that Ag NPs can have the significant influence to environmental organisms. Ag NPs have been detected in wastewater, rivers, and even in soil, indicating their potential to accumulate in the environment (T. Zhou et al., 2021).

On the other hand, it is also worth mentioning that Ag NPs have been shown to exhibit anti-inflammatory and wound-healing properties. These properties make them a promising candidate for wound dressings and medical implants, as they can promote tissue regeneration and prevent bacterial infections (Paladini, 2019). Nevertheless, the safety of Ag NPs in these applications remains a concern, and their use in medical devices should be evaluated. Responsible and sustainable use of Ag NPs can help maximize their benefits and minimize their negative impacts on the world around us.

## **1.1.2 Antimicrobial properties of Cu and CuO NPs**

### **1.1.2.1 Antibacterial properties of Cu and CuO NPs**

Cu NPs have been also found to possess relatively good antibacterial properties, which make them a promising material for medical purposes. The use of Cu NPs as an antibacterial agent has several advantages over traditional antibiotics, including their broad-spectrum activity, low toxicity to mammalian cells, and reduced risk of bacterial resistance (Mahmoodi et al., 2018). Cu NPs possess multiple antibacterial mechanisms that contribute to their efficacy against a range of bacterial species (Ameh et al., 2022).

Several studies have demonstrated the effectiveness of Cu NPs against a range of bacteria, including *Escherichia coli* (*E. coli*), *Staphylococcus aureus* (*S. aureus*), and *Pseudomonas aeruginosa* (*P. aeruginosa*) (Ermini & Voliani, 2021). One mechanism is the

production of **ROS**, which can damage the cellular components of bacteria and ultimately lead to cell death. Cu NPs can generate ROS through a process called Fenton-like reaction, in which Cu ions interact with hydrogen peroxide to produce highly reactive hydroxyl radicals. The hydroxyl radicals can then react with the bacterial cell membrane and cause damage to the membrane proteins and lipids, leading to membrane disruption and cell death (Ameh et al., 2022).

Another mechanism by which Cu NPs can kill bacteria is through the **release of Cu ions**. When Cu NPs come into contact with water or biological fluids, they release Cu ions that are highly toxic to bacteria. Cu ions can interact with bacterial cell walls and cause the membrane to become more permeable, leading to the leakage of cellular contents and eventual cell death (Ma et al., 2022).

Cu NPs, through release of Cu ions, impact bacterial DNA and interfere with replication and transcription processes. Cu ions can bind to the DNA strands and cause structural changes, leading to disruption of the DNA replication machinery and the formation of abnormal proteins that can be toxic to the bacteria (Linder, 2012).

In summary, Cu NPs possess multiple antibacterial mechanisms that contribute to their efficacy against bacterial species. These mechanisms include the production of ROS, release of Cu ions, interaction with bacterial DNA, and induction of oxidative stress. The synergistic effect of these mechanisms makes Cu NPs a promising antibacterial agent for various applications. However, further research is needed to fully understand the mechanisms of action of Cu NPs and their potential impact on the environment and human health.

#### **1.1.2.2 Antiviral Cu**

Cu NPs have also been investigated for their potential antiviral properties. Several studies have shown that Cu NPs can be effective against a range of viruses, including influenza A (Ha et al., 2022), herpes simplex virus (Tavakoli & Hashemzadeh, 2020), C-hepatitis virus (Hang et al., 2015) and others (Tortella et al., 2022).

In case of coronavirus SARS-CoV-2, recent studies have shown that Cu surfaces inactivate this virus more effectively compared to plastic, glass cardboard, steel or nickel (Warnes et al., 2015).

The exact mechanism of action of Cu NPs is not fully understood. Cu NPs have been shown to interfere with the viral replication process, disintegration of viral envelope (Warnes et al., 2015) and inhibit virus entry into host cells (Hang et al., 2015).

However, as in case with Ag NPs, it is important to consider the potential toxicity of Cu NPs.

#### **1.1.3 Antimicrobial synergy effect between Ag and Cu components**

Within the scope of standard antibiotics, the idea of combinatory synergy is presently considered as one of the most promising strategies for handling bacterial infections and mitigating resistance (Theuretzbacher, 2020). By integrating diverse drugs, it becomes feasible to diminish their dosage, thereby resulting in fewer side effects as opposed to monotherapy (León-Buitimea et al., 2020). A set of recent studies, including our own research, suggest that the antibacterial action of NPs can be significantly enhanced when used in combinations. However, much of the existing literature predominantly focuses on the combined impact of metal ions rather than NPs (Fisher et al., 2009), (Vaidya et al., 2017), (Yayha et al., 1999), (Landeem et al., 1989). Considering the numerous combinations of metals studied (such as Ag with Cu, Zn, Co, Cd, and Ni), the combination of Ag and Cu

displayed the most substantial synergistic antibacterial impact against both Gram-negative and Gram-positive bacteria (Garza-Cervantes et al., 2017).

Lately, there has been an escalating interest in the synergy between Cu and Ag, as indicated by an increasing number of published articles in recent years. Most of these studies focused on the antibacterial effects of Cu/Ag nanoalloys (F. Zhou et al., 2022), (Tao et al., 2022) or Cu/Ag combined with additional metals, for instance, tungsten (Bankier et al., 2019). Additionally, research by Jang et al. displayed remarkable antibacterial, anti-biofilm, and wound healing capabilities of Cu/Ag/Graphene Oxide composites in an infected wound model in mice (Jang et al., 2020).

Very few or previous articles proposed potential synergistic mechanisms, suggesting that Ag mainly affects the bacterial cell membrane, while Cu acts on the nucleic acids and various internal biomolecules and cellular structures (Fisher et al., 2009), (Vaidya et al., 2017), (Garza-Cervantes et al., 2017), (Bankier et al., 2019), but the specific mechanisms driving this synergy remained largely unexplored. Not a single article was found where antiviral synergistic properties between metal NPs were considered.

#### **1.1.4 Antimicrobial properties of filter materials with NPs**

The exceptional virucidal properties of metal-based NPs make them suitable candidates for application on frequent contact surfaces, aimed at curbing the transmission of infections. Antimicrobial coatings composed of Cu, Ag, and Zn have demonstrated potent virucidal effectiveness in managing the spread of various viruses such as influenza A virus, HIV-1, Dengue virus type 2, and Human Herpesvirus 1 (Rai et al., 2016), (Hodek et al., 2016). A substantial decline in the infectivity of human coronavirus HuCoV-229E was observed on surfaces infused with Cu, after 30 minutes of exposure (Warnes et al., 2015). Cu-treated surfaces are currently employed in hospital settings as a preventive measure against microbial spread and potential viral transmissions (Michels et al., 2015).

Lately, a multitude of organic polymer compounds, including biopolymers, have exhibited potential as antibacterial and antiviral agents, geared toward curbing the spread of infectious diseases (Balasubramaniam et al., 2021). These polymer matrices serve as effective carriers for metal NPs and metals. Metals can be permanently integrated into these materials, resulting in metal-polymer composites with efficient antimicrobial activity. Polymers and their fiber derivatives are used as constituents in fabrics, textiles, and filter materials. Conventionally, the integration of metal additives into polymer matrices is achieved by coating metals onto fiber surfaces or impregnating them into polymer fiber blends (Palza, 2015).

Most of these materials are synthetic in nature. For instance, typical surgical masks comprise plastic-based polymers such as polypropylene, polyurethane, polyacrylonitrile, polystyrene, polycarbonate, polyethylene, or polyester. However, the preference is shifting towards bio-based polymers for the development of future biodegradable materials.

To develop safe and efficient nano-based materials, it is crucial to understand their mechanism of action and toxicity. Thus, this focused on closing the knowledge gaps and utilizing the new knowledge to develop new innovative materials with improved antimicrobial properties.

##### **1.1.4.1 Safety of metal-based NPs for mammalian cells**

Although metal NPs can have great antimicrobial properties, the toxic effect to human cells also have reported. Ag NPs have been showed to induce oxidative stress in human cells, leading to reduced cell viability, DNA damage, and apoptosis. In particular, they



have demonstrated cytotoxic effects on various human cell types, including fibroblasts, keratinocytes, and epithelial cells. Ag NPs are known to induce oxidative stress via the production of ROS. This process can lead to various cellular impairments such as DNA disruption, the stimulation of antioxidant enzymes, the reduction of antioxidant substances like glutathione, protein incapacitation through binding, and damage to the cellular membrane (McShan et al., 2014). Furthermore, Ag NPs can interfere with protein function, potentially leading to abnormal cellular activity and the initiation of cell death pathways (Gupta et al., 2022).

Copper oxide (CuO) NPs similar to Ag NPs, possess broad antimicrobial properties. However, an increasing body of evidence suggests potential cytotoxic effects, particularly in relation to human cells. Studies have shown that CuO NPs can reduce cell viability in a range of human cell lines (Karlsson et al., 2008). They achieve this through various mechanisms, including the induction of oxidative stress, mitochondrial damage, and initiation of apoptotic pathways. CuO NPs have been shown to generate ROS, which leads to oxidative stress, causing damage to DNA, proteins, and lipids (Naz et al., 2020).

The safety profile of metal-based nanoparticles can be altered by surface functionalization, as documented in previous studies (Nel et al., 2009), (Kubo et al., 2018). For instance, nanoparticle functionalization with compounds like PEG, chitosan, or dextran can inhibit nanoparticle opsonization – the process where a biocorona of proteins and other biomolecules adsorb onto the nanoparticles' surface – subsequently reducing macrophage uptake and toxicity (Sheng et al., 2009), (Jenkins et al., 2016), (Wonder et al., 2018). Conversely, nanoparticles functionalized with positively charged entities such as polyethylenimine PEI, or amine group, compared to those functionalized with neutrally charged coatings or negatively charged ones have exhibited greater toxicity to mammalian cells (Líbalová et al., 2018).

While Ag and CuO NPs exhibit unique properties beneficial to various industries, their potential cytotoxic effects on human cells cannot be ignored. The potential for cytotoxicity underscores the urgent need for additional research into the functionalization and combination of nanoparticles. Investigating how different forms of functionalization can modulate the effects of nanoparticles could provide a pathway to safer, more effective antibacterial materials. The integration of varying nanoparticles could also offer unforeseen synergistic effects, underscoring the vast potential for innovation within the sphere of antibacterial materials.

## 2 Aims of the study

The main objective of this study was to characterize antimicrobial effects and safety of differently functionalized metal-based NPs, determine their mechanism of action and to develop new antimicrobial materials.

The main objective was approached through the following sub-tasks:

- 1) To compare the toxicity and mechanisms of differently functionalized Cu and Ag NPs to bacteria, viruses and mammalian cells *in vitro*.
- 2) To understand the antimicrobial mechanism of action (synergy) of Cu and Ag NPs combinations.
- 3) To develop and characterize new nanoparticle-based antibacterial and antiviral materials.

### 3 Materials and methods

#### 3.1 Bacterial cells

Bacterial and viral strains used in the study are showed in Table 1. In total, 6 different bacterial strains, both Gram-positive and Gram-negative, were used and 3 RNA viruses. Also, 1 luminescent bacterial strain has been used in luminescence assay for understanding of antimicrobial mechanisms.

**Table 1.** Bacterial and viral strains used in the study

Microbes	Type	Reference (publication)
<i>Streptococcus dysgalactiae</i> (DSM 23147)	Gram-positive bacteria	II
<i>Staphylococcus aureus</i> (ATCC 25923)	Gram-positive bacteria	II, III
<i>Enterococcus faecalis</i> ATCC (29212)	Gram-positive bacteria	II
<i>Escherichia coli</i> K-12 (MG1655)	Gram-negative bacteria	I, II, III
<i>Escherichia coli</i> (MC1061, pSLcueR/pDNPCopAlux)	Gram-negative bacteria	I, II
<i>Escherichia coli</i> (clinical isolate, ESBL)	Gram-negative bacteria	II
<i>Pseudomonas aeruginosa</i> (PAO1)	Gram-negative bacteria	II
Influenza A (H1N1, A/WSN/1933)	enveloped single-stranded (+)RNA virus	III
Transmissible gastroenteritis virus	enveloped single-stranded (-)RNA virus	III
Severe acute respiratory syndrome-related coronavirus 2	enveloped single-stranded (+)RNA virus	III

#### 3.2 Mammalian cells

Mammalian cell cultures used in the study are showed in Table 2. THP-1 and HACAT were used for investigation of toxicity of NPs and understanding their mechanisms. MDCK-2 cells were used for influenza virus propagation and titration; Vero-E6 cells were used for SARS-CoV-2 propagation and titration, and ST cells were used for Transmissible gastroenteritis virus (TGEV) propagation and titration.

**Table 2.** Mammalian cell cultures used in the study.

Human cell line	type of cell line	Reference (publication)
THP-1	human monocytes	I
HACAT	human keratinocytes	I
MDCK-2	canine kidney epithelial cells	III
Vero E-6	monkey kidney epithelial cells	III
ST cells	porcine fibroblasts	III

### 3.3 Methods

Methods used in the study are showed in Table 3.

**Table 3.** Methods used in the study

Methods	Test was conducted: institution (person)	Reference (publication)
<b>Alamar Blue Assay</b> for human cells viability evaluation	KBFI (Vasiliev G)	I
<b>Alamar Blue Assay</b> for bacteria viability evaluation	KBFI (Kubo AL)	I
Measurement of Cu and Ag bioavailability to bacteria using <b>recombinant biosensor bacteria <i>E. coli</i> MC1061 (pSLcueR/pDNPcopAlux)</b>	KBFI (Vasiliev G)	I, II
Hydrodynamic size and zeta potential measurement using <b>Dynamic Light Scattering</b>	KBFI (Vasiliev G)	I, II
Measurement of reactive oxygen species using <b>2',7'-dichlorodihydrofluorescein diacetate (H<sub>2</sub>DCFA-DA) Assay.</b>	KBFI (Kubo AL)	I, II
Measurement Cu and Ag content (metal content in NPs, dissolution analysis) in samples using <b>Atomic Absorption Spectroscopy (AAS)</b>	KBFI (Vasiliev G)	I, II, III
Measurement of TNF-a using <b>Enzyme-Linked Immunosorbent Assay</b>	KBFI (Kubo AL, Vasiliev G)	I
<b>Confocal Microscopy</b>	TalTech (Krishtal J)	I
Evaluation of the minimum bactericidal concentration using <b>Spot Test</b>	KBFI (Vasiliev G)	II
Evaluation of bacterial outer membrane integrity using <b>N-Phenylnaphthalen-1-amine (1-NPN) Assay</b>	KBFI (Vasiliev G)	II
Detection of Cu <sup>+</sup> in suspension using the <b>iodometric method</b>	TalTech (Bondar D)	II
<b>Electrospinning</b> of filter materials	TalTech (Krumme A)	III
<b>Antibacterial Diffusion Assay</b>	KBFI (Vasiliev G)	III
Assessment of antiviral activity in suspension and in filter material using <b>Plaque Assay</b>	TÜ (Rausalu K)	III

Short descriptions of tests performed by G. Vasiliev are below:

### **3.3.1 Characterization of NPs and materials**

#### **3.3.1.1 Hydrodynamic size and zeta potential measurement using Dynamic Light Scattering**

The hydrodynamic size, polydispersity index, and zeta potential of the NPs were assessed using a Malvern zetasizer (Zetasizer Nano-ZS, Malvern Instruments, UK). These measurements were taken in suspensions containing 100 mg/l of nanoparticles, either in MQ water or RPMI CCM (Roswell Park Memorial Institute cell culture media).

#### **3.3.1.2 Measurement Cu and Ag content (metal content in NPs, dissolution analysis) in samples using AAS**

The metal content of the analyzed samples was evaluated using AAS (contrAA 800, Analytik Jena Ag) according to instrument manual. For the dissolution analysis, a solution of 100 mg/l of components was incubated in MQ or a RPMI CCM under conditions of 37 °C, 5% CO<sub>2</sub>, and 95% humidity for periods of either 0 hours, 30 minutes, or 24 hours. Following this, the solution was centrifuged at 320,000 × g for 30 minutes using a Bekman Coulter ultracentrifuge. The supernatants were collected and then analyzed using AAS (contrAA 800, Analytik Jena Ag).

### **3.3.2 Tests with bacteria**

#### **3.3.2.1 Evaluation of the minimum bactericidal concentration using Spot Test**

The Minimum Bactericidal Concentration (MBC) was determined as the lowest concentration that completely abolished bacterial growth, using the spot test method. After an overnight growth and further 4-hour incubation to reach the exponential phase, a bacterial suspension was prepared with an optical density at 620 nm (OD<sub>620</sub>) of 0.07 in either MQ, RPMI CCM, or bacterial medium. This bacterial suspension (100 µL) was combined with 100 µL of components alone or their mixture in the medium. This setup was carried out in 96-well microplates and incubated at 30 °C for 24 hours in the absence of light and without shaking, either in MQ, RPMI CCM, or bacterial medium. After the incubation period, 3 µL of the treated suspension was transferred onto bacterial agar medium, and bacterial cell viability was visually assessed (presence of bacterial “spot”) after an additional 24 hours of incubation.

#### **3.3.2.2 Antibacterial Diffusion Assay**

Bacteria were cultivated overnight in 3 mL of RPMI CCM at a constant temperature of 37 °C, with agitation at 200 rpm. Subsequently, 400 µL of the overnight cultures were combined with 20 mL of bacterial medium, and then incubated for 4 hours to attain the exponential growth phase. Bacterial suspension with an absorbance of 0.1 at OD<sub>620</sub> was prepared. Next, 500 µL of the suspension was dispersed over a square Petri dish (10 cm x 10 cm) that contained Luria-Bertani (LB) agar. The filter materials were then placed on the freshly inoculated LB agar and incubated at 37 °C for 24 hours. The antibacterial efficacy of the materials was subsequently assessed through visual inspection.

#### **3.3.2.3 Evaluation of bacterial outer membrane integrity using 1-NPN Assay**

The permeabilization of bacterial cell walls was determined by measuring the uptake of 1-NPN. The fluorescent properties of 1-NPN, which are significantly boosted in hydrophobic environments like the membrane lipid bilayer, as opposed to hydrophilic ones, make it a suitable dye to examine the integrity of gram-negative bacteria's outer membrane. In brief, a black microplate was prepared by adding 50 µL of 40 µM 1-NPN

and 50  $\mu\text{L}$  of the tested substance in 50 mM 3-(N-morpholino)propanesulfonic acid adjusted with tris(hydroxymethyl)aminomethane base to pH 7.2 to each well. Each well then received 100  $\mu\text{L}$  of bacterial suspension in 50 mM this buffer with  $\text{OD}_{620}$  of 0.5, after which the fluorescence was measured following a 30-minute incubation period at room temperature. The uptake factor of 1-NPN by cells was calculated and depicted as a ratio of the fluorescence intensity values of the bacterial suspension incubated with and without the tested compounds.

#### **3.3.2.4 Measurement of Cu and Ag bioavailability to bacteria using recombinant biosensor bacteria *E. coli* MC1061 (pSLcueR/pDNPCopAlux)**

The measurement of intracellular Ag and Cu ions' effect on bioluminescence (BL) in bacteria was conducted using recombinant biosensor bacteria *E. coli* MC1061 (pSLcueR/pDNPCopAlux). This strain's response to intracellular Ag and Cu ions is driven by the CueR activator protein and its regulated copA promoter, which is coupled to genes encoding BL. Consequently, when Ag and Cu ions are present in the cells at sub-toxic levels, they cause an increase in BL in these recombinant bacteria, which is directly proportional to the ion concentration.

The biosensor assay process and the preparation of the test bacteria were akin to the bacterial growth inhibition assay, with one distinct difference: The growth medium for bioluminescent Ag-biosensor *E. coli* MC1061 (pSLcueR/pDNPCopAlux) included 100  $\mu\text{g}/\text{l}$  of ampicillin and 10  $\mu\text{g}/\text{l}$  of tetracycline during overnight cultivation to ensure the maintenance of the recombinant plasmids. A Berthold Detection Systems Orion II plate luminometer was utilized for the bioluminescence readings. *E. coli* at an  $\text{OD}_{620}$  of 0.1 was exposed to 100  $\mu\text{l}$  of bacterial suspension containing either the compounds or their mixture in RPMI CCM (sample), or just RPMI CCM (background), and this was kept at 30  $^{\circ}\text{C}$  for 4 hours. The Ag and Cu biosensor's dose-response curves were plotted by setting the applied Cu and Ag concentrations against the biosensor's BL in the respective samples. The concentration that yielded the highest bioluminescence value from each component was identified as the peak of the luminescence curve.

### **3.3.3 Tests with human cells**

#### **3.3.3.1 Alamar Blue Assay for human cells viability evaluation**

The cells were grown at RPMI CCM in medium to confluency  $10^5/\text{ml}$ . On the day of the test, the cell culture medium was discarded, and the cells were thoroughly rinsed with Phosphate-Buffered Saline (PBS). Following this, the cells were treated with either 100  $\mu\text{l}$  of the cell culture medium alone or the same volume of Cu compounds suspended in the cell culture medium. This treatment was left in place for 24 hours under conditions of 37  $^{\circ}\text{C}$  and 5%  $\text{CO}_2$ . After this exposure period, the supernatant was discarded, the cells were given another rinse with PBS and then subjected to a 2-hour incubation at 37  $^{\circ}\text{C}$  with 5%  $\text{CO}_2$  in the presence of 100  $\mu\text{l}$  of Alamar Blue at a concentration of 150  $\mu\text{g}/\text{ml}$ . Alamar Blue fluorescence was measured using Fluoroskan (Fluoroskan Ascent FL, Thermo Labsystems) with excitation at 530 nm and emission at 590 nm. The  $\text{EC}_{50}$  values were computed using MS Excel macro Regtox ([https://www.normalesup.org/~vindimian/en\\_download.html](https://www.normalesup.org/~vindimian/en_download.html)).

#### **3.3.3.2 Measurement of TNF- $\alpha$ using Enzyme-Linked Immunosorbent Assay**

Differentiated THP-1 cells were set up at a density of  $10^5$  cells per well and subjected to treatment with CuO NPs and  $\text{CuSO}_4$  at varying concentrations ranging from 25 to 400  $\text{mg}/\text{l}$  in RPMI CCM. Following a 24-hour period of exposure, the supernatants were

harvested, centrifuged at 10,000 x g for 10 minutes, and preserved in a frozen state at  $-80\text{ }^{\circ}\text{C}$ . To quantify the amount of TNF- $\alpha$ , an Enzyme-Linked Immunosorbent Assay (ELISA) was employed using a kit from Invitrogen (88-7346), with all procedures carried out in line with the instructions provided by the manufacturer, with readings taken from 96-well plates. Colorimetric measurement was done by Spectramax Paradigm spectrophotometer (Molecular Devices, USA).

## 4 Results and discussion

### 4.1 Physico-chemical characteristics of NPs

Table 4 displays the characterization of the NPs utilized in the PhD thesis. The zeta-potential of CuO NPs (CuO) and CuO functionalized with amino groups (CuO-NH<sub>2</sub>) was positive, while CuO functionalized with carboxyl groups (CuO-COOH) and with polyethylene glycol (CuO-PEG) had a negative zeta-potential. Among the tested Ag NPs, all exhibited a significantly negative zeta-potential, with coated silver nanoparticles (cAg) having a value of -56.6 mV and nano-silver (nAg) having a value of -27.7 mV. In the RPMI CCM, all NPs zeta-potentials were negative, ranging from -8.9 mV (CuO-NH<sub>2</sub>) to -10.8 mV (CuO). This is likely due to the adsorption of serum proteins on the NP surface, known as the “protein corona”, which is a dynamic camouflage formed by protein adherence. This phenomenon was previously suggested before (Ivask et al., 2015).

The primary size of NPs was comparable, with the exception of nAg with larger size compared to other used NPs. In medium, hydrodynamic size was different and most probably reflected agglomeration of some NPs, such as functionalized Cu NPs.

**Table 4.** Physico-chemical characteristics of nanoparticle (NPs) used in the study

Metal-based NPs or metal salts	Primary size, nm ± standard deviation	Hydrodynamic diameter in MQ water, nm (pdi) ± standard deviation	Zeta-potential in MQ water, mV ± standard deviation	Metal content, % ± standard deviation	Reference (publication)
CuO	15.9 ± 5.2	237 ± 31 (0.25)	27.5 ± 1.8	76.8 ± 5.7	I, II, III
CuO-NH <sub>2</sub>	6.9 ± 2.2	733 ± 252 (0.24)	25.8 ± 1.3	46.2 ± 4.0	I, II, III
CuO-COOH	9.2 ± 2.5	1124 ± 128 (0.35)	-12.0 ± 2.2	33.6 ± 3.2	I, II, III
CuO-PEG	12.1 ± 3.2	1244 ± 254	-21.9 ± 3.3	11.7 ± 1.0	I
cAg	12.5 ± 4	45.88 ± 0.21 (0.261)	-56.6 ± 1.91	83.0 ± 9.8	I, III
nAg	85.7 ± 29.3	109.4 ± 1.3 (0.447)	-27.7 ± 1.65	71.8 ± 12.0	I, II
Ag <sub>2</sub> O	23 ± 16.8	81.265 ± 9.04 (0.604)	-50.97 ± 4.15	80.1 ± 11.3	II



## 4.2 Antibacterial properties of CuO ja Ag NP with different functionalization (Publication II)

Next, characterized NPs were studied for their antibacterial properties, providing critical insights towards the development of advanced antimicrobial agents. These NPs comprised of Ag and CuO, each subjected to different surface functionalizations. The NPs were dosed based on their metal content MBC for different gram-positive and negative bacteria was determined as described above.

The table 5 provides data regarding the MBC of various NPs against a range of bacterial strains. The MBC represents the lowest concentration of an antibacterial agent required to kill a specific bacterium. The data shows cAg NPs displayed the most promising antibacterial properties against all bacteria, especially it was very effective against *S. dysgalactiae* with an MBC of  $10.07 \pm 3.76$  mg/L. nAg, Ag<sub>2</sub>O and AgNO<sub>3</sub> were tested only with *E. coli* K-12. AgNO<sub>3</sub> have shown the most effective antibacterial properties due to best dissolution of salt. This is probably because released Ag<sup>+</sup> ions are the main antibacterial mechanism in Ag NPs (Bondarenko et al., 2013).

**Table 5.** Minimal bactericidal concentrations with standard deviation for nanoparticles (NPs) in different bacteria. Adopted and changed from Publication II.

NPs	MBC ± SD (mg/L) for <i>E. coli</i> K-12	MBC ± SD (mg/L) for <i>E. coli</i> ESBL	MBC ± SD (mg/L) for <i>S. aureus</i>	MBC ± SD (mg/L) for <i>S. dysgalactica</i>	MBC ± SD (mg/L) for <i>P. aeruginosa</i> PAO1	MBC ± SD (mg/L) for <i>E. faecalis</i>
CuO	215.38 ± 114.35	133.33 ± 57.74	60 ± 22.36	133.33 ± 57.74	1400 ± 400	233.33 ± 152.75
CuO-NH <sub>2</sub>	157.14 ± 51.36	100 ± 0	80 ± 27.39	133.33 ± 57.74	200 ± 122.47	266.67 ± 115.47
CuO-COOH	350 ± 90.45	333.33 ± 115.47	110 ± 54.77	200 ± 0	800 ± 0	400 ± 0
CuSO <sub>4</sub>	217.65 ± 72.76	200 ± 0	90 ± 22.36	133.33 ± 57.74	720 ± 178.89	200 ± 0
cAg	34.04 ± 13.13	45.83 ± 9.73	16.25 ± 5.88	10.07 ± 3.76	28.91 ± 15.63	58.33 ± 19.46
AgNO <sub>3</sub>	10.16 ± 8.20	ND	ND	ND	ND	ND
nAg	1333.33 ± 427.62	ND	ND	ND	ND	ND
Ag <sub>2</sub> O	66.67 ± 24.62	ND	ND	ND	ND	ND

Among different CuO NPs, positively charged CuO and CuO-NH<sub>2</sub> were more effective against bacteria and especially CuO-NH<sub>2</sub> in some cases (*P. aeruginosa*). In general, CuO NPs were not so efficient against bacteria compared to Ag NPs. However some CuO NPs had promising results against *S. aureus*. The most resistant bacteria to Cu components were *P. aeruginosa* PAO1 as indicated by its MBC of 1400 ± 400 mg/L and most susceptible was *S. aureus*, which MBC was lower than 100 mg/L.

Despite to promising antibacterial properties of Ag and CuO NPs, it is important to test toxicity of these components on human cells and compare their toxicity to bacterial and mammalian cell to have a therapeutic window for usage. While Ag and CuO NPs display promising antibacterial properties, assessing the toxicity of these components on human cells and comparing their toxicity to bacterial and mammalian cells is crucial to establish a therapeutic window for their use.

It's well known that this therapeutic window (antibacterial efficacy versus cytotoxicity), usually does not exist according to studies (O. Bondarenko et al., 2013), yet there is limited knowledge regarding the impact of surface functionalization on this overlap. We therefore tested a hypothesis that the therapeutic window of NPs might be influenced by different surface functionalizations of NPs. As such, further research in this area could lead to optimized NP designs with better safety profiles.

#### **4.3 Comparison of antibacterial properties and toxicity for human cells using different functionalization in CuO NPs (Publication I)**

Because some CuO NP were found potent against bacteria and Ag NPs have well-known toxic effects for human cells (McShan et al., 2014), we decided to compare the toxicity to human cells with toxicity to bacteria *in vitro* for CuO NPs which had to have better safety profile, since it is vital microelement. The cytotoxic effects of these NPs were tested by Alamar Blue Assay test with THP-1 and HACAT cells, with particular attention paid to the impact of surface functionalization.

In terms of surface functionalization, it was found that cationic unmodified CuO and CuO-NH<sub>2</sub> NPs displayed higher toxicity to human cells compared to bacteria. In contrast, the CuO-COOH and CuO-PEG, which were negatively charged, were less toxic to human cells but had a significantly greater impact on bacteria (Figure 1). Interestingly, the results showed that the toxicity of these NPs to human cells was not solely dictated by the Cu content. This is evidenced by the fact that the Cu-adjusted half maximal effective concentration (EC<sub>50</sub>) values of CuO-NH<sub>2</sub> NPs were significantly lower than that of CuSO<sub>4</sub>, despite CuSO<sub>4</sub> having a higher Cu concentration. This indicates that toxicity mechanisms beyond mere Cu content play a role in the cytotoxicity of CuO-NH<sub>2</sub> NPs.

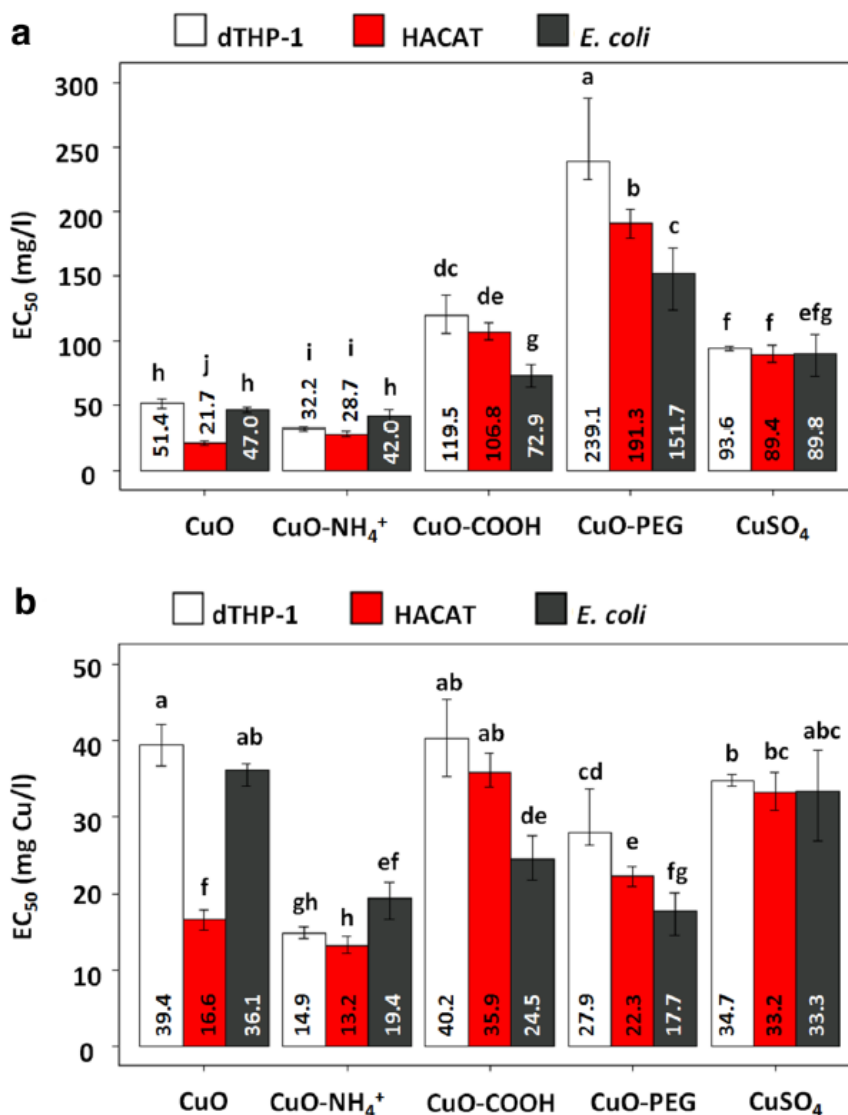


**Figure 1.** Toxicity of Cu compounds to bacteria *Escherichia coli* (*E. coli*), HACAT keratinocytes and differentiated THP-1 cells (dTHP-1). The average compound-based 24-h half maximal effective concentration ( $EC_{50}$ ) values with 95% confidence intervals mg/l (a) and the clustering of average compound-based 24-h  $EC_{50}$  (b), and the clustering of average copper adjusted 24-h  $EC_{50}$ . Adopted and changed from Publication I.

In an attempt to understand the mechanisms underlying this differential toxicity, we investigated the NPs' ability to induce ROS under abiotic conditions and their potential to provoke inflammation in mammalian cells. We also conducted detailed studies on their interactions with human cells in vitro, focusing primarily on NPs localization and uptake mechanisms.

#### 4.4 Mechanisms of toxicity of CuO NPs with different functionalization (Publication I)

Our findings demonstrated that the toxicity of CuO NPs to human cells can be manipulated by varying the NP surface functionalization and form. Additionally, the data highlighted that Cu content alone does not define toxicity, pointing towards the contribution of other toxicity mechanisms to understand them by which Cu compounds exert their toxicity. Our first consideration was the bioavailability and dissolution of these compounds. To assess this, we used recombinant bioluminescent *E. coli* that showed increased bioluminescence in response to bioavailable Cu ions. This offered insight into the role of internalized Cu ions in the antibacterial potential of Cu compounds.

Generally, Cu compounds exhibited similar behavior in the sub-toxic region, resulting in an increase in bioluminescence in *E. coli* MC1061 (pSLcueR/pDNPcopAlux) in proportion to the increase in Cu concentration. A distinctive exception was found with CuO-NH<sub>2</sub>, which exhibited toxic properties at noticeably low concentrations, indicating an antibacterial effect independent of dissolved Cu ions. In contrast to other NPs, the biosensor response to CuO-NH<sub>2</sub> was less related to the Cu content and NPs dissolution.

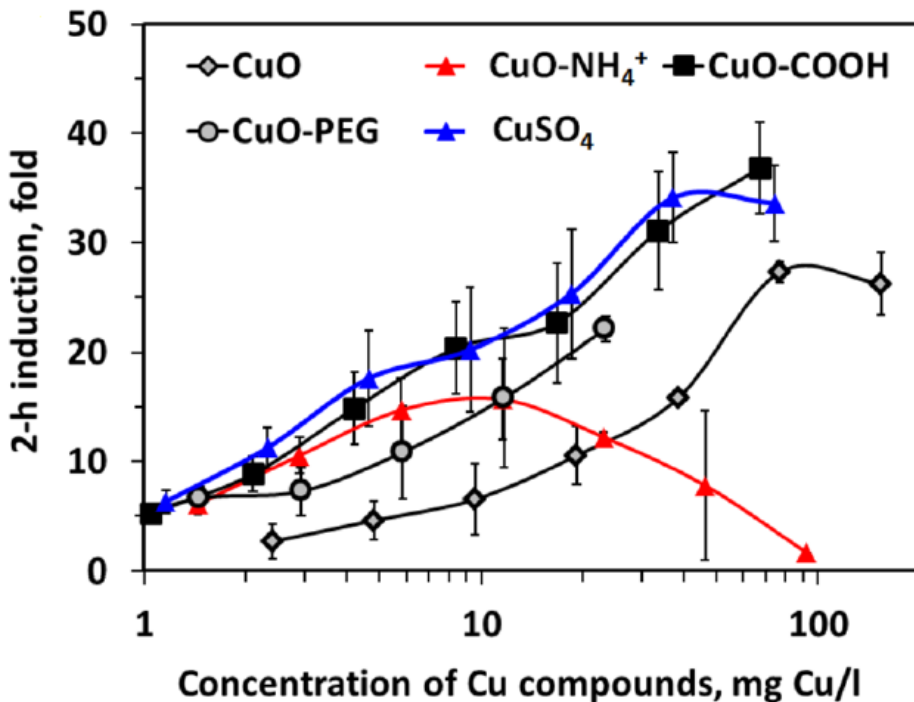


**Figure 2.** Bioavailability of Cu compounds. Induction of bioluminescence in *E. coli* biosensor in response to Cu compounds in cell culture medium 2 incubation with standard deviations. Adopted and changed from Publication I.

We further explored the ability of Cu compounds to generate ROS and induce inflammation. CuO-NH<sub>2</sub> were highly potent inducers of ROS. Intriguingly, they also demonstrated the highest capability to induce TNF- $\alpha$ , a pro-inflammatory cytokine. Additionally, we noted significant vacuolization in THP-1 cells exposed to CuO-NH<sub>2</sub>, which could be indicative of inflammation and cell death.

To comprehend the toxicity mechanisms of Cu compounds, we evaluated the “cell-associated Cu”, comprising intracellular Cu, NPs, and possibly cell surface-bound Cu. Our data suggested that the toxicity of Cu compounds was not purely caused by Cu ions alone. Specifically, CuO-NH<sub>2</sub> NPs had lower cell-associated Cu, hinting at additional toxicity mechanisms. We also found exceptionally high levels of cell-associated Cu in cells exposed CuO-COOH, indicating a high tolerance of these cells to Cu in this particular form. To gain more insights, we investigated the cellular localization of Cu compounds in mammalian cells through confocal microscopy. We discovered a significantly higher association of CuO-COOH NPs with cells compared to other NPs, with most of the CuO-COOH NPs located inside the cells. This suggests that these macrophages have an extraordinarily high tolerance for internal Cu in CuO-COOH.

Our research has shown that the toxicity of Cu compounds towards bacteria and human cells is influenced by several factors, including their bioavailability, dissolution, ability to induce ROS and inflammation, and their interaction with the cells, including uptake and cellular localization. These findings expand our understanding of the toxicity mechanisms of CuO-based NPs and will be invaluable for future design and application of these NPs in biomedical fields.

#### **4.5 Antibacterial synergy between Cu and Ag components (Publication II)**

In our research, we hypothesized that the synergistic antibacterial activity of CuO and Ag NPs results from their distinct, yet complementary, modes of action, like the classical synergy between different classes of antibiotics (Kohanski et al., 2010). The suggestion was that Ag NPs compromise the integrity of bacterial cell walls, which then paves the way for CuO NPs / Cu ions to pass into bacterial cells. Once inside, CuO NPs and Cu ions interfere with intracellular structures and functions. We first discerned the synergistic antibacterial effects of Cu and Ag compounds in a medium similar to a tissue infection transudate, the RPMI cell culture testing medium, which contains blood serum and growth factors. Figure 3 illustrates an example of this synergy, with the MBC serving as the measure of the lowest concentration that prevented visible bacterial growth on an agarized growth medium. For instance, to inactivate *E. coli* permanently, we required 40 mg/l of Ag NPs or 400 mg/l of CuSO<sub>4</sub> independently, but when used together, we needed only 5 mg/l of cAg and 25 mg/l of CuSO<sub>4</sub>.

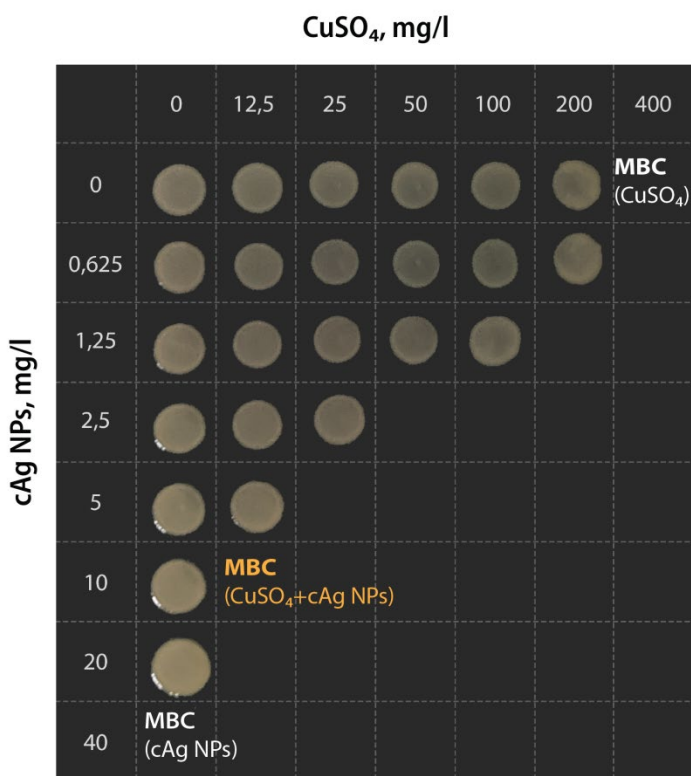


**Figure 3.** The antibacterial synergy between CuSO<sub>4</sub> and coated silver nanoparticles (cAg). *E. coli* K-12 suspension was incubated with different concentrations of either cAg, CuSO<sub>4</sub> or their combinations in RPMI cell culture medium for 24 h. After incubation 3 µl of the bacteria-NP mixture was pipetted onto agarized broth and minimal bactericidal concentration (MBC, the lowest tested concentration yielding no visible bacterial growth after 24 h incubation at 37C in the dark) was determined. The concentrations of cAg and CuSO<sub>4</sub> are shown on the axes. The minimal bactericidal concentration of CuSO<sub>4</sub> and cAg were 400 mg/L and 40 mg/L respectively. Published from publication II with permission from journal.

We introduced the term “coefficient of antibacterial synergy” (K(AbS)) to quantify and compare the synergistic effect among various NPs and bacterial strains. This coefficient represents the combined antibacterial efficiency of NPs, contrasting it with the sum of the MBC values of the individual NPs (Equation 1). This coefficient has previously been applied to metal mixtures (Vaidya et al., 2017). If K(AbS) > 1, there is synergy; if K(AbS) = 1, there is an additive effect; if K(AbS) < 1, there is antagonism.

Equation 1:

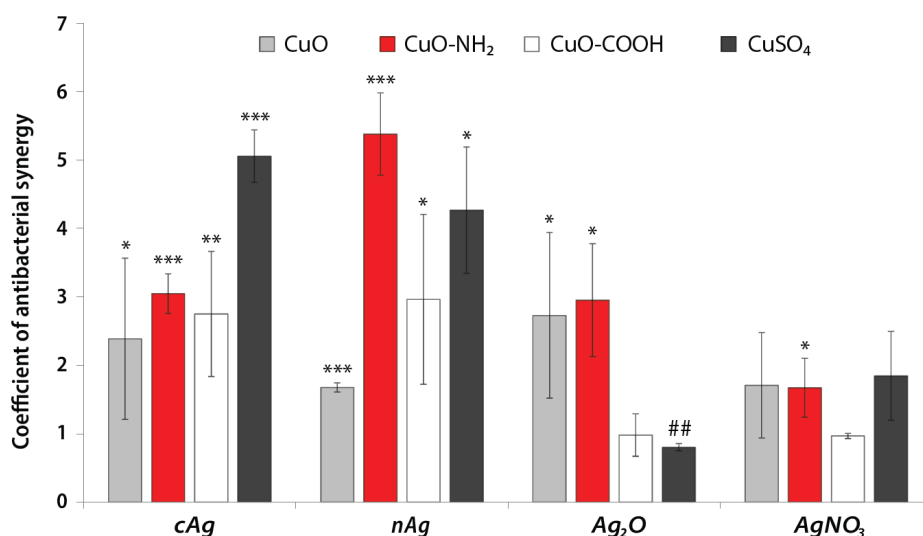
$$K(AbS) = 1 / \left( \frac{\text{MBC of antibacterial A in mix}}{\text{MBC of antibacterial A alone}} + \frac{\text{MBC of antibacterial B in mix}}{\text{MBC of antibacterial B alone}} \right)$$

Figure 3 clearly demonstrates that the MBC of a Cu component and Ag NP mixture is considerably lower than the MBC of the separate components. Based on our K(AbS) formula, the antibacterial effect of this mixture is 5.33 times higher than the sum of the

separate components' antibacterial effects. Different combinations of  $\text{CuSO}_4$  / cAg ratios yielded different K(AbS) results, with the highest K(AbS) most frequently observed using the 1:1 to 12.5:1 Cu/Ag ratio.

The antibacterial synergy depended on the type of Cu component used (Figure 4). MBC values of different Cu components, both alone and in combination with cAg, varied among different bacteria, except for *P. aeruginosa*, which resisted Cu compounds, despite the similar cAg MBC for *P. aeruginosa* and other bacteria.

Among CuO NPs, the highest K(AbS) with cAg was observed with unfunctionalized CuO and especially CuO-NH<sub>2</sub>, both of which are positively charged. However, the lowest K(AbS) was observed with negatively charged CuO-COOH. This implies that the inherent charge of CuO NPs influenced antibacterial synergy. On the other hand, the highest K(AbS) had well-dissolved  $\text{CuSO}_4$  salt and it means that presence of  $\text{Cu}^{2+}$  ions the mayor role in antibacterial synergy between cAg and Cu components (Figure 4).



**Figure 4.** Coefficient of antibacterial synergy (K(AbS)) between different Ag and Cu components in RPMI cell culture media with *E. coli* K-12 strain. \* -  $P < 0.05$ ; \*\* -  $< 0.01$ ; \*\*\* -  $< 0.001$ , ## -  $P < 0.01$  antagonism. Note: K(AbS) has been calculated as mean K(AbS) from different experiments, not from mean MBC of components in the mix or alone. The mean values with standard deviation are shown. Abbreviations: coated silver nanoparticles (cAg), nanosilver (nAg), silver oxide ( $\text{Ag}_2\text{O}$ ), silver nitrate ( $\text{AgNO}_3$ ), copper oxide (CuO), copper oxide coated with amino groups ( $\text{CuO-NH}_2$ ), copper oxide coated with carboxy groups ( $\text{CuO-COOH}$ ) and copper sulphate ( $\text{CuSO}_4$ ). Published from publication II with permission from journal.

Interestingly, the antibacterial synergy also relied on the Ag component. Various Ag NPs and  $\text{AgNO}_3$  were examined to determine which would display stronger antibacterial synergy with Cu components. The highest antibacterial synergy was showed when mixed non-oxidized Ag NPs with Cu salt.  $\text{AgNO}_3$  did not show strong antibacterial synergy with Cu components.

## 4.6 Mechanisms of antibacterial synergy (Publication II)

To understand antibacterial synergistic effect between Cu and Ag, several tests were conducted. It was hypothesized that their synergy could be linked to their different cellular targets in/on bacterial cells. A popular example of such synergy is seen between beta-lactam antibiotics, which impair bacterial cell membranes, and aminoglycosides, which obstruct bacterial protein synthesis. The heightened effect of aminoglycosides when used with  $\beta$ -lactams is said to be due to the  $\beta$ -lactam-induced membrane damage that boosts the uptake of aminoglycosides (Kohanski et al., 2010).

We hypothesized that one component (Cu or Ag component) might be causing more membrane damage, facilitating the other component's entry into the cell, thus further damaging the internal structures. In an attempt to corroborate this hypothesis, we assessed the outer membrane permeability of two Gram-negative bacteria, *E. coli* K-12 and *P. aeruginosa* PAO1. Our findings indicated that AgNO<sub>3</sub> and cAg were able to damage the outer membrane of both bacteria. Although cAg took longer to cause damage compared to AgNO<sub>3</sub>, and *P. aeruginosa*'s membrane was more resistant to damage compared to *E. coli*'s. However, CuO NPs and CuSO<sub>4</sub> did not cause significant membrane damage, especially in *P. aeruginosa*. This implies that Ag compounds might be inactivating cells by rupturing the bacteria's outer membranes, while Cu compounds seem to target other cell structures. Additionally, mixing Cu and Ag compounds didn't significantly alter the damaging action on the membrane. Thus, we discovered that the synergy between Cu and Ag did not result from damaging the bacterial outer membrane (Figure 5).

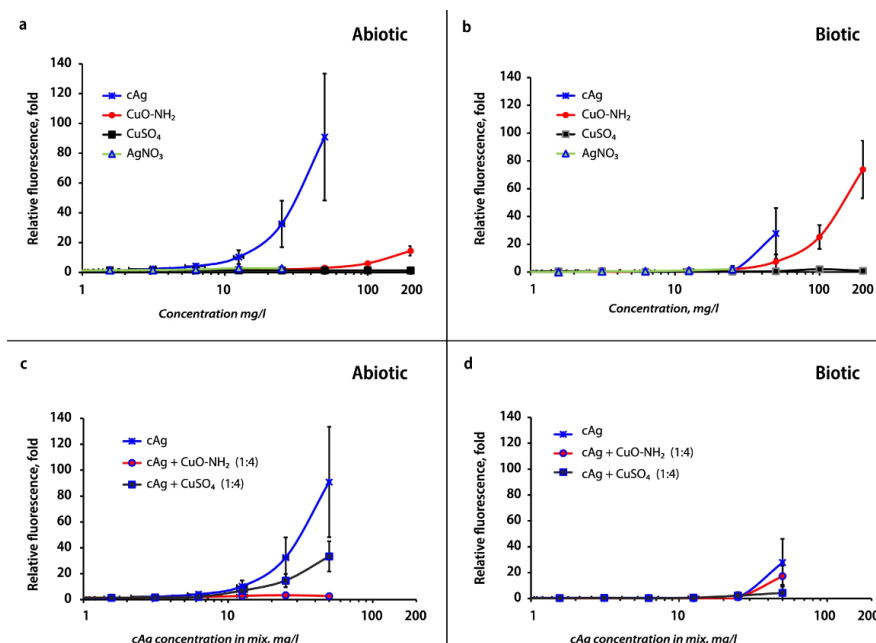


**Figure 5.** Production of reactive oxygen species (ROS) in suspensions. Measurement of induction of ROS in abiotic (a, c) and biotic (b, d) conditions. Measurement of ROS induction was performed after incubation with components alone (a, b) or in the mix of cAg and Cu components in a ratio 1:4 (c, d). cAg, Coated silver nanoparticles; AgNO<sub>3</sub>, Silver nitrate; CuO, Copper oxide; CuO-NH<sub>2</sub>, Copper oxide coated with amino groups; CuSO<sub>4</sub>, Copper sulphate; RFU, Relative fluorescence units. Published from publication II with permission from journal.



We also examined the potential role of ROS in the synergy of Cu and Ag. The Fenton-like reaction capacity of Cu ions to redox-cycle between  $\text{Cu}^+/\text{Cu}^{2+}$  which can generate ROS leading to lipid peroxidation, protein oxidation and DNA damage was investigated. However, our tests showed that the addition of  $\text{CuO-NH}_2$  or  $\text{CuSO}_4$  to cAg did not enhance ROS production, both in the presence and absence of bacteria, contradicting the idea that ROS might be the reason for the observed synergy between Cu and Ag components.

We further studied the dissolution of Ag NPs in water and RPMI CCM, with and without the addition of  $\text{CuSO}_4$ . Interestingly, there was a marked increase in the dissolution of Ag NPs with  $\text{CuSO}_4$  addition. This suggests an improved dissolution of Ag NPs in the presence of  $\text{Cu}^{2+}$ , possibly due to a redox reaction between Cu and Ag components (Figure 6).

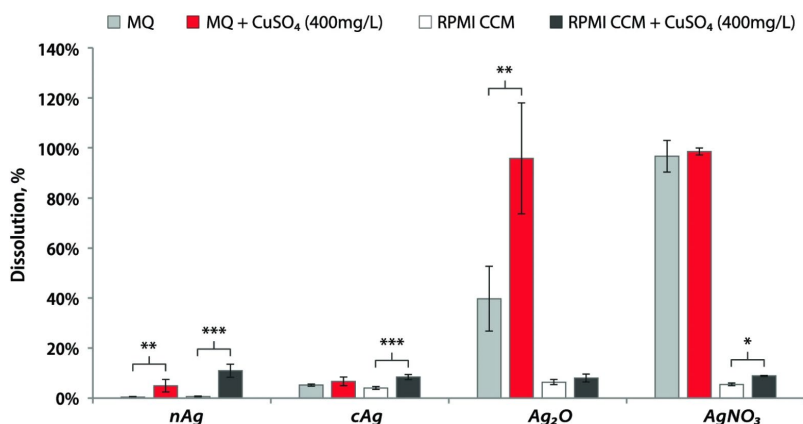


**Figure 6.** Dissolution of silver nanoparticles. Dissolution percentage of silver components (100 mg/L) in water and in RPMI CCM with and without the addition of  $\text{CuSO}_4$  (400 mg/L) after 24 h of incubation in a shaker at 37 °C. \* $P < 0.05$ ; \*\* $P < 0.01$ ; \*\*\* $P < 0.001$ . cAg, Coated silver nanoparticles; nAg, Nanosilver;  $\text{Ag}_2\text{O}$ , Silver oxide;  $\text{AgNO}_3$ , Silver nitrate;  $\text{CuSO}_4$ , Copper sulphate; RPMI CCM, Roswell Park Memorial Institute cell culture media. Published from publication II with permission from journal.

Lastly, in line with the aforementioned redox reaction,  $\text{Cu}^+$  is produced in the mix of Ag NPs and  $\text{Cu}^{2+}$  ions. We conducted a qualitative chemical reaction that proved the presence of  $\text{Cu}^+$  in the mixture, but not in nAg suspension,  $\text{AgNO}_3$ , or  $\text{CuSO}_4$  solutions separately. Since  $\text{Cu}^+$  has a higher antibacterial effect compared to  $\text{Cu}^{2+}$  due to its capacity to generate OH radicals, the formation of additional  $\text{Cu}^+$  ions in the solution may be among the main factors driving the antibacterial synergy of the Ag NP/ $\text{Cu}^{2+}$  system.

Our work demonstrates that a combination of non-oxidized Ag NPs and Cu ions is vital for achieving antibacterial synergy. We propose at least three reasons for this synergistic effect. Firstly, Cu ions enhance the oxidation of non-oxidized  $\text{Ag}^0$  in a redox reaction, resulting in improved dissolution of  $\text{Ag}^+$  from Ag NPs. Secondly, the production of more antibacterial  $\text{Cu}^+$  ions occurs in the same redox reaction. Lastly, the presence of  $\text{Cu}^{2+}$  reduces Ag ion binding to proteins in the culture medium, thereby increasing the concentration of free  $\text{Ag}^+$  in the solution. Therefore,  $\text{Cu}^{2+}$  ions' release from CuO NPs is essential for this synergistic action. These processes can occur both outside and within cells, with the latter causing more harm to cell homeostasis. Additional factors, like zeta-potential and NP surface functionalization, might have minor impacts on antibacterial synergy, warranting further investigation.

Understanding these mechanisms provides a critical foundation for the development of more efficient antimicrobial materials. In-depth knowledge of these processes allows for the creation of synergistic combinations of antimicrobial agents, thereby enhancing their overall efficacy against pathogenic bacteria.

#### 4.7 Antiviral properties of CuO and Ag NPs (Publication III)

Understanding the antiviral properties of NPs is, also, crucial as it opens up new avenues for developing effective therapies and preventive measures against various viral infections, especially respiratory viral infections which is very popular topic today. It aids in the design of advanced materials such as protective clothing, filters, and surfaces with inherent antiviral properties, enhancing public health safety, particularly during pandemics. We evaluated the antiviral properties of Ag, Cu, and Zn NPs and their corresponding salts using plaque assays on suspensions of influenza A virus and coronaviruses TGEV and SARS-CoV-2. For safety reasons, TGEV served as a Biosafety Level 2 model for SARS-CoV-2 susceptibility evaluation. We used metallic salts as controls during these NP tests. To ensure no cytotoxic effects were induced by the tested compounds, we confirmed their absence in vitro on cell lines, as the infection process in the plaque assay inherently involved the suspension of cells with these compounds. We sought to develop and assess materials with high efficacy, hence, we conducted the antiviral efficacy assessments of metal compounds in suspensions at the 1-hour mark.

Our suspension tests revealed that CuSO<sub>4</sub> was the most effective component against all tested viruses, including A/WSN/1933 (H1N1), SARS-CoV-2, and TGEV (half maximal inhibitory concentration (IC<sub>50</sub>) values of 1.40, 0.45, and 4.44 mg/L respectively) (Table 6). This highlights the superior antiviral capabilities of Cu, particularly Cu ions. CuO, CuO-NH<sub>2</sub>, and CuO-COOH NPs exhibited lower antiviral effectiveness compared to CuSO<sub>4</sub>, with the exception of CuO-COOH, which demonstrated an IC<sub>50</sub> value of 0.57 mg/L against A/WSN/1933 (H1N1). This could be attributed to the enhanced antiviral efficiency due to carboxylation, as carboxyl groups can bind to viral RNA.

**Table 6.** Antiviral efficacy (half maximal inhibitory concentration (IC<sub>50</sub>)) of metal salts and metal NPs against influenza A virus, SARS-CoV-2, and TGEV in water suspensions. Adopted and changed from Publication III.

Substance	IC <sub>50</sub> (mg/L)		
	Influenza A Virus	SARS-CoV-2	TGEV
CuSO <sub>4</sub>	1.40	0.45	4.44
CuO	49.25	>100	383.4
CuO-NH <sub>2</sub>	1.88	149.1	8.8
CuO-COOH	0.57	79.68	13.75
ZnSO <sub>4</sub>	3.39	35.65	ND
ZnO	134.8	ND	ND
AgNO <sub>3</sub>	>100	NA	>100
nAg	>1000	NA	NA

NA—not applicable: since nAg NPs and AgNO<sub>3</sub> were toxic to VeroE6 cells used for tests with SARS-CoV-2 already at 10 mg/L. ND—not determined, half maximal inhibitory concentration IC<sub>50</sub>.

AgNO<sub>3</sub> was ineffective at even the highest concentration (100 mg/L) tested in our study and failed to significantly reduce the titers of A/WSN/1933 (H1N1) and TGEV to calculate an IC<sub>50</sub>. The zinc sulfate (ZnSO<sub>4</sub>) displayed lesser antiviral effectiveness against the tested influenza and coronavirus strains compared to CuSO<sub>4</sub>. Antiviral synergy between Cu and Ag components has not been detected. As we pointed out in the previous paragraph, the main reason for the antibacterial synergy is the increase in free Ag ions in the solution in the presence of Cu ions. But since Ag components did not showed strong antiviral properties, antiviral synergy does not occur in this case.

Due to significant antiviral effect of Cu components, we chose them for incorporation into filter materials. Unfortunately, the CuO-NH<sub>2</sub> and CuO-COOH NPs that underwent functionalization aggregated in solvents, which is evidenced by high polydispersity index values ranging from 0.7 to 1 (data not shown). As a result, these NPs were unsuitable for electrospinning. Consequently, surface-functionalized NPs were not employed in the production of filter materials. However, the unfunctionalized CuO NPs, and CuSO<sub>4</sub> salt, exhibited exceptional compatibility for integration into CA filter materials. Hence, these were utilized in the fabrication of the filter materials.

#### 4.8 Characterization of produced filter materials (Publication III)

We leveraged electrospinning techniques and utilized cellulose acetate (CA) as a polymer to incorporate CuO NPs and CuSO<sub>4</sub>, with a view to develop novel filter materials (Table 7).

**Table 7.** Characteristics of electrospun filter materials. Adopted and changed from Publication III.

Samples	Mat thickness, mm	Diameter, nm	Air Permeability, Pa/cm <sup>2</sup>	Hydrophobic /Hydrophilic Measuring	Cu Content, %	Released Cu Content, 1h, %
CA	0.051	750	125.0	Hydrophobic	0	ND
CA_7.5% CuSO <sub>4</sub>	0.062	972	54.1	Hydrophobic	4.68 ± 1.1	46
CA_10% CuO	0.163	759	47.4	Hydrophobic	8.01 ± 0.39	0
CA_thymol	0.036	545	45.4	Hydrophilic	0	ND
CA_thymol_7.5% CuSO <sub>4</sub>	ND	431	55.9	Hydrophilic	7.38 ± 0.61	78

Additionally, we employed thymol during the electrospinning process to enhance the porosity and hydrophilicity of the fibers in the filter materials, as suggested in prior articles (Chen et al., 2020). We hypothesized that an increased porosity, courtesy of thymol, will augment metal release and thereby bolster the antimicrobial properties of the filter materials. Furthermore, heightened hydrophilicity should facilitate superior metal ion release, leading to more effective virus inactivation.

The fabricated filter materials were categorised as follows: CA (CA without antimicrobial components); CA\_7.5%CuSO<sub>4</sub> (CA containing 7.5% CuSO<sub>4</sub>); CA\_10%CuO (CA containing 10% CuO); CA\_thymol (CA containing 10% thymol); and CA\_thymol\_7.5%CuSO<sub>4</sub> (CA combined with 10% thymol and 7.5% CuSO<sub>4</sub>). All indicated percentages were determined based on Cu content.

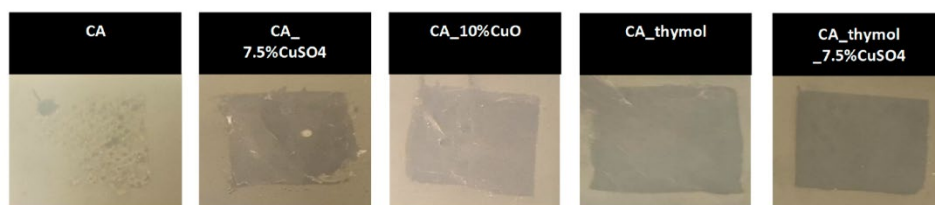
The maximum Cu concentration derived from CuSO<sub>4</sub> and CuO that we successfully integrated into CA was up to 8% (Table 7). To illustrate, when 7.5% of Cu derived from CuSO<sub>4</sub> was incorporated into CA polymer solutions (sample denoted as CA\_7.5%CuSO<sub>4</sub>), the final filter material displayed a measured Cu concentration of 4.68%. Thymol notably facilitated the integration of CuSO<sub>4</sub> into CA. When 7.5% of Cu from CuSO<sub>4</sub> was amalgamated with CA containing thymol, the final filter material's Cu concentration was almost identical to the nominal, at 7.38%.

The developed filter materials were evaluated for fiber morphologies, material thickness, hydrophilicity/hydrophobicity, and air-filtration parameters. Thymol resulted in improved material hydrophilicity and enhanced Cu release by 1.7 times compared to CA fibers without thymol (Table 7).

#### 4.8.1 Antibacterial properties of filter materials (Publication III)

Subsequently, we assessed the antibacterial potential of the developed filter materials against *E. coli* and *S. aureus*. Antibacterial activity against these bacterial strains was evaluated using the agar diffusion assay and visualized in Figure 7. As predicted, CA alone (control) did not inhibit bacterial growth. All other filter materials demonstrated exceptional antibacterial activity against both *E. coli* and *S. aureus*. Intriguingly, even CA incorporating thymol exhibited antibacterial effects without any Cu compound incorporation. The most potent antibacterial effect (largest bacteria-free zone) was observed for CA integrated with CuSO<sub>4</sub> and CA combined with thymol and CuSO<sub>4</sub>.

##### *Escherichia coli* K12



##### *Staphylococcus aureus* (ATCC 25923)

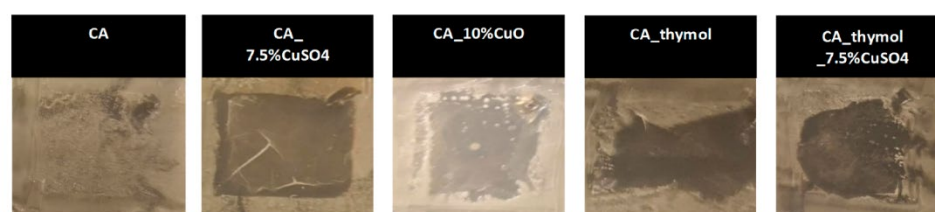


**Figure 7.** Antibacterial activity of filter materials against bacteria *E. coli* and *S. aureus*. The filter materials were removed for the images to demonstrate the bacteria-free area under the materials. Published from publication III with permission from journal.

#### **4.8.2 Antiviral properties of filter materials (Publication III)**

In the previous stages of our research, we assessed the antiviral efficacy of NPs in suspension (Table 6). We then analyzed the antiviral activity of our fabricated filter materials against A/WSN/1933 (H1N1), SARS-CoV-2, and TGEV viruses. This was done by incubating the virus stock with the material and subsequently evaluating its effect on the virus titer using the plaque assay.

The most substantial virucidal effect (expressed as the reduction of viral titers post 5-minute and 1-hour exposure) was recorded for filter materials CA with CuSO<sub>4</sub> and CA combined with thymol and CuSO<sub>4</sub> (Figure 8). These CuSO<sub>4</sub>-infused materials decreased influenza A virus titers by 1.1–1.8 log after 5 minutes of exposure and by 1.6–1.8 log after 1 hour of exposure (Figure 8A).

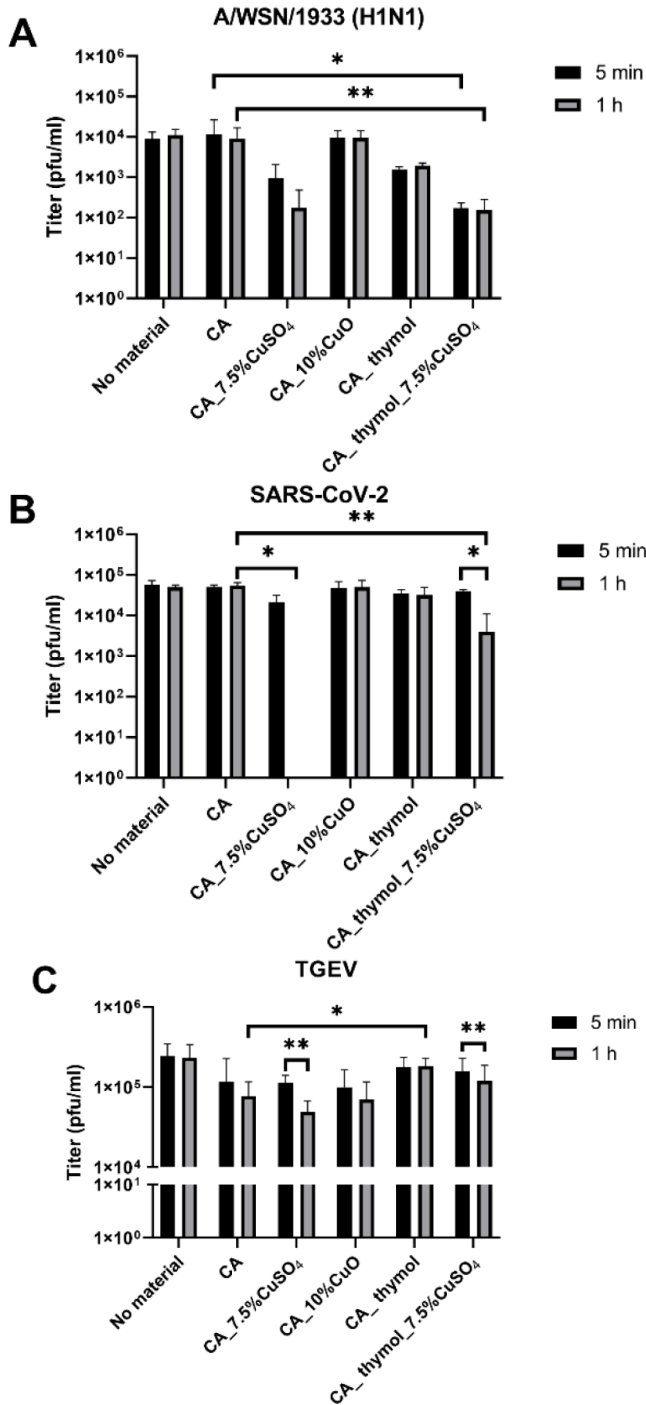


**Figure 8.** Antiviral properties of CA without additives (control), 7.5% CuSO<sub>4</sub> and 10% CuO in CA against influenza A/WSN/1933 (H1N1) virus (A), SARS-CoV-2 (B), and transmissible gastroenteritis coronavirus TGEV (C). Statistical significance is represented as follows: \*  $p < 0.05$ ; \*\*  $p < 0.01$ . Published from publication III with permission from journal.

Out of the three tested viruses, TGEV was the least affected by the virucidal effect of all filter materials: a modest 0.2 log reduction was observed after 1-hour exposure for CA material with  $\text{CuSO}_4$ . No significant effect was noted when thymol was added to the same material (Figure 8C).

The most potent virucidal effect of filter materials were observed against SARS-CoV-2: CA fibers with 7.5% Cu from  $\text{CuSO}_4$  entirely neutralized the infectivity of SARS-CoV-2 after 1 hour of contact exposure, while the CA\_thymol\_7.5% $\text{CuSO}_4$  material reduced the titer by 1.14 logs (Figure 8B).

Interestingly, contrary to the filter materials containing  $\text{CuSO}_4$ , those with 10% CuO didn't show effectiveness against any of the tested viruses. However, the addition of thymol alone to the CA material led to a reduction of A/WSN/1933 (H1N1) titer by approximately 0.7 logs compared to the CA control material without additives. Still, the difference was not statistically significant (Figure 8A).

Thymol's antiviral effect was found to be specific to the influenza virus in our experiments, as the CA\_thymol material didn't decrease the titers of coronaviruses. This outcome highlights the significance of hydrophobicity in antiviral efficacy.

We suggested that the influenza virus is more susceptible to Cu ions, while SARS-CoV-2 is more vulnerable to the material's hydrophobic interactions. In conclusion, filter materials containing  $\text{CuSO}_4$  demonstrated superior antiviral properties. Additionally, material hydrophilicity and hydrophobicity seemed to play a crucial role.

## 5 Conclusions

In this comprehensive investigation, we aimed to characterize the antimicrobial effects and safety of differently functionalized Cu and Ag NPs, dissect their mechanism of action, alone and in combination and developed new antimicrobial materials based on investigated NPs.

Firstly, we systematically compared the toxicity and mechanisms of Cu and Ag NPs with varying surface functionalizations to bacteria, viruses, and mammalian cells *in vitro*. We discovered that the toxicity of NPs to human cells can be significantly attenuated by functionalization of NPs with negatively charged groups, effectively broadening the therapeutic window. This finding presents a promising avenue for the creation of efficient and safe antimicrobials, thus opening up potential novel therapeutic strategies in combating bacterial infections.

Secondly, our research discovered an intriguing antibacterial synergy between Ag and Cu components, an interaction which underlying mechanisms we further elucidated. Our results showed that the combination of non-oxidized Ag NPs and  $\text{Cu}^{2+}$  ions was crucial for antibacterial synergy. This was attributed to three core processes: the enhancement of oxidation of  $\text{Ag}^0$  NPs through a redox reaction, instigated by Cu ions, leading to a greater dissolution of  $\text{Ag}^+$  from the NPs; the increased production of antibacterial  $\text{Cu}^+$  ions in the same redox reaction, which are more toxic to bacteria; and the diminished binding of Ag ions to proteins in the culture medium when in the presence of Cu ions. It leads to increased concentration of free  $\text{Ag}^+$  in the solution. We found that this synergistic effect could be highly instrumental in antibacterial applications, such as in wound dressings for treating infected wounds or filter materials preventing bacterial and viral infections.

Thirdly, we ventured into the realm of material development, focusing on creating new NPs-based antibacterial and antiviral materials. Our endeavours have resulted in innovative filter materials that incorporate  $\text{CuSO}_4$  or CuO NPs, exhibiting potent antiviral and antibacterial properties. These materials have demonstrated remarkable efficacy against a spectrum of pathogens, including SARS-CoV-2, Influenza A and bacteria such as *E. coli* and *S. aureus*. We envisage their applications in medical settings to mitigate the spread of infectious agents.

In conclusion, the research undertaken in this study has greatly contributed to our understanding of the mechanisms and potential applications of metal-based NPs in antimicrobial treatments. We have offered novel insights into the differential toxic effects of these NPs on human and bacterial cells, discovered mechanisms of the synergistic antibacterial action of Ag and Cu components, and advanced the development of NPs-based antimicrobial materials. Our findings set a robust foundation for further exploration and optimization of these promising materials, bringing us a step closer to more effective antimicrobial solutions.



## References

- Abushaheen, M. A., Muzahed, Fatani, A. J., Alosaimi, M., Mansy, W., George, M., Acharya, S., Rathod, S., Divakar, D. D., Jhugroo, C., Vellappally, S., Khan, A. A., Shaik, J., & Jhugroo, P. (2020). Antimicrobial resistance, mechanisms and its clinical significance. *Disease-a-Month*, *66*(6). <https://doi.org/10.1016/j.disamonth.2020.100971>
- Adeyemi, O. S., Shittu, E. O., Akpor, O. B., Rotimi, D., & Batiha, G. E. S. (2020). Silver nanoparticles restrict microbial growth by promoting oxidative stress and DNA damage. *EXCLI Journal*, *19*, 492–500. <https://doi.org/10.17179/excli2020-1244>
- Alavi, M., Kamarasu, P., McClements, D. J., & Moore, M. D. (2022). Metal and metal oxide-based antiviral nanoparticles: Properties, mechanisms of action, and applications. *Advances in Colloid and Interface Science*, *306*(June), 102726. <https://doi.org/10.1016/j.cis.2022.102726>
- Ameh, T., Gibb, M., Stevens, D., Pradhan, S. H., Braswell, E., & Sayes, C. M. (2022). Silver and Copper Nanoparticles Induce Oxidative Stress in Bacteria and Mammalian Cells. *Nanomaterials*, *12*(14). <https://doi.org/10.3390/nano12142402>
- Aruoja, V., Pokhrel, S., Sihtmäe, M., Mortimer, M., Mädler, L., & Kahru, A. (2015). Toxicity of 12 metal-based nanoparticles to algae, bacteria and protozoa. *Environmental Science: Nano*, *2*(6), 630–644. <https://doi.org/10.1039/C5EN00057B>
- Balasubramaniam, B., Prateek, Ranjan, S., Saraf, M., Kar, P., Singh, S. P., Thakur, V. K., Singh, A., & Gupta, R. K. (2021). Antibacterial and Antiviral Functional Materials: Chemistry and Biological Activity toward Tackling COVID-19-like Pandemics. *ACS Pharmacology and Translational Science*, *4*(1), 8–54. <https://doi.org/10.1021/acspsci.0c00174>
- Bankier, C., Matharu, R. K., Cheong, Y. K., Ren, G. G., Cloutman-Green, E., & Ciric, L. (2019). Synergistic Antibacterial Effects of Metallic Nanoparticle Combinations. *Scientific Reports*, *9*(1), 16074. <https://doi.org/10.1038/s41598-019-52473-2>
- Baram-Pinto, D., Shukla, S., Perkas, N., Gedanken, A., & Sarid, R. (2009). Inhibition of herpes simplex virus type 1 infection by silver nanoparticles capped with mercaptoethane sulfonate. *Bioconjugate Chemistry*, *20*(8), 1497–1502. <https://doi.org/10.1021/bc900215b>
- Bondarenko, O., Juganson, K., Ivask, A., Kasemets, K., Mortimer, M., & Kahru, A. (2013). Toxicity of Ag, CuO and ZnO nanoparticles to selected environmentally relevant test organisms and mammalian cells in vitro: A critical review. In *Archives of Toxicology* (Vol. 87, Issue 7, pp. 1181–1200). <https://doi.org/10.1007/s00204-013-1079-4>
- Bondarenko, O. M., Heinlaan, M., Sihtmäe, M., Ivask, A., Kurvet, I., Joonas, E., Jemec, A., Mannerström, M., Heinonen, T., Rekulapelly, R., Singh, S., Zou, J., Pyykkö, I., Drobne, D., & Kahru, A. (2016). Multilaboratory evaluation of 15 bioassays for (eco)toxicity screening and hazard ranking of engineered nanomaterials: FP7 project NANOVALID. *Nanotoxicology*, *10*(9), 1229–1242. <https://doi.org/10.1080/17435390.2016.1196251>
- Bondarenko, O. M., Sihtmäe, M., Kuzmičiova, J., Ragelienė, L., Kahru, A., & Daugelavičius, R. (2018). Plasma membrane is the target of rapid antibacterial action of silver nanoparticles in *Escherichia coli* and *Pseudomonas aeruginosa*. *International Journal of Nanomedicine*, *Volume 13*, 6779–6790. <https://doi.org/10.2147/IJN.S177163>
- Chen, Y., Qiu, Y., Chen, W., & Wei, Q. (2020). Electrospun thymol-loaded porous cellulose acetate fibers with potential biomedical applications. *Materials Science and Engineering C*, *109*(December 2019), 110536. <https://doi.org/10.1016/j.msec.2019.110536>

- Delay, M., & Frimmel, F. H. (2012). Nanoparticles in aquatic systems. *Analytical and Bioanalytical Chemistry*, 402(2), 583–592. <https://doi.org/10.1007/s00216-011-5443-z>
- Elechiguerra, J. L., Burt, J. L., Morones, J. R., Camacho-Bragado, A., Gao, X., Lara, H. H., & Yacaman, M. J. (2005). Interaction of silver nanoparticles with HIV-1. *Journal of Nanobiotechnology*, 3, 1–10. <https://doi.org/10.1186/1477-3155-3-6>
- Ermini, M. L., & Voliani, V. (2021). Antimicrobial Nano-Agents: The Copper Age. In *ACS Nano* (Vol. 15, Issue 4, pp. 6008–6029). American Chemical Society. <https://doi.org/10.1021/acsnano.0c10756>
- Ferdous, Z., & Nemmar, A. (2020). Health impact of silver nanoparticles: A review of the biodistribution and toxicity following various routes of exposure. In *International Journal of Molecular Sciences* (Vol. 21, Issue 7). <https://doi.org/10.3390/ijms21072375>
- Fisher, K., Pope, M., & Phillips, C. (2009). Combined effect of copper and silver against *Pseudomonas aeruginosa*. *Journal of Hospital Infection*, 73(2), 180–182. <https://doi.org/10.1016/j.jhin.2009.06.022>
- Garza-Cervantes, J. A., Chávez-Reyes, A., Castillo, E. C., García-Rivas, G., Antonio Ortega-Rivera, O., Salinas, E., Ortiz-Martínez, M., Gómez-Flores, S. L., Peña-Martínez, J. A., Pepi-Molina, A., Treviño-González, M. T., Zarate, X., Elena Cantú-Cárdenas, M., Enrique Escarcega-Gonzalez, C., & Morones-Ramírez, J. R. (2017). Synergistic Antimicrobial Effects of Silver/Transition-metal Combinatorial Treatments. *Scientific Reports*, 7(1), 903. <https://doi.org/10.1038/s41598-017-01017-7>
- Gupta, G., Cappellini, F., Farcal, L., Gornati, R., Bernardini, G., & Fadeel, B. (2022). Copper oxide nanoparticles trigger macrophage cell death with misfolding of Cu/Zn superoxide dismutase 1 (SOD1). *Particle and Fibre Toxicology*, 19(1), 1–27. <https://doi.org/10.1186/s12989-022-00467-w>
- Ha, T., Pham, T. T. M., Kim, M., Kim, Y. H., Park, J. H., Seo, J. H., Kim, K. M., & Ha, E. (2022). Antiviral Activities of High Energy E-Beam Induced Copper Nanoparticles against H1N1 Influenza Virus. *Nanomaterials*, 12(2). <https://doi.org/10.3390/nano12020268>
- Hang, X., Peng, H., Song, H., Qi, Z., Miao, X., & Xu, W. (2015). Antiviral activity of cuprous oxide nanoparticles against Hepatitis C Virus in vitro. *Journal of Virological Methods*, 222, 150–157. <https://doi.org/10.1016/j.jviromet.2015.06.010>
- He, Q., Lu, J., Liu, N., Lu, W., Li, Y., Shang, C., Li, X., Hu, L., & Jiang, G. (2022). Antiviral Properties of Silver Nanoparticles against SARS-CoV-2: Effects of Surface Coating and Particle Size. *Nanomaterials*, 12(6), 1–13. <https://doi.org/10.3390/nano12060990>
- Heinlaan, M., Ivask, A., Blinova, I., Dubourguier, H. C., & Kahru, A. (2008). Toxicity of nanosized and bulk ZnO, CuO and TiO<sub>2</sub> to bacteria *Vibrio fischeri* and crustaceans *Daphnia magna* and *Thamnocephalus platyurus*. *Chemosphere*, 71(7), 1308–1316. <https://doi.org/10.1016/j.chemosphere.2007.11.047>
- Hodek, J., Zajíčová, V., Lovetinská-Šlamborová, I., Stibor, I., Müllerová, J., & Weber, J. (2016). Protective hybrid coating containing silver, copper and zinc cations effective against human immunodeficiency virus and other enveloped viruses. *BMC Microbiology*, 16(1), 1–12. <https://doi.org/10.1186/s12866-016-0675-x>

- Holt, K. B., & Bard, A. J. (2005). Interaction of silver(I) ions with the respiratory chain of *Escherichia coli*: An electrochemical and scanning electrochemical microscopy study of the antimicrobial mechanism of micromolar Ag. *Biochemistry*, *44*(39), 13214–13223. <https://doi.org/10.1021/bi0508542>
- Huang, Y. W., Cambre, M., & Lee, H. J. (2017). The Toxicity of Nanoparticles Depends on Multiple Molecular and Physicochemical Mechanisms. *International Journal of Molecular Sciences*, *18*(12). <https://doi.org/10.3390/ijms18122702>
- Ivask, A., Kurvet, I., Kasemets, K., Blinova, I., Aruoja, V., Suppi, S., Vija, H., Kakinen, A., Titma, T., Heinlaan, M., Visnapuu, M., Koller, D., Kisand, V., & Kahru, A. (2014). Size-dependent toxicity of silver nanoparticles to bacteria, yeast, algae, crustaceans and mammalian cells in vitro. *PLoS ONE*, *9*(7). <https://doi.org/10.1371/journal.pone.0102108>
- Ivask, A., Titma, T., Visnapuu, M., Vija, H., Kakinen, A., Sihtmae, M., Pokhrel, S., Madler, L., Heinlaan, M., Kisand, V., Shimmo, R., & Kahru, A. (2015). Toxicity of 11 Metal Oxide Nanoparticles to Three Mammalian Cell Types In Vitro. *Current Topics in Medicinal Chemistry*, *15*(18), 1914–1929. <https://doi.org/10.2174/1568026615666150506150109>
- Jang, J., Lee, J. M., Oh, S. Bin, Choi, Y., Jung, H. S., & Choi, J. (2020). Development of Antibiofilm Nanocomposites: Ag/Cu Bimetallic Nanoparticles Synthesized on the Surface of Graphene Oxide Nanosheets. *ACS Applied Materials and Interfaces*, *12*(32), 35826–35834. <https://doi.org/10.1021/acsami.0c06054>
- Jenkins, S. I., Weinberg, D., Al-Shakli, A. F., Fernandes, A. R., Yiu, H. H. P., Telling, N. D., Roach, P., & Chari, D. M. (2016). “Stealth” nanoparticles evade neural immune cells but also evade major brain cell populations: Implications for PEG-based neurotherapeutics. *Journal of Controlled Release*, *224*, 136–145. <https://doi.org/10.1016/j.jconrel.2016.01.013>
- Jeremiah, S. S., Miyakawa, K., Morita, T., Yamaoka, Y., & Ryo, A. (2020). Potent antiviral effect of silver nanoparticles on SARS-CoV-2. *Biochemical and Biophysical Research Communications*, *533*(1), 195–200. <https://doi.org/10.1016/j.bbrc.2020.09.018>
- Karlsson, H. L., Cronholm, P., Gustafsson, J., & Möller, L. (2008). Copper oxide nanoparticles are highly toxic: A comparison between metal oxide nanoparticles and carbon nanotubes. *Chemical Research in Toxicology*, *21*(9), 1726–1732. <https://doi.org/10.1021/tx800064j>
- Kohanski, M. A., Dwyer, D. J., & Collins, J. J. (2010). How antibiotics kill bacteria: from targets to networks. *Nature Reviews Microbiology*, *8*(6), 423–435. <https://doi.org/10.1038/nrmicro2333>
- Kubo, A. L., Capjak, I., Vrček, I. V., Bondarenko, O. M., Kurvet, I., Vija, H., Ivask, A., Kasemets, K., & Kahru, A. (2018). Antimicrobial potency of differently coated 10 and 50 nm silver nanoparticles against clinically relevant bacteria *Escherichia coli* and *Staphylococcus aureus*. *Colloids and Surfaces B: Biointerfaces*, *170*, 401–410. <https://doi.org/10.1016/j.colsurfb.2018.06.027>
- Landeen, L. K., Yahya, M. T., & Gerbal, C. P. (1989). *Efficacy of Copper and Silver Ions and Reduced Levels of Free Chlorine in Inactivation of Legionella pneumophila* (Vol. 55, Issue 12).
- Lara, H. H., Ayala-Nuñez, N. V., Ixtapan-Turrent, L., & Rodriguez-Padilla, C. (2010). Mode of antiviral action of silver nanoparticles against HIV-1. *Journal of Nanobiotechnology*, *8*, 1–10. <https://doi.org/10.1186/1477-3155-8-1>

- León-Buitimea, A., Garza-Cárdenas, C. R., Garza-Cervantes, J. A., Lerma-Escalera, J. A., & Morones-Ramírez, J. R. (2020). The Demand for New Antibiotics: Antimicrobial Peptides, Nanoparticles, and Combinatorial Therapies as Future Strategies in Antibacterial Agent Design. *Frontiers in Microbiology*, *11*(July), 1–10. <https://doi.org/10.3389/fmicb.2020.01669>
- Líbalová, H., Costa, P. M., Olsson, M., Farcál, L., Ortelli, S., Blosi, M., Topinka, J., Costa, A. L., & Fadeel, B. (2018). Toxicity of surface-modified copper oxide nanoparticles in a mouse macrophage cell line: Interplay of particles, surface coating and particle dissolution. *Chemosphere*, *196*, 482–493. <https://doi.org/10.1016/j.chemosphere.2017.12.182>
- Linder, M. C. (2012). The relationship of copper to DNA damage and damage prevention in humans. In *Mutation Research - Fundamental and Molecular Mechanisms of Mutagenesis* (Vol. 733, Issues 1–2, pp. 83–91). <https://doi.org/10.1016/j.mrfmmm.2012.03.010>
- Lu, L., Sun, R. W. Y., Chen, R., Hui, C. K., Ho, C. M., Luk, J. M., Lau, G. K. K., & Che, C. M. (2008). Silver nanoparticles inhibit hepatitis B virus replication. *Antiviral Therapy*, *13*(2), 252–262. <https://doi.org/10.1177/135965350801300210>
- Luceri, A., Francese, R., Lembo, D., Ferraris, M., & Balagna, C. (2023). Silver Nanoparticles: Review of Antiviral Properties, Mechanism of Action and Applications. *Microorganisms*, *11*(3), 629. <https://doi.org/10.3390/microorganisms11030629>
- Ma, X., Zhou, S., Xu, X., & Du, Q. (2022). Copper-containing nanoparticles: Mechanism of antimicrobial effect and application in dentistry—a narrative review. In *Frontiers in Surgery* (Vol. 9). Frontiers Media S.A. <https://doi.org/10.3389/fsurg.2022.905892>
- Mahmoodi, S., Elmi, A., & Hallaj Nezhadi, S. (2018). Copper Nanoparticles as Antibacterial Agents. *Journal of Molecular Pharmaceutics & Organic Process Research*, *06*(01). <https://doi.org/10.4172/2329-9053.1000140>
- McNeilly, O., Mann, R., Hamidian, M., & Gunawan, C. (2021). Emerging Concern for Silver Nanoparticle Resistance in *Acinetobacter baumannii* and Other Bacteria. In *Frontiers in Microbiology* (Vol. 12). Frontiers Media S.A. <https://doi.org/10.3389/fmicb.2021.652863>
- McShan, D., Ray, P. C., & Yu, H. (2014). Molecular toxicity mechanism of nanosilver. *Journal of Food and Drug Analysis*, *22*(1), 116–127. <https://doi.org/10.1016/j.jfda.2014.01.010>
- Michels, H. T., Keevil, C. W., Salgado, C. D., & Schmidt, M. G. (2015). From laboratory research to a clinical trial: copper alloy surfaces kill bacteria and reduce hospital-acquired infections. *Health Environments Research and Design Journal*, *9*(1), 64–79. <https://doi.org/10.1177/1937586715592650>
- Mishra, A., Pradhan, D., Halder, J., Biswasroy, P., Rai, V. K., Dubey, D., Kar, B., Ghosh, G., & Rath, G. (2022). Metal nanoparticles against multi-drug-resistance bacteria. *Journal of Inorganic Biochemistry*, *237*(July), 111938. <https://doi.org/10.1016/j.jinorgbio.2022.111938>
- Murray, C. J., Ikuta, K. S., Sharara, F., Swetschinski, L., Robles Aguilar, G., Gray, A., Han, C., Bisignano, C., Rao, P., Wool, E., Johnson, S. C., Browne, A. J., Chipeta, M. G., Fell, F., Hackett, S., Haines-Woodhouse, G., Kashef Hamadani, B. H., Kumaran, E. A. P., McManigal, B., ... Naghavi, M. (2022). Global burden of bacterial antimicrobial resistance in 2019: a systematic analysis. *The Lancet*, *399*(10325), 629–655. [https://doi.org/10.1016/S0140-6736\(21\)02724-0](https://doi.org/10.1016/S0140-6736(21)02724-0)

- Naz, S., Gul, A., & Zia, M. (2020). Toxicity of copper oxide nanoparticles: A review study. *IET Nanobiotechnology*, *14*(1), 1–13. <https://doi.org/10.1049/iet-nbt.2019.0176>
- Nel, A. E., Mädler, L., Velegol, D., Xia, T., Hoek, E. M. V., Somasundaran, P., Klaessig, F., Castranova, V., & Thompson, M. (2009). Understanding biophysicochemical interactions at the nano-bio interface. In *Nature Materials* (Vol. 8, Issue 7, pp. 543–557). <https://doi.org/10.1038/nmat2442>
- Orłowski, P., Kowalczyk, A., Tomaszewska, E., Ranożek-Soliwoda, K., Węgrzyn, A., Grzesiak, J., Celichowski, G., Grobelny, J., Eriksson, K., & Krzyżowska, M. (2018). Antiviral activity of tannic acid modified silver nanoparticles: Potential to activate immune response in herpes genitalis. *Viruses*, *10*(10), 1–15. <https://doi.org/10.3390/v10100524>
- Paladini, F. (2019). *Antimicrobial Silver Nanoparticles for Wound Healing Application : Progress and Future Trends*.
- Palza, H. (2015). Antimicrobial polymers with metal nanoparticles. *International Journal of Molecular Sciences*, *16*(1), 2099–2116. <https://doi.org/10.3390/ijms16012099>
- Park, S. J., Ko, Y. S., Lee, S. J., Lee, C., Woo, K., & Ko, G. P. (2018). Inactivation of influenza A virus via exposure to silver nanoparticle-decorated silica hybrid composites. *Environmental Science and Pollution Research*, *25*(27), 27021–27030. <https://doi.org/10.1007/s11356-018-2620-z>
- Rai, M., Deshmukh, S. D., Ingle, A. P., Gupta, I. R., Galdiero, M., & Galdiero, S. (2016). Metal nanoparticles: The protective nanoshield against virus infection. *Critical Reviews in Microbiology*, *42*(1), 46–56. <https://doi.org/10.3109/1040841X.2013.879849>
- Sanità, G., Carrese, B., & Lamberti, A. (2020). Nanoparticle Surface Functionalization: How to Improve Biocompatibility and Cellular Internalization. *Frontiers in Molecular Biosciences*, *7*(November). <https://doi.org/10.3389/fmolb.2020.587012>
- Shady, N. H., Khattab, A. R., Ahmed, S., Liu, M., Quinn, R. J., Fouad, M. A., Kamel, M. S., Muhsinah, A. Bin, Krischke, M., Mueller, M. J., & Abdelmohsen, U. R. (2020). Hepatitis c virus ns3 protease and helicase inhibitors from red sea sponge (Amphimedon) species in green synthesized silver nanoparticles assisted by in silico modeling and metabolic profiling. *International Journal of Nanomedicine*, *15*, 3377–3389. <https://doi.org/10.2147/IJN.S233766>
- Sheng, Y., Liu, C., Yuan, Y., Tao, X., Yang, F., Shan, X., Zhou, H., & Xu, F. (2009). Long-circulating polymeric nanoparticles bearing a combinatorial coating of PEG and water-soluble chitosan. *Biomaterials*, *30*(12), 2340–2348. <https://doi.org/10.1016/j.biomaterials.2008.12.070>
- Suppi, S., Kasemets, K., Ivask, A., Künnis-Beres, K., Sihtmäe, M., Kurvet, I., Aruoja, V., & Kahru, A. (2015). A novel method for comparison of biocidal properties of nanomaterials to bacteria, yeasts and algae. *Journal of Hazardous Materials*, *286*, 75–84. <https://doi.org/10.1016/j.jhazmat.2014.12.027>
- Tao, Y., Zhou, F., Wang, K., Yang, D., & Sacher, E. (2022). AgCu NP Formation by the Ag NP Catalysis of Cu Ions at Room Temperature and Their Antibacterial Efficacy: A Kinetic Study. *Molecules*, *27*(20). <https://doi.org/10.3390/molecules27206951>
- Tavakoli, A., & Hashemzadeh, M. S. (2020). Inhibition of herpes simplex virus type 1 by copper oxide nanoparticles. *Journal of Virological Methods*, *275*. <https://doi.org/10.1016/j.jviromet.2019.113688>
- Theuretzbacher, U. (2020). Dual-mechanism antibiotics. *Nature Microbiology*, *5*(8), 984–985. <https://doi.org/10.1038/s41564-020-0767-0>

- Theuretzbacher, U., Outterson, K., Engel, A., & Karlén, A. (2020). The global preclinical antibacterial pipeline. *Nature Reviews Microbiology*, 18(5), 275–285. <https://doi.org/10.1038/s41579-019-0288-0>
- Tortella, G. R., Pieretti, J. C., Rubilar, O., Fernández-Baldo, M., Benavides-Mendoza, A., Diez, M. C., & Seabra, A. B. (2022). Silver, copper and copper oxide nanoparticles in the fight against human viruses: progress and perspectives. In *Critical Reviews vasiliein Biotechnology* (Vol. 42, Issue 3, pp. 431–449). Taylor and Francis Ltd. <https://doi.org/10.1080/07388551.2021.1939260>
- Vaidya, M. Y., McBain, A. J., Butler, J. A., Banks, C. E., & Whitehead, K. A. (2017). Antimicrobial Efficacy and Synergy of Metal Ions against *Enterococcus faecium*, *Klebsiella pneumoniae* and *Acinetobacter baumannii* in Planktonic and Biofilm Phenotypes. *Scientific Reports*, 7(1), 5911. <https://doi.org/10.1038/s41598-017-05976-9>
- Wang, L., Hu, C., & Shao, L. (2017). The-antimicrobial-activity-of-nanoparticles--present-situati. *International Journal of Nanomedicine*, 12, 1227–1249.
- Warnes, S. L., Little, Z. R., & Keevil, C. W. (2015). Human coronavirus 229E remains infectious on common touch surface materials. *MBio*, 6(6). <https://doi.org/10.1128/mBio.01697-15>
- Wonder, E., Simón-Gracia, L., Scodeller, P., Majzoub, R. N., Kotamraju, V. R., Ewert, K. K., Teesalu, T., & Safinya, C. R. (2018). Competition of charge-mediated and specific binding by peptide-tagged cationic liposome–DNA nanoparticles in vitro and in vivo. *Biomaterials*, 166, 52–63. <https://doi.org/10.1016/j.biomaterials.2018.02.052>
- Yang, X. X., Li, C. M., & Huang, C. Z. (2016). Curcumin modified silver nanoparticles for highly efficient inhibition of respiratory syncytial virus infection. *Nanoscale*, 8(5), 3040–3048. <https://doi.org/10.1039/c5nr07918g>
- Yayha, M. T., Kutz, S. M., Landeen, L. K., & Gerba, C. P. (n.d.). Swimming Pool Disinfection: An evaluation of the efficacy of copper: silver ions. In *Source: Journal of Environmental Health* (Vol. 51, Issue 5).
- Zhang, R., Lin, Z., Lui, V. C., Wong, K. K., Tam, P. K., Lee, P., Lok, C. N., Lamb, J. R., Chen, Y., & Xia, H. (2017). Silver nanoparticle treatment ameliorates biliary atresia syndrome in rhesus rotavirus inoculated mice. *Nanomedicine: Nanotechnology, Biology, and Medicine*, 13(3), 1041–1050. <https://doi.org/10.1016/j.nano.2016.11.013>
- Zhou, F., Zhu, Y., Yang, L., Yang, D. Q., & Sacher, E. (2022). Ag NP catalysis of Cu ions in the preparation of AgCu NPs and the mechanism of their enhanced antibacterial efficacy. *Colloids and Surfaces A: Physicochemical and Engineering Aspects*, 632. <https://doi.org/10.1016/j.colsurfa.2021.127831>
- Zhou, S. Y. D., Huang, F. Y., Zhou, X. Y., Lin, C., Jin, M. K., Neilson, R., Li, H., & Su, J. Q. (2022). Conurbation size drives antibiotic resistance along the river. *Science of the Total Environment*, 823. <https://doi.org/10.1016/j.scitotenv.2022.153822>
- Zhou, T., Prasher, S., Qi, Z., George, S., Mawof, A., Nzediegwu, C., Dhiman, J., & Patel, R. (2021). Impact of Silver Nanoparticles in Wastewater on Heavy Metal Transport in Soil and Uptake by Radish Plants. *Water, Air, and Soil Pollution*, 232(7). <https://doi.org/10.1007/s11270-021-05227-8>

## Acknowledgements

The work was financially supported by PUT1015 and GOVSG16 grants from the Estonian Research Council, Arengufond\_OB Grant from Development Fund of National Institute of Chemical Physics and Biophysics, grant from the Estonian Connected Health Cluster and WomenTech EU grant and EIC Accelerator grant No. 190199469 (NANOWOUND) from the European Commission. This work has been partially supported by “TUT Institutional Development Program for 2016-2022” Graduate School in Clinical medicine” receiving funding from the European Regional Development Fund under program ASTRA 2014-2020.4.01.16-0032 in Estonia.

I would like to express my deepest gratitude to my supervisor, **Dr. Olesja Bondarenko**, whose expertise, understanding, and patience, added considerably to my doctoral experience. Her mentorship was paramount in providing a well-rounded experience consistent with my long-term career goals. Her perpetual energy and enthusiasm in research, and unflinching support have been key to this work.

I am incredibly thankful to the Head of the Laboratory of Environmental Toxicology (National Institute of Chemical Physics and Biophysics), Academician **Anne Kahru**, for her invaluable guidance, support, and encouragement. Her insights and wisdom have inspired me throughout my academic journey, for which I am profoundly grateful.

Special thanks go to my co-worker, **Dr. Anna-Liisa Kubo**, for her cooperation, immense knowledge, and motivation that immensely helped me throughout the research.

I extend my heartfelt thanks to **Mariliis Sihtmäe**. Her assistance and support at every stage of my PhD journey have been invaluable, and I deeply appreciate her kindness and commitment.

I extend my heartfelt thanks to **Dr. Pirjo Spuul** for her pivotal role in the doctoral school management. Also, her diligent guidance and thorough feedback were important during the process of thesis writing.

I would also like to acknowledge the diligent and dedicated **members of Laboratory of Environmental Toxicology (National Institute of Chemical Physics and Biophysics)**. Their collaborative efforts, insightful comments, and feedback played an instrumental role in shaping this research.

Finally, to all who contributed directly or indirectly to this thesis, your assistance was a milestone in the accomplishment of this research. I am eternally grateful for your unwavering belief in my capabilities.

## Abstract

# Synergistic Mechanisms and Toxicity Profiles of Silver and Copper Nanoparticles for the Development of Novel Antimicrobial Materials

This research provides a comprehensive data on antimicrobial properties and safety profiles of differently functionalized copper (Cu) and silver (Ag) nanoparticles (NPs) and mechanisms of their synergy. In addition, on the basis of characterized NPs, we developed innovative NP-based antibacterial and antiviral materials that showed excellent antibacterial and antiviral properties and thus, promising prospects in the medical field.

At the core of this research, we conducted an extensive comparison of the toxicity and mechanism of action of Cu and Ag NPs, specifically those with differing functionalizations, against bacteria, viruses, and mammalian cells *in vitro*. The findings highlighted a notable reduction in toxicity of NPs to human cells when NPs were functionalized with negatively charged groups. This observation found the crucial role of NP surface charge in influencing cytotoxicity and uncovered a new dimension in nanosafety. By widening the therapeutic window for the treatment of bacterial infections, this discovery set a precedent for the future design of antimicrobial agents that balance antibacterial efficacy with reduced cytotoxicity to human cells, thereby resulting more efficient and safe antimicrobials.

After understanding the mechanisms of NPs, we focused on antibacterial synergistic effects of Ag and Cu NP combinations. We discovered that the combined antibacterial action of Ag and Cu in NPs goes beyond the additive effect of their individual antibacterial properties. Three key processes were identified as responsible for this synergistic action. First,  $\text{Cu}^{2+}$  ions were found to enhance the oxidation of non-oxidized Ag in a redox reaction, leading to an augmented dissolution of  $\text{Ag}^+$ . Simultaneously, the same redox reaction led to the generation of a higher quantity of antibacterial  $\text{Cu}^+$  ions, which are more antibacterial. Lastly, the presence of  $\text{Cu}^{2+}$  was observed to reduce the binding of Ag ions to proteins in the culture medium, thereby increasing the concentration of free  $\text{Ag}^+$  in the solution. With these findings, we propose that the interplay of Cu and Ag in NPs can be optimized to create a synergistic antibacterial action, which can be exploited for more efficient antimicrobial applications.

The third significant achievement of this research was the development of new NP-based antibacterial and antiviral filter materials, especially those incorporating  $\text{CuSO}_4$  or CuO NPs. We tested these materials against a range of pathogens, including SARS-CoV-2, Influenza A, *E. coli*, and *S. aureus*. Impressively, they exhibited potent virucidal and bactericidal effects, with  $\text{CuSO}_4$ -based filter materials being especially effective against SARS-CoV-2. The development of these advanced filter materials represents an important step towards creating practical inventions to mitigate the spread of bacterial and viral pathogens.

In summary, this doctoral research advances the current understanding of the antimicrobial potential of metal-based NPs, particularly those based on Cu and Ag. By offering new insights into NP cytotoxicity, antibacterial synergy, and material development, it builds a solid foundation for the future design and optimization of NP-based antimicrobials and materials. It helps to bring the medical field closer to efficacious, safer, and practical antimicrobial solutions.



## Lühikokkuvõte

# Vase ja hõbeda nanoosakeste sünergilise koosmõju mehhanismid ja rakendamine uute antimikroobsete materjalide arendamiseks

Antud doktoritöö keskendub vase (Cu) ja hõbeda (Ag) nanoosakeste (NPs) antimikroobsetele omadustele, nende ohutusele, koosmõjule ja toimemehhanismidele. Töö viimases osas kirjeldatakse antud nanoosakeste põhjal arendatud uudsete bakteri- ja viirusvastaste filtermaterjalide loomist ja omadusi.

Uuringu käigus leidsime, et erinevalt funktsionaliseeritud negatiivse pinnalaenguga Ag ja Cu nanoosakesed olid inimrakkudele *in vitro* tingimustes ohutumad kui erinevalt funktsionaliseeritud positiivse pinnalaenguga nanoosakesed, olles siiski piisavalt efektiivsed bakteritega võitlemiseks. See, et negatiivselt laetud Ag ja Cu nanoosakesed olid inimrakkudele vähem toksilised kui bakterirakkudele võimaldab laiendada nende osakeste terapeutilise kasutamise 'akent', mis omakorda on oluline tõhusamate ja ohutumate antimikroobsete nanoosakeste ja nendel põhinevate materjalide loomisel.

On märkimisväärne tulemus, et Ag ja Cu nanoosakeste kooskasutamisel ilmnes sünergiline bakterivastane toime, mille selgituseks pakkusime välja kolm põhilist mehhanismi: (i)  $\text{Cu}^{2+}$  ioonid suurendasid redoks-reaktsioonis mitte-oküdeerunud Ag oksüdatsiooni, mis viis  $\text{Ag}^+$  lahustumise suurenemiseni; (ii) redoks-reaktsioon viis suurema hulga antibakteriaalsete  $\text{Cu}^+$  ionide vabanemiseni, millel on tugevam bakterivastane toime võrreldes  $\text{Cu}^{2+}$ ioonidega; (iii)  $\text{Cu}^{2+}$  juuresolu vähendas  $\text{Ag}^+$  ionide sidumist katsekeskkonnas olevate valkudega, suurendades seeläbi vaba  $\text{Ag}^+$  kontsentratsiooni lahuses. Kõiki neid teadmisi kasutades on võimalik luua tõhusamaid antimikroobseid rakendusi

Uurimistöö kolmas oluline saavutus oli uute nanoosakeste baasil antibakteriaalsete ja viirusevastaste filtrimaterjalide arendamine.  $\text{CuSO}_4$  või  $\text{CuO}$  sisaldavad materjalid olid eriti tõhusad bakterite ja viiruste vastu, sealhulgas SARS-CoV-2, gripp A, *Escherichia coli* ja *Staphylococcus aureus* vastu. Selliste uudsete filtrimaterjalide arendamine on oluline samm mikroobsete patogeenide leviku tõkestamisel.

Kokkuvõtteks laiendab antud doktoritöö praegust arusaama vase- ja hõbedapõhiste nanoosakeste antimikroobsest potentsiaalist, mehhanismidest ja koostoimest. Doktoritöö käigus saadud tulemused nanoosakeste tsütotoksilisusest ja antibakteriaalsest sünergiast võimaldavad luua uusi antimikroobseid materjale, mis omakorda tõhustab võitlust infektsioonide ja bakterite antibiootikumiresistentsusega.

## Appendix 1

### Publication I

Kubo, A.-L., **Vasiliev, G.**, Vija, H., Krishtal, J., Tõugu, V., Visnapuu, M., Kisand, V., Kahru, A., & Bondarenko, O. M. (2020). Surface carboxylation or PEGylation decreases CuO nanoparticles' cytotoxicity to human cells in vitro without compromising their antibacterial properties. *Archives of Toxicology*, 94(5), 1561–1573. <https://doi.org/10.1007/s00204-020-02720-7>





# Surface carboxylation or PEGylation decreases CuO nanoparticles' cytotoxicity to human cells in vitro without compromising their antibacterial properties

Anna-Liisa Kubo<sup>1</sup> · Grigory Vasiliev<sup>1,2</sup> · Heiki Vija<sup>1</sup> · Jekaterina Krishtal<sup>2</sup> · Vello Tõugu<sup>2</sup> · Meeri Visnapuu<sup>3</sup> · Vambola Kisand<sup>3</sup> · Anne Kahru<sup>1,4</sup> · Olesja M. Bondarenko<sup>1</sup>

Received: 31 January 2020 / Accepted: 26 March 2020 / Published online: 7 April 2020  
© The Author(s) 2020

## Abstract

Clinical use of CuO nanoparticles (NPs) as antibacterials can be hampered by their toxicity to human cells. We hypothesized that certain surface functionalizations of CuO NPs may render NPs toxic to bacteria, but still be relatively harmless to human cells. To control this hypothesis, the toxicity of differently functionalized CuO NPs to bacteria *Escherichia coli* vs human cells (THP-1 macrophages and HACAT keratinocytes) was compared using similar conditions and end points. CuO NPs functionalized with polyethylene glycol (CuO–PEG), carboxyl (CuO–COOH, anionic), ammonium (CuO–NH<sub>4</sub><sup>+</sup>, cationic) and unfunctionalized CuO NPs and CuSO<sub>4</sub> (controls) were tested. In general, the toxicity of Cu compounds decreased in the following order: CuO–NH<sub>4</sub><sup>+</sup> > unfunctionalized CuO > CuSO<sub>4</sub> > CuO–COOH > CuO–PEG. Positively charged unfunctionalized CuO and especially CuO–NH<sub>4</sub><sup>+</sup> proved most toxic (24-h EC<sub>50</sub> = 21.7–47 mg/l) and had comparable toxicity to bacterial and mammalian cells. The multivariate analysis revealed that toxicity of these NPs was mostly attributed to their positive zeta potential, small hydrodynamic size, high Cu dissolution, and induction of reactive oxygen species (ROS) and TNF-α. In contrast, CuO–COOH and CuO–PEG NPs had lower toxicity to human cells compared to bacteria despite efficient uptake of these NPs by human cells. In addition, these NPs did not induce TNF-α and ROS. Thus, by varying the NP functionalization and Cu form (soluble salt vs NPs), it was possible to “target” the toxicity of Cu compounds, whereas carboxylation and PEGylation rendered CuO NPs that were more toxic to bacteria than to human cells envisaging their use in medical antibacterial products.

**Keywords** Surface coating · Nanosafety · Nanomedicine · Antibacterial · Immunotoxicity · Particle internalization

**Electronic supplementary material** The online version of this article (<https://doi.org/10.1007/s00204-020-02720-7>) contains supplementary material, which is available to authorized users.

- ✉ Anne Kahru  
anne.kahru@kbfi.ee
- ✉ Olesja M. Bondarenko  
olesja.bondarenko@kbfi.ee

<sup>1</sup> Laboratory of Environmental Toxicology, National Institute of Chemical Physics and Biophysics, Akadeemia tee 23, Tallinn, Estonia

<sup>2</sup> Department of Chemistry and Biotechnology, School of Science, TalTech, Akadeemia tee 15, Tallinn, Estonia

<sup>3</sup> Institute of Physics, University of Tartu, W. Ostwaldi 1, Tartu, Estonia

<sup>4</sup> Estonian Academy of Sciences, Kohtu 6, Tallinn, Estonia

## Introduction

Increasing resistance of bacteria to conventional antibiotics necessitates the development of alternatives such as silver and copper-based antimicrobials, including in nanoformulations. Copper is known since long time as a metal with antibacterial effect that can be used to inhibit bacterial spreads by employing Cu on surfaces (Rosenberg et al. 2018), in aqueous suspension (Bastos et al. 2018) and in textiles (Teli and Sheikh 2013; Mantecca et al. 2017). For living organisms, including humans, Cu is an essential microelement. Cu is vital for, e.g., functioning of the innate and adaptive immune system (Percival 1995, 1998) and is the necessary component of the key enzymes (O'Dell 1976). Previous studies have shown that CuO NPs support wound healing (Borkow et al. 2010) and bone regeneration (Shi et al. 2016). For instance, mesoporous silica NPs containing 2.5–5% Cu

were suggested for the use in bone regeneration, since they up-regulated the genes contributing to osteogenic and angiogenic factors and were not toxic in the range of 10–500 mg/l (i.e., 0.5–25 mg Cu/l) to murine macrophages RAW 264.7, whereas Cu significantly contributed to the beneficial properties of these NPs (Shi et al. 2016).

Given the above-mentioned properties, CuO NPs are ideal candidates for the use in medicine as wound dressings and/or internal implants by combining two functions: antimicrobial activity and increased wound healing or osteogenesis. However, the excessive copper is toxic and plays a role in the pathogenesis of several diseases (Klaassen and Curtis 2008; Brewer 2010; Montes et al. 2014). In case of topical use (e.g., in wound dressings), CuO NPs will be in close contact with keratinocytes and in case of internal use (e.g., implants), with the macrophages residing in the blood and tissues. Thus, it is important to avoid toxicity of CuO NPs to these cell types. Previous studies have shown that pristine (unfunctionalized) CuO NPs were toxic to murine macrophage cell line RAW264.7 (Líbalová et al. 2018) and other human cell models in vitro such as epidermal keratinocytes NHEK (Murugan et al. 2017), lung adenocarcinoma cells A549 (Karlsson et al. 2008), hepatoma cell line HepG2 (Piret et al. 2017), epithelial colon carcinoma cells Caco-2 (Käkinen et al. 2016) and differentiated Caco-2 (in vitro model for the cells of small intestine) (Ude et al. 2017) with the range of  $EC_{50}$  values of 13–100 mg/l (Bondarenko et al. 2013). However, the antibacterial concentrations of CuO NPs were in the range of 20–280 mg/l, implying that the therapeutic use of the existing (mostly unfunctionalized) CuO NPs as antibacterials is rather limited, since the CuO NPs effective in killing bacteria were also toxic to human cells in vitro (Bondarenko et al. 2013, 2016). Thus, successful commercialization of antibacterial CuO NPs necessitates a compromise of reasonable antibacterial properties with reasonable safety to human cells. As the prerequisite of the toxic action of chemicals/NPs is adversely influencing or crossing the main biological barrier (the cell wall/membrane that is different in bacterial and mammalian cells), we hypothesized that certain type of surface functionalization of CuO NPs may render NPs toxic to bacteria, but still be relatively benign to human cells. Indeed, surface functionalization of metal-based NPs may change the safety profile of NPs (Nel et al. 2009; Kubo et al. 2018). For example, functionalization of NPs with PEG, chitosan or dextran prevented the opsonization of NPs (i.e., adsorption of bio-corona of proteins and other biomolecules onto their surface) and, thus, reduced the uptake of NPs by macrophages and, hence, toxicity (Sheng et al. 2009; Jenkins et al. 2016; Wonder et al. 2018). In contrast, compared with NPs functionalized with neutrally (e.g., with PVP) or negatively charged coatings (e.g., citrate), functionalization of NPs with positively charged groups such as polyethylenimine (PEI),

branched PEI or amine group rendered NPs that were more toxic to mammalian cells including murine macrophage cell line RAW264.7 (Líbalová et al. 2018), epithelial cells BEAS-2B and human monocytes THP-1 (Li et al. 2014).

While there are many articles on the biological effects of unfunctionalized CuO, the information on differently functionalized CuO NPs is rare (Bondarenko et al. 2013; Juganson et al. 2015). Although there are various protocols available for the synthesis of CuO NPs functionalized with, e.g., peptides, antibodies and oligonucleotides (Tauran et al. 2013), these NPs were mostly intended for bioanalytical applications and thus not tested for their potential toxic effects. Our search in PubMed (performed in December 2019) using the keywords “copper nano\* tox\*” identified in total 215 research articles, and only 8 of these addressed the biological effects of differently functionalized CuO NPs with the focus on the “green” functionalization such as chitosan (Worthington et al. 2013; Vanti et al. 2019), plant latex (Valodkar et al. 2011), albumin (Azizi et al. 2017) and a set of coatings including citrate, sodium ascorbate, polyvinylpyrrolidone, polyethylenimine (Líbalová et al. 2018) and, similarly to this study, carboxyl, PEG and ammonium (Meissner et al. 2019; Ilves et al. 2019). None of the studies compared the antibacterial properties of NPs with their safety to human cells in vitro or in vivo.

This study is the first report on the comparison of the antimicrobial efficiency and safety toward human cells of CuO NPs with different surface functionalizations: CuO-NH<sub>4</sub><sup>+</sup>, CuO-COOH, CuO-PEG and unfunctionalized CuO NPs as well as CuSO<sub>4</sub> as an ionic control. THP-1-derived macrophages were used as a model for immunotoxicity, HACAT keratinocytes in vitro as the model for human skin cells and *Escherichia coli* as model bacteria. We chose Gram-negative bacterium *E. coli* as there is a warning rise of multidrug resistance in Gram-negative bacteria becoming a challenge in health care (Exner et al. 2017). To minimize the effects of speciation of copper on test results, the toxicity of Cu compounds to THP-1 cells and bacteria was tested in comparable conditions using RPMI medium supplemented with 10% fetal bovine serum and 24-h Alamar Blue to determine cell viability. In addition, we compared the potential mechanisms of toxicity of studied Cu compounds to different cell types with the focus on reactive oxygen species (ROS), dissolution, cellular internalization of CuO and their ability to induce inflammation in mammalian cells, and revealed the main parameters contributing to toxicity using statistical multivariate analysis.

## Materials and methods

The manuscript does not contain clinical studies or patient data.

## Chemicals

All the purchased chemicals were at least of analytical grade. Dulbecco's phosphate-buffered saline (DPBS, Biog-nost), Alamar Blue (AppliChem),  $\text{CuSO}_4$  (Alfa Aesar), 2',7'-dichlorodihydrofluorescein diacetate ( $\text{H}_2\text{DCF-DA}$ , Life Technologies), phosphate buffered saline (PBS pH = 7.2, Biognost), tryptone (LabM), yeast extract (LabM), agar (LabM) and NaCl (Sigma-Aldrich) were used.

## Nanoparticles

Four types of differently functionalized and unfunctionalized CuO NPs were obtained via the consortium of EU FP7 project NANOSOLUTIONS (<https://nanosolutionsfp7.com/>) as a kind gift from Prof. Bengt Fadeel (Karolinska Institutet, Sweden). CuO NPs were synthesized by PlasmaChem (Germany) by decomposition of  $\text{Cu}_2\text{CO}_3(\text{OH})_2$ , followed by the introduction of the surface groups via treatment with mercaptopropionic acid. CuO NPs were provided as dry powders, and the suspensions were prepared each time freshly before the tests at concentrations 1000–2000 mg compound/l in endotoxin free bi-distilled water (DI water). Ten milliliters of CuO NP suspensions were vortexed and sonicated using probe sonication (Branson 450 Sonifier, USA) for 5 min with acoustic power of 13 W corresponding to the specific energy of  $3.9 \cdot 10^5 \text{ kJ/m}^3$  (Käkinen et al. 2016).

The morphology and primary size of NPs were studied using transmission electron microscope (TEM) Tecnai G2 Spirit BioTwin (FEI) at 120 kV. A drop of a 200 mg/l NP suspension in methanol was deposited onto 200 mesh formvar/carbon coated copper grid (Agar Scientific, UK). Sixty particles were measured from TEM images using ImageJ software to obtain nanoparticle primary size. TEM figure for CuO-PEG was provided by NANOSOLUTIONS consortium (Fig. S1d).

Fourier transform infrared spectroscopy (FTIR) spectra were measured in the  $1000\text{--}4000 \text{ cm}^{-1}$  range with  $2 \text{ cm}^{-1}$  resolution using Bruker VERTEX 70 spectrometer with an attenuated total reflection (ATR) accessory.

Hydrodynamic size (Dh), polydispersity index (pdi) and zeta potential (Z-potential) of NPs were measured in 100 mg/l suspensions in DI water or cell culture medium using Malvern zetasizer (Zetasizer Nano-ZS, Malvern Instruments, UK).

The endotoxin content in CuO dispersions was assessed using the chromogenic Limulus amoebocyte lysate (LAL) assay (Charles River Endosafe, Charleston, SC) according to the manufacturer's instructions and was below the detection limit of the assay.

The Cu content of the tested Cu compounds was determined using total reflection X-ray fluorescence (TXRF, Picofox S2, Bruker Corporation) from 100 mg/l suspensions.

Briefly, 40  $\mu\text{l}$  of the sample was mixed with 40  $\mu\text{l}$  of the reference element (2 mg/l Ga) and 3  $\mu\text{l}$  of the mixture was pipetted onto quartz sample holder (Analyslide Petri Dish, Pall Corporation). The measurements were done in triplicate in at least two independent experiments.

For the dissolution analysis, 100 mg/l CuO NPs or  $\text{CuSO}_4$  (a recovery control) was incubated in cell culture medium (at  $37^\circ\text{C}$ , 5%  $\text{CO}_2$  and 95% humidity) for 0 h, 30 min or 24 h and centrifuged at  $320,000 \times g$  for 30 min (Bekman Coulter ultracentrifuge). After centrifugation, the supernatants were collected and analyzed by TXRF as described above.

## Human cell lines

The cell lines were obtained from American Type Culture Collection (ATCC) and cultured according to ATCC guidelines. The cells were subcultured up to 20 passages, and the toxicity tests were performed after at least two passages.

The human monocytic leukemia cell line THP-1 (ATCC TIB-202) was grown in Roswell Park Memorial Institute medium with L-glutamine (RPMI-1640, Corning) supplemented with 10% fetal bovine serum (FBS, Corning), 100 mM sodium pyruvate solution (Na-Pyr, Gibco) and 10,000 U/ml penicillin and 10,000  $\mu\text{g/ml}$  streptomycin (PEST, Gibco) that is further referred to as the complete cell culture medium (CCM). THP-1 cells (growing in suspension) were subcultured by adding fresh CCM. Before the assays, THP-1 cells were differentiated into macrophage like cells by culturing them with 100 ng/ml phorbol myristate acetate (PMA, InvivoGen) in CCM. For that, THP-1 cells were seeded into 96-well plates (Corning Falcon) at a density of  $10^5$  cells per well and incubated with 100 ng/ml phorbol myristate acetate (PMA) for 3 days at  $37^\circ\text{C}$  and 5%  $\text{CO}_2$ .

The human HACAT cell line, immortalized keratinocytes (ATCC PCS-200-011), were grown in Dulbecco's modified Eagle's medium with 4.5 g/l glucose, L-glutamine and sodium pyruvate (DMEM, Corning) supplemented with 10% FBS and 1% PEST. Before the tests, cells were seeded into 96-well plates at a density of  $10^4$  cells per well and incubated for 1 day at  $37^\circ\text{C}$ , 5%  $\text{CO}_2$  and 95% humidity. The composition of the test media used is shown in Table S1.

## Bacterial cells

*Escherichia coli* MG1655 (obtained from the *E. coli* genetic stock center, Yale University) and recombinant bioluminescent *E. coli* MC1061 (pSLcueR/pDNpcopAlux) [constructed in our laboratory previously (Ivask et al. 2009)] were stored on agarized Luria–Bertani medium (LB, 1% tryptone, 0.5% yeast extract, 0.5% NaCl, 1.5% agar) and before the toxicity tests cultivated in 3 ml of LB medium at  $37^\circ\text{C}$  with shaking at 200 rpm overnight. In case of recombinant bacteria,

LB was supplemented with 100 µg/l ampicillin and 10 µg/l tetracycline to retain the bioluminescence-encoding plasmid.

### Toxicity assays

The toxicity of Cu compounds to *E. coli* and THP-1 cells was assessed in similar conditions (24-h incubation in CCM medium at 37 °C and using Alamar Blue assay for viability evaluation) with minor differences: (1) PEST was removed from *E. coli* exposure medium; (2) human cells were incubated in humidified conditions (5% CO<sub>2</sub>). Details on the test conditions are summarized in Table S1. All reported concentrations were nominal and EC<sub>50</sub> values were calculated either based on the compound (compound-based concentrations, Figs. 1a and S3, left panel) or on copper (copper-adjusted concentrations, Figs. 1c and S3, right panel) to estimate the contribution of Cu to the toxicity. The concentration of copper in Cu compounds was determined by TXRF as described above.

*E. coli* cells were grown in LB medium overnight, followed by removal of the medium by centrifugation and resuspension of bacterial pellet in CCM without PEST to ~5 × 10<sup>5</sup> colony forming units (CFU/ml). For the toxicity assay, 100 µl of bacterial suspension was exposed to 100 µl of either cell culture medium (control) or 6.25–400 mg/l CuO suspensions/CuSO<sub>4</sub> in CCM in transparent 96-well plates for 24 h at 37 °C. The bacterial viability was estimated using Alamar Blue assay. For that, the exposed cells were washed and Alamar Blue (AppliChem, final concentration of 150 µg/ml) in CCM without PEST was added to the cells for 2 h at 37 °C. After incubation, fluorescence was read by Fluoroscan (Fluoroskan Ascent FL, Thermo LabSystems) with excitation at 530 nm and emission at 590 nm. The metabolic activity (viability) of the exposed cells was expressed in % by comparing their fluorescence with that of untreated cells. The EC<sub>50</sub> values were calculated as described in "Statistical analysis". Tests were performed in five biological experiments in duplicate. To assess possible interference of NPs with assay reagents, NPs with Alamar Blue were also incubated in abiotic conditions (no unspecific reactions were observed).

For the toxicity assay with human cells, the cell culture medium was removed, cells were washed with PBS and exposed to 100 µl of either cell culture medium or Cu compounds in cell culture medium for 24 h at 37 °C and 5% CO<sub>2</sub>. After the exposure, the supernatant was removed, cells were washed once with PBS and incubated with 100 µl of 150 µg/ml Alamar Blue for 2 h at 37 °C and with 5% CO<sub>2</sub>.

### Bioavailability of Cu to bacteria

Quantification of intracellular Cu ions was performed using recombinant biosensor bacteria *E. coli* MC1061 (pSLcueR/

pDNPcopAlux) in which Cu ion-inducible promoter *copA* is genetically coupled to the bioluminescence-encoding genes *luxCDABE* (Ivask et al. 2009). Thus, bioluminescence of this recombinant *E. coli* increases in response to sub-toxic concentrations of intracellular Cu ions in a dose-dependent manner. In the toxic concentration range, the bioluminescence of bacteria gradually decreases.

The overnight bacterial culture was diluted 1:20 into fresh LB medium supplemented with 100 µg/l ampicillin and 10 µg/l tetracycline, grown till OD = 0.5–0.8 and diluted in CCM without PEST to OD = 0.1 corresponding to a final concentration of 10<sup>6</sup> CFU/ml. 100 µl of the appropriate dilution of Cu compounds in CCM without PEST was pipetted into the wells of white 96-well microplates and 100 µl of bacterial culture in CCM without PEST was added. The test plates were incubated at 37 °C for 2 h, and bioluminescence was measured using Orion II plate luminometer (Berthold Detection Systems). Fold increase in bioluminescence in response to Cu compounds was calculated as a function of increased bioluminescence of biosensor in the sample (CuO and CuSO<sub>4</sub> dilutions in CCM without PEST) compared to the background (CCM without PEST).

### Measurement of reactive oxygen species

The ability of CuO NPs and CuSO<sub>4</sub> to generate ROS was measured in abiotic conditions in DI water with H<sub>2</sub>DCFDA as described by Aruoja et al. (2015). 100 µl of 6.25–200 mg/l CuO NPs and CuSO<sub>4</sub> and 100 µl of H<sub>2</sub>DCF were incubated at room temperature (RT) for 60 min. Fluorescence (excitation at 485 nm and emission at 527 nm) was quantified using a microplate fluorometer (Fluoroskan Ascent FL, Thermo LabSystems, Finland). The ability of Cu compounds to induce ROS was expressed in % in relation to the control.

### Chemical analysis of cell-associated Cu

THP-1 monocytes were seeded into 96-well plates (Corning Falcon) at a density of 10<sup>5</sup> cells/well and differentiated with 100 ng/ml PMA for 72 h. Cells were exposed to Cu compounds in CCM at EC<sub>20</sub> concentrations for 24 h (27.3 mg/l for CuO NPs, 22.2 mg/l for CuO-NH<sub>4</sub><sup>+</sup>, 90.6 mg/l for CuO-COOH, 211.4 mg/l for CuO-PEG and 85.4 mg/l for CuSO<sub>4</sub>).

HACAT cells were seeded into 96-well plates at density 10<sup>4</sup> cells/well and allowed to attach for 24 h. The cells were exposed to Cu compounds at EC<sub>20</sub> concentrations (11.6 mg/l for CuO NPs, 14.9 mg/l for CuO-NH<sub>4</sub><sup>+</sup>, 73.7 mg/l for CuO-COOH, 142.0 mg/l for CuO-PEG and 57.6 mg/l for CuSO<sub>4</sub>) for 24 h.

After 24 h exposure, the cells were washed, detached and washed again twice with PBS by centrifugation at 150×g for 5 min. 10 µl cell suspension was mixed with 10 µl trypan

blue and the cell number and cell viability were determined. The supernatant was aspirated and the pellet was lyophilized. The Cu content was quantified with TXRF, normalized on total cell number basis and designated as “cell-associated Cu”, referring to the sum of the following fractions: intracellular Cu and extracellular Cu bound to the cell surface.

### Measurement of TNF- $\alpha$

Differentiated THP-1 cells at density  $10^5$  cells/well were exposed to CuO NPs and CuSO<sub>4</sub> at concentrations from 25 to 400 mg/l in CCM. After 24-h exposure, the supernatants were collected, centrifuged for 10 min at  $10,000\times g$  and stored frozen at  $-80^\circ\text{C}$ . TNF- $\alpha$  was measured on 96-well plates using Enzyme-Linked Immunosorbent Assay (ELISA) kit (Invitrogen 88-7346) according to the manufacturer’s instructions.

### Microscopy

For the automatic photographing, THP-1 cells were differentiated in 24-well plates, exposed to NPs (24-h EC<sub>20</sub> concentrations), washed, stained with Giemsa Stain (Sigma-Aldrich) according to manufacturer’s instructions and visualized using Automated Digital Morphology System CellaVision®. Before the analysis, differentiated THP-1 cells were mixed with human red blood cells to improve the cell recognition by the software.

For the confocal microscopy, THP-1 cells were differentiated on glass coverslips in 12-well plates, stained with  $5\ \mu\text{g}/\text{ml}$  Cell Mask Orange (CMO) cell membrane dye (Invitrogen), fixed with 4% paraformaldehyde (Sigma) and stained with 1:300 diluted DAPI (Sigma). Finally, the coverslips were rinsed and mounted with ProLong® Gold antifade reagent (Life Technologies) for 12–24 h at room temperature in the dark. Cells and NPs were visualized using a confocal microscope Zeiss Duo 510 META with  $63\times$  oil immersion objective 1.4 NA. To set up the reflectance optical configuration, the main beam splitter was set to NT80/20 and the channel was set up for reflectance using the 488 nm laser. CMO was excited with 561 nm laser and DAPI was visualized with 405 nm laser. Z-stacks from the coverslip to the top of the cell were acquired at a step size of 320 nm. For three-dimensional (3D) reconstruction Imaris 6.4.2 software was used.

### Statistical analysis

All tests were performed in at least three individual experiments in duplicate. The EC<sub>50</sub> values were calculated using MS Excel macro Regtox ([https://www.normalesup.org/~vindimian/en\\_download.html](https://www.normalesup.org/~vindimian/en_download.html)) and the results were

presented with 95% confidence intervals. The statistical significance between the EC<sub>50</sub> values was estimated assuming equal variances at  $p < 0.05$  with one-way ANOVA followed by Tukey’s HSD post hoc test. Heatmap and dendrogram were done with R Language and Environment for Statistical Computing (<https://www.R-project.org>). Heatmaps and dendrograms were generated using heatmap function (incorporating Euclidean distance and complete method).

Principal component analysis (PCA) was used to obtain a multiparametric estimation of the variables that contributed to the toxicity (average compound-based EC<sub>50</sub> values) of CuO NPs. Scores of the first two PCs which accounted for 87–95% of the variance were used to generate the biplots. For visualization, data were scaled by dividing the (centered) columns of  $x$  by their standard deviations.

## Results

### Physico-chemical characterization of CuO NPs

The primary sizes of CuO NPs were measured by transmission electron microscopy (TEM, Fig. S1) and the presence of the different organic functional groups on the functionalized NPs was verified with Fourier transform infrared spectroscopy (FTIR) (Fig. S2). CuO NPs mostly formed agglomerates of a few hundred nanometers with the primary particle sizes of  $15.9 \pm 5.2$ ,  $6.9 \pm 2.2$ ,  $9.2 \pm 2.5$  and  $12.1 \pm 3.2$  nm for the CuO, CuO–COOH, CuO–NH<sub>4</sub><sup>+</sup> and CuO–PEG NPs, respectively (Fig. S1; Table 1).

FTIR spectra proved the presence of organic functional groups as absorption peaks characteristic to O–H, C–H, C=O, N–H and C–O vibrational bands were identified in the measured spectra (Fig. S2).

Hydrodynamic size (Dh) of NPs was in the range of 204 nm (CuO NPs) to 1268 nm (CuO-PEG) (Table 1). The polydispersity index (pdi) values did not exceed 0.35 in the DI and increased to 0.45–0.88 in the cell culture medium, confirming the tendency of NPs, especially CuO–PEG (pdi = 0.88), to agglomerate in the test medium. The Z-potential reflecting the particle surface charge in DI water was positive for CuO and CuO–NH<sub>4</sub><sup>+</sup> and negative for CuO–COOH and CuO–PEG. In the cell culture medium, the Z-potential of NPs was negative for all the particles ranging from  $-8.9$  mV (CuO–NH<sub>4</sub><sup>+</sup>) to  $-10.8$  mV (CuO), most likely due to the adsorption of the serum proteins (the Z-potential of the test medium alone was  $-10.4$  mV) as suggested previously by Ivask et al. (2015) or the interference of the serum proteins [such as negatively charged bovine serum albumin tending to adsorb to the particles (Jachimska and Pajor 2012)] with the measurement. Measured total Cu content was the highest for CuO (76.8%), followed by CuO–NH<sub>4</sub><sup>+</sup> (46.2%), CuO–COOH (33.6%)



and CuO–PEG (11.7%). The measured total Cu content in CuSO<sub>4</sub> was 37.1 ± 4.5%, in agreement with the calculated amount of Cu in CuSO<sub>4</sub> (39.8%), and Cu content in CuO was 76.8 ± 5.7% close to the calculated amount of Cu in CuO (79.9%) (Table 1).

**Toxicity of Cu compounds**

The loss of viability of the cells after 24-h exposure to different copper compounds is shown in Fig. S3. Figure 1 depicts the average 24-h EC<sub>50</sub> values calculated on the basis of the dose–response curves from Fig. S3 (left panel) and dendrogram showing the clustering of these EC<sub>50</sub> values (Fig. 1b). While the 24-h EC<sub>50</sub> values of CuSO<sub>4</sub> were very similar for all cell types, the toxicity of NPs to different cells significantly varied (Fig. 1a). Namely, unfunctionalized CuO and CuO–NH<sub>4</sub><sup>+</sup> were more toxic to human cells in vitro than to bacteria, whereas negatively charged NPs—CuO–COOH and CuO–PEG—were significantly more toxic to bacteria compared to human cells. Thus, clearly, by varying the NP

surface functionalization and also Cu form (soluble salt vs NPs), it was possible to tune the toxicity of Cu compounds to bacteria vs to human cells.

Dendrogram analysis of the average 24-h EC<sub>50</sub> values pointed out several clusters: most toxic NPs—unfunctionalized CuO and CuO–NH<sub>4</sub><sup>+</sup>—clustered together, whereas CuO and CuSO<sub>4</sub> formed another cluster and the least toxic CuO–PEG NPs a separate cluster (Fig. 1b). Since the most toxic NPs (unfunctionalized CuO and CuO–NH<sub>4</sub><sup>+</sup> NPs) contained the highest % of Cu (Table 1), the 24-h EC<sub>50</sub> values of Cu compounds were re-calculated based on Cu content (from Table 1) and presented in Fig. 1c. Cu-adjusted EC<sub>50</sub> of CuSO<sub>4</sub> proved to be around 33 mg Cu/l for all cell types. Cu-adjusted EC<sub>50</sub> values of CuO NPs were mostly lower or the same as for CuSO<sub>4</sub> depending on the surface functionalization and cell type showing that not only Cu contributed to the toxicity. Interestingly, Cu-adjusted EC<sub>50</sub> values clustered differently, highlighting that CuO–NH<sub>4</sub><sup>+</sup>, CuO–PEG and CuO–COOH NPs are the most potent antibacterials (Fig. 1d). While CuO–PEG and especially CuO–COOH

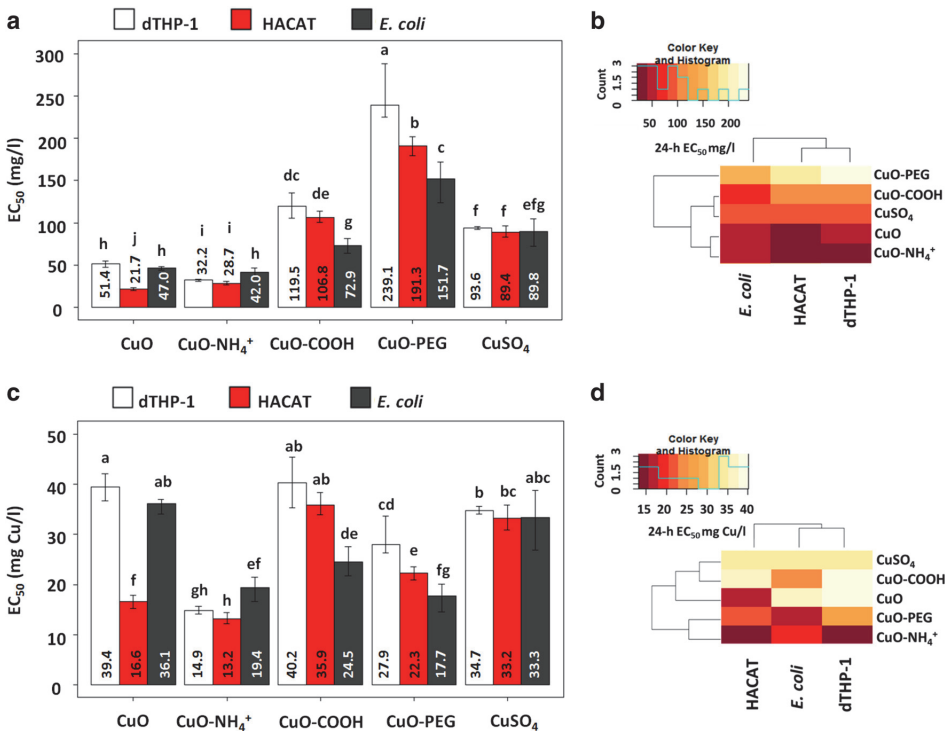


**Fig. 1** Toxicity of Cu compounds to bacteria *Escherichia coli* (*E. coli*), HACAT keratinocytes and differentiated THP-1 cells (dTHP-1). The average compound-based 24-h EC<sub>50</sub> values with 95% confidence intervals mg/l (a) and the clustering of average compound-based 24-h EC<sub>50</sub> (b). The average copper-adjusted 24-h EC<sub>50</sub> values with 95%

confidence intervals mg/l (c) and the clustering of average copper-adjusted 24-h EC<sub>50</sub> (d). Data presented as bars with the same letters are not statistically significant, whereas data presented as bars with different letters are statistically significant

**Table 1** Physico-chemical characteristics of Cu compounds

Cu compounds	Primary size, nm <sup>a</sup>	Hydrodynamic diameter (Dh) in DI water <sup>b</sup> nm (pdi <sup>c</sup> )	Dh in cell culture medium <sup>b</sup> , nm (pdi)	Z-potential in DI water <sup>b</sup> , mV	Z-potential in cell culture medium <sup>b</sup> , mV	Cu content <sup>d</sup> , %
CuO NPs	15.9 ± 5.2	237 ± 31 (0.25)	204 ± 13 (0.45)	27.5 ± 1.8	- 10.8 ± 1.4	76.8 ± 5.7
CuO-NH <sub>4</sub> <sup>+</sup> NPs	6.9 ± 2.2	733 ± 252 (0.24)	936 ± 229 (0.67)	25.8 ± 1.3	- 8.9 ± 0.8	46.2 ± 4.0
CuO-COOH NPs	9.2 ± 2.5	1124 ± 128 (0.35)	303 ± 84 (0.70)	- 12.0 ± 2.2	- 10.2 ± 0.8	33.6 ± 3.2
CuO-PEG NPs	12.1 ± 3.2	1244 ± 254 (0.35)	1268 ± 315 (0.88)	- 21.9 ± 3.3	- 10.0 ± 1.8	11.7 ± 1.0
CuSO <sub>4</sub>	NA	NA	NA	NA	NA	37.1 ± 4.5

NA not applicable

<sup>a</sup>Measured by transmission electron microscopy (TEM)

<sup>b</sup>Measured by Malvern Zetasizer from 100 mg/l suspensions

<sup>c</sup>Polydispersity index

<sup>d</sup>Analyzed by TXRF from 100 mg/l suspensions

NPs were less toxic to human cells compared to bacteria, CuO-NH<sub>4</sub><sup>+</sup> NPs were more toxic to mammalian cells. In addition, the Cu-based EC<sub>50</sub> values of CuO-NH<sub>4</sub><sup>+</sup> NPs were about twice lower than that of CuSO<sub>4</sub> (Fig. 1c), suggesting that the toxicity of CuO-NH<sub>4</sub><sup>+</sup> NPs cannot be solely explained by Cu content and additional toxicity mechanisms played a role in its toxicity. Thus, we determined the ability of Cu compounds to induce ROS in abiotic conditions and inflammation in mammalian cells and studied in detail their interactions with bacterial and human cells in vitro with the focus on NP localization and uptake mechanisms.

## Mechanisms of toxicity of Cu compounds

### Bioavailability and dissolution of Cu compounds

Recombinant bioluminescent *E. coli* increasing the bioluminescence in response to bioavailable Cu ions was applied to determine the role of internalized Cu ions in the antibacterial potency of Cu compounds (Fig. 2a). In parallel, chemical analysis was done to reveal dissolution of CuO (Fig. 2b). In the sub-toxic region, Cu compounds acted quite similar on sensor bacteria by increasing the bioluminescence of *E. coli* biosensor in parallel to the increase of the concentration of copper. There was, however, one exception: CuO-NH<sub>4</sub><sup>+</sup> NPs showed toxic properties (decline of luminescence) already at remarkably low concentrations (starting from 5 mg Cu/l), thus demonstrating the antibacterial effect independent of dissolved Cu ions (Fig. 2a). For other NPs, biosensor response was a function of Cu content and NP dissolution, being lowest for CuO (that had the lowest 0.5-h dissolution, 40%, Fig. 2b).

Thus, Cu biosensor suggested that Cu compounds exhibited antibacterial effects through bioavailable ionic Cu with the exception of CuO-NH<sub>4</sub><sup>+</sup> NPs. In contrast, CuO-NH<sub>4</sub><sup>+</sup> NPs were different from all the other Cu compounds by

killing bacteria at remarkably low concentrations, even before the bioluminescence of biosensor was induced by Cu. Thus, we hypothesized that CuO-NH<sub>4</sub><sup>+</sup> exhibits specific partly Cu-independent antibacterial mechanism and studied the toxicity mechanisms of CuO-NH<sub>4</sub><sup>+</sup> and other NPs in more detail.

### Ability of Cu compounds to induce ROS and inflammation

The results of the assay measuring abiotic ROS indicated that CuO-NH<sub>4</sub><sup>+</sup> NPs were very potent inducers of ROS (46-fold induction at concentration 200 mg/l), whereas other NPs were relatively poor ROS inducers (6- to 11-fold). CuSO<sub>4</sub> did not induce ROS at any tested concentration (Fig. 3a). In addition, ELISA test revealed that CuO-NH<sub>4</sub><sup>+</sup> and also CuO NPs were the most potent inducers of TNF-α in differentiated THP-1 cells inducing TNF-α already at 50 mg/l, whereas CuO-COOH and CuSO<sub>4</sub> induced TNF-α production starting from 100 mg/l (Fig. 3b) and CuO-PEG starting from 400 mg/l (data not shown). In general, TNF-α production correlated well with the EC<sub>50</sub> numbers (Fig. 1a) and can be therefore considered as a marker of the cell death (Fink and Cookson 2005).

Using light microscopy, we also noticed extensive vacuolization in the cells exposed to CuO and especially to CuO-NH<sub>4</sub><sup>+</sup> NPs (Fig. 3c). Vacuolization has previously been suggested as a sign of inflammation and cell death (Shubin et al. 2016) and may indicate a distinct mechanism of toxicity of CuO-NH<sub>4</sub><sup>+</sup> NPs also in mammalian cells (macrophages) in vitro.

### Measurement of cell-associated Cu from Cu compounds

To reveal the mechanisms of toxicity of Cu compounds, differentiated THP-1 cells and HACAT cells were exposed to

equitoxic (24-h  $EC_{20}$ ) concentrations of Cu compounds for 24 h, washed and analyzed for Cu content. We assumed that Cu content mostly referred to intracellular Cu, but it cannot be excluded that some fraction of CuO NPs or dissolved Cu was tightly bound to cell surface and also detected by our analysis. Thus, the measured fraction was designated as “cell-associated Cu” combining intracellular Cu and CuO NPs and possible cell surface-bound Cu. We hypothesized that (i) if the toxicity of Cu compounds was caused solely by Cu ions, the amount of cell-associated Cu in the cells exposed to equitoxic concentrations of Cu compounds would be equal; (ii) if the toxicity was caused by additional factors (as suggested for  $CuO-NH_4^+$ ), the amount of cell-associated Cu would be lower compared to the other CuO NPs and  $CuSO_4$ . The experiment proved the latter option: there was significantly less Cu in both differentiated THP-1 and HACAT cells exposed to  $CuO-NH_4^+$ , than in case of other exposures (Fig. 4a and Fig. S4). Surprisingly, we observed about five- and eightfold higher amounts of cell-associated Cu in case of  $CuO-COOH$  compared to other NPs in both HACAT and differentiated THP-1 cells, respectively, suggesting that both cell lines had exceptional capacity to tolerate cell-associated Cu in the form of  $CuO-COOH$ . Therefore, we conducted the confocal microscopy study to confirm this result and visualize the cellular localization of CuO NPs.

### Cellular localization of Cu compounds in mammalian cells

Differentiated THP-1 cells were exposed to equitoxic (24-h  $EC_{20}$ ) concentrations of Cu compounds for 24 h as in previous experiments and visualized with confocal microscopy (Figs. 4b, S5). The reflective mode of the microscope was optimized to visualize CuO NPs. However, some reflectance

was seen also in a control group (shown in Fig. S5) that might be the dense inclusions of early lysosomes typical for macrophages (Douglas and Tuluc 2010). By combining Z-stacks into three-dimensional image, we observed that significantly more of  $CuO-COOH$  NPs were associated with cells compared to other NPs (Fig. 4b). Furthermore, confocal microscopy images indicated that most of the  $CuO-COOH$  NPs localized inside the cells (Supplementary video 1). Thus, the tolerance of THP-1 macrophages to internal Cu was exceptionally high for  $CuO-COOH$  NPs and low for  $CuO-NH_4^+$  NPs. Interestingly, a similar phenomenon was previously shown for differently functionalized polystyrene NPs: the uptake of COOH-functionalized NPs by human monocyte-derived macrophages as well THP-1 monocytes was significantly higher than the uptake of polystyrene- $NH_2$  NPs (Lunov et al. 2011a), but despite that polystyrene- $NH_2$  NPs were toxic to the macrophages after 72-h exposure, while polystyrene- $COOH$  NPs were not toxic (Lunov et al. 2011b).

### Multivariate analysis for CuO

Finally, multivariate analysis was performed to evaluate the variability of different properties of CuO NPs and, thus, to estimate their contribution to the net toxicity. For this, toxicity data (Fig. 1a) and physico-chemical characterization data (Table 1, Figs. 1, 3) were fitted into scores plot that comprises the eigenvectors. The principal component analysis (PCA) was applied resulting in NP positions according to their variability (Fig. 5).

Since arrows indicated the direction of the increase of the values, 24-h  $EC_{50}$  vector denoted the direction of lower toxicity (increasing  $EC_{50}$  value) that was the most characteristic for  $CuO-COOH$  and  $CuO-PEG$  (Fig. 5a–c). To estimate

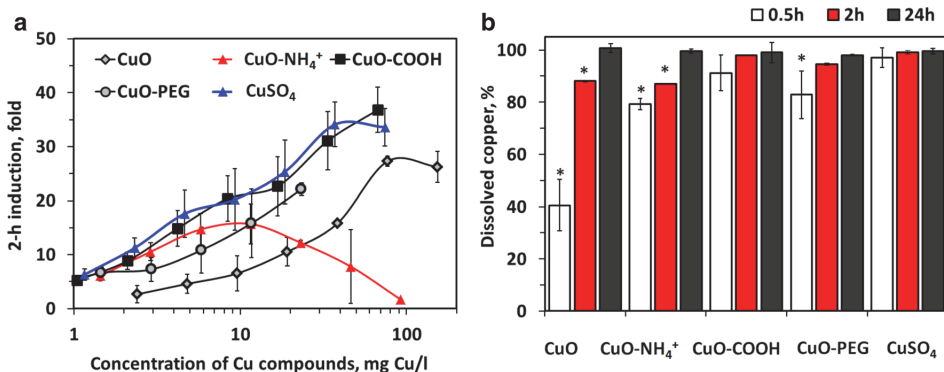


**Fig. 2** Bioavailability and dissolution of Cu compounds. Induction of bioluminescence in *E. coli* biosensor in response to Cu compounds (a) and abiotic dissolution of Cu compounds in cell culture medium

(100 mg/l, 37 °C) after 0.5, 2 and 24-h incubation with standard deviations (b). Asterisks designate the statistically significant difference ( $p < 0.05$ ) compared to the highest value in the group

the contribution of different physico-chemical parameters to NPs` toxicity, we focused on the properties localizing in the area as opposed to the  $EC_{50}$  value vector. Figure 5 shows that the properties contributing to increased toxic effects of unfunctionalized CuO and  $CuO-NH_4^+$  NPs were more positive zeta-potential, higher Cu content, higher 24-h dissolution, ability to produce more abiotic ROS and in case of THP-1 cells also higher production of  $TNF-\alpha$ . Importantly, the localization and the direction of the eigenvectors on the plot were strictly similar in case of mammalian cells (Fig. 5a, b) and bacteria (Fig. 5c), suggesting that the toxicity of CuO NPs to different cell types is influenced by the same variables.

## Discussion

Antibacterial metal-based NPs such as Ag, ZnO and CuO are usually purposely designed to inhibit the undesired growth of bacteria and are widely applied in medical and commercial products. However, it was shown that the toxicity range of CuO and Ag NPs to bacterial and mammalian cells in vitro may overlap, indicating the potential hazard of these NPs to human cells (Greulich et al. 2012; Bondarenko et al. 2013). In our comprehensive review on the toxicity of

Ag, ZnO and CuO NPs to different organisms, we showed that among all studied NPs, CuO NPs had clear “particle-specific” toxic effect, i.e., NPs were more toxic than the Cu ions (on basis of Cu concentration) (Bondarenko et al. 2013). Among all organisms, this effect was only evident for mammalian cells in vitro and yeast cells.

That brought us to the current study: to test new surface functionalizations that would possibly render CuO NPs less toxic to mammalian cells than to bacterial cells. Despite wide commercial use and toxicity of CuO NPs, there were no attempts to identify the surface functionalizations of NPs that would decrease the cytotoxicity of NPs to human cells without compromising antibacterial functions.

In the current study, we compared the toxicity and revealed the mechanisms of toxicity of unfunctionalized CuO NPs,  $CuO-COOH$ ,  $CuO-NH_4^+$ ,  $CuO-PEG$  and  $CuSO_4$  to bacteria *Escherichia coli* and to human cells: HACAT keratinocytes and macrophages differentiated from THP-1 monocytes in vitro. Our main aim was to identify the NP surface functionalizations that would improve the safety profile of CuO NPs to mammalian cells in vitro, while retaining sufficient antibacterial activity. We showed that the effect of the surface functionalizations of CuO NPs on toxicity is different for bacteria and human cells. Namely, while the toxicity of ionic  $CuSO_4$  was nearly identical to bacterial

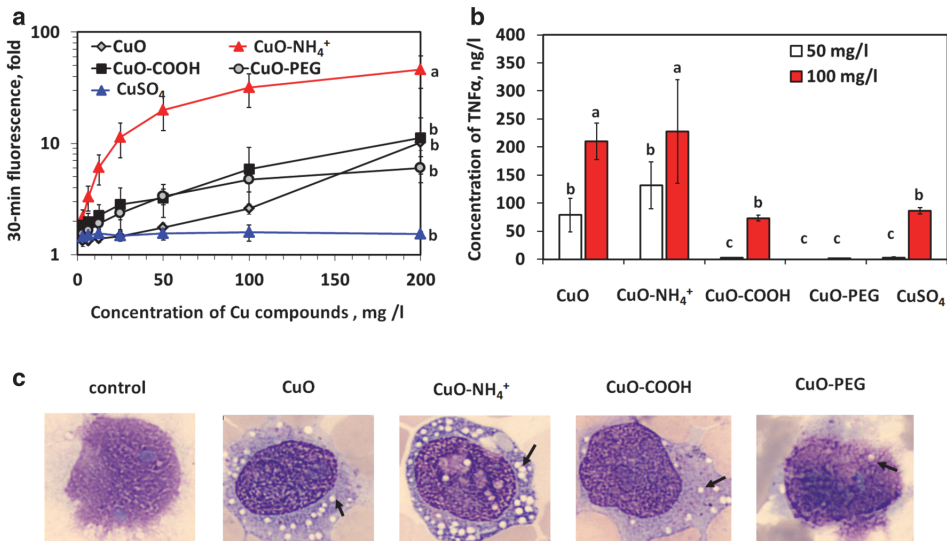


**Fig. 3** Oxidative and inflammatory potential of Cu compounds. Fluorescence of  $H_2DCFA$  reflecting the ability of Cu compounds to produce reactive oxygen species in abiotic conditions in DI water (a). Concentrations of  $TNF-\alpha$  in the supernatants of differentiated THP-1 cells exposed to Cu compounds in cell culture medium for 24 h (b) and representative light microscopy pictures of differentiated THP-1

cells exposed to equitoxic compound-based concentrations (24-h  $EC_{20}$ ) of Cu compounds for 24 h (c). Data presented as bars with the same letters are not statistically significant ( $p > 0.05$ ) according to ANOVA analysis, whereas data presented as bars with different letters are statistically significant ( $p < 0.05$ ). Arrows indicate localisation of the vacuoles

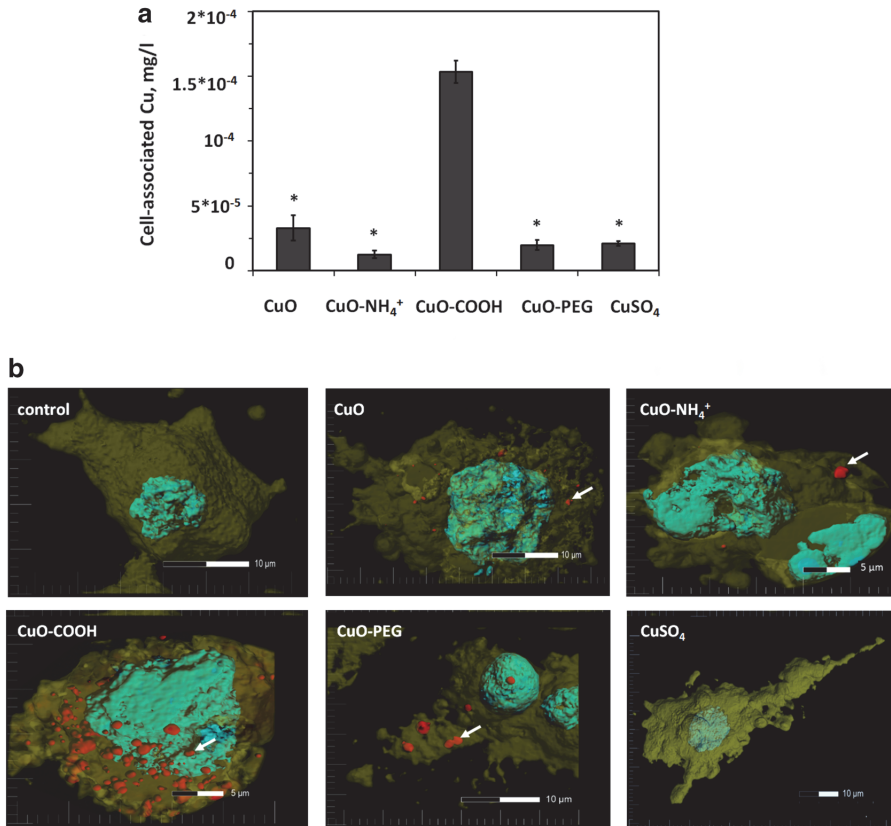


**Fig. 4** Interaction of Cu compounds with THP-1 cells. Concentration of copper associated with differentiated THP-1 cells after 24-h exposure to the equitoxic ( $EC_{20}$ ) concentrations of CuO NPs and CuSO<sub>4</sub> (**a**). Asterisks show the statistically different values ( $p < 0.001$ ). Representative confocal microscopy images of differentiated THP-1 macrophages exposed to equitoxic concentrations (24-h  $EC_{20}$ ) of Cu com-

pounds for 24 h (**b**). Cell membranes were stained with Cell Mask Orange (yellow) and cell nucleus with DAPI (blue). Nanoparticles were visualized in red using reflective mode of the microscope. The arrows indicate the cellular localisation of the CuO NPs (color figure online)

and human cells, CuO–COOH and CuO–PEG were significantly more toxic to bacteria than to human cells in vitro. In contrast, CuO–NH<sub>4</sub><sup>+</sup> was more toxic to human cells than to bacterial cells.

The effects of positively vs negatively charged nanomaterials to mammalian cells in vitro was previously addressed using, e.g., polystyrene NPs and carbon nanotubes. For example, it was shown that polystyrene–NH<sub>2</sub> induced toxicity, lysosomal leakage and inflammasome activation and IL-1 $\beta$  production in primary human monocyte-derived macrophages (Loos et al. 2014), while polystyrene–COOH NPs were not toxic to the macrophages (Lunov et al. 2011b). In another study, carbon nanotubes functionalized with negatively charged COOH and PEG groups decreased the production of pro-fibrogenic

cytokines and growth factors in human cell lines BEAS-2B and THP-1 compared to carbon nanotubes functionalized with NH<sub>2</sub> or PEI (Li et al. 2014). In a recent study, it was shown that pristine, carboxylated and methylaminated, but not PEGylated, NPs worsened the pulmonary effects of CuO NPs in allergic airway inflammation mice model (Ilves et al. 2019). All these results are in line with our findings, showing that NH<sub>4</sub><sup>+</sup> functionalization renders CuO NPs that are especially toxic to human cells. Interestingly, from the studied NPs, CuO–NH<sub>4</sub><sup>+</sup>-functionalized NPs were also the most toxic to bacteria, indicating additional universal mechanisms of toxicity unrelated to the active NP uptake, lysosomal damage and inflammation (that are not existing in bacteria). Most probably, unspecific toxicity component of CuO–NH<sub>4</sub><sup>+</sup> was mediated via

ROS (Fig. 3a) and binding to the cell surface (Fig. 4). Surprisingly, the most common unfunctionalized CuO NPs were almost as toxic as CuO–NH<sub>4</sub><sup>+</sup> NPs to human cells in vitro (Figs. 1, 5a,b), especially for HACAT cells (24-h EC<sub>50</sub> = 21.7 mg/l, the lowest toxicity value obtained in this study). It was previously demonstrated that 24-h EC<sub>50</sub> of unfunctionalized CuO NPs to HACAT was around 30 mg/l (MTT reduction assay), and that CuO induced ROS, oxidative stress, DNA damage and apoptosis in HACAT cells (Alarifi et al. 2013). In our study, CuO induced ROS tenfold in abiotic conditions, but at irrelevantly high concentration (200 mg/l, Fig. 3a). Furthermore, CuO–NH<sub>4</sub><sup>+</sup> induced significantly more ROS, but was less toxic to HACAT than unfunctionalized CuO, suggesting that ROS-related mechanism was most likely not the primary mechanism of toxicity of unfunctionalized CuO to HACAT.

Our multivariate analysis of the properties contributing to the toxicity of Cu compounds revealed very similar patterns for mammalian cells in vitro and bacteria (Fig. 5). Zeta-potential, Cu content, dissolution and ability to induce ROS were the most significant parameters defining toxicity to all cell types, suggesting that the toxicity mechanisms of CuO NPs to bacterial and mammalian cells are largely similar. Thus, in addition to the surface functionalization (that can modulate the specificity of CuO NPs to some extent as shown in this study), attention should be paid to the specific targeting of bacterial cells using bacterial cell wall components-binding peptides, antibiotics or their combinations with NPs to achieve more specificity and enlarged therapeutic window.

Summarizing, CuO–COOH and CuO–PEG NPs can be considered as promising antibacterials to be used in biomedical applications, since they were significantly more toxic to bacteria than to human cells in vitro. It is well known that functionalization of NPs with PEG prevents the adsorption of proteins and, thus, the uptake of NPs by macrophages (Nguyen and Lee 2017) that most likely explains the reduced toxicity of CuO–PEG NPs to mammalian cells in our study. The reason why mammalian cells were able to tolerate high intracellular concentration of CuO–COOH NPs remains to be addressed. We speculate that COOH functionalization guides the NPs to the specific receptors and non-inflammatory pathway, since it is known that NP interactions with the cell receptors impact their cellular localization, inflammatory properties and toxicity (Dobrovolskaia and McNeil 2007; Xia et al. 2008).

## Conclusions

Here, we report the benefits of the surface functionalization of CuO with carboxyl- or polyethylene glycol compared to unfunctionalized and ammonium-functionalized CuO NPs. Specifically, we showed that CuO–NH<sub>4</sub><sup>+</sup> NPs were

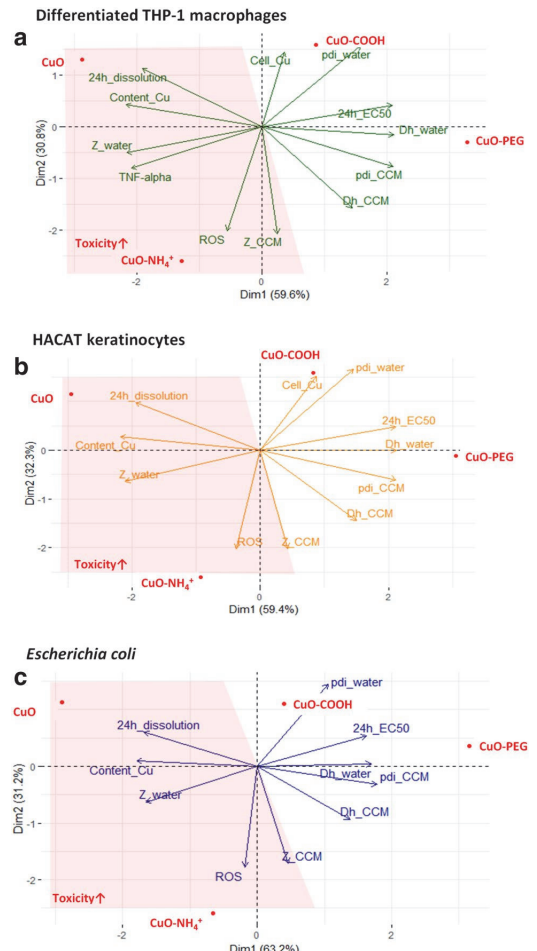


**Fig. 5** Properties contributing to toxicity of CuO compounds. Multivariate analysis of properties contributing to the variability of the toxicity of CuO, CuO–NH<sub>4</sub><sup>+</sup>, CuO–COOH and CuO–PEG NPs to differentiated THP-1 macrophages (a), *E. coli* (b) and HACAT keratinocytes (c). *Z*<sub>water</sub> surface charge in distilled (DI) water, *Z*<sub>CCM</sub> surface charge in cell culture medium, *Cell*<sub>Cu</sub> cell-associated Cu, *Dh*<sub>water</sub> hydrodynamic size in DI water, *Dh*<sub>CCM</sub> hydrodynamic size in cell culture medium, *pdi*<sub>CCM</sub> *pdi* in cell culture medium, *pdi*<sub>water</sub> *pdi* in water, *ROS* abiotic reactive oxygen species, *Content*<sub>Cu</sub> copper content. More toxic compounds are highlighted in the red area (color figure online)

significantly more toxic to human cells in vitro than to *E. coli* cells, probably because of their ability to induce inflammation (TNF- $\alpha$ ) in human cells and ROS. The best therapeutic window was observed for CuO–COOH and CuO–PEG that can be recommended as antimicrobials.

Summarizing, we showed that the antibacterial potency vs safety profile of CuO NPs can be tuned with the surface

functionalizations, and the effect of the surface functionalizations is different for bacteria and human cells. This knowledge can be used for the synthesis of more efficient and safer antimicrobials.

**Acknowledgements** This work was supported by the Estonian Research Council grants PUT1015, IUT23-5 and by European Regional Development Fund projects TK134, IMPAKT 2014-2020.4.01.16-0041 and NAMUR+2014-2020.4.01.16-0123. Olesja Bondarenko and Anna-Liisa Kubo were also supported by Graduate School in Clinical Medicine, receiving funding from the European Regional Development Fund under program ASTRA 2014-2020.4.01.16-0032. Dr. Carsten Jost, Dr. Alexei Antipov (PlasmaChem) and Prof. Bengt Fadeel (Karolinska Institutet, Sweden) are acknowledged for copper oxide nanoparticles, Dr. Aljona Lukjanova and Dr. Valeriy Verchenko (National Institute of Chemical Physics and Biophysics, Estonia) for the technical help with microscopy and consultations in material characterization, respectively; Dr. Taavi Päll (University of Tartu, Estonia) and Dr. Pekka Kohonen (Karolinska Institutet, Sweden) for the feedback on the multivariate analysis and Oleg Barotov (West Tallinn Central Hospital, Estonia) for the photographs of THP-1 cells with the CellaVision.

**Author contributions** AL participated in planning, performed most of the experimental work, analyzed the data, prepared most of the figures and participated in writing, GV participated in planning, conducted experiments with mammalian cells and participated in writing, HV performed TXRF analysis and participated in writing, JK performed confocal microscopy and participated in writing, VT participated in writing, MV and VK performed and interpreted TEM and FTIR, AK participated in planning and refining of the writing, OB initiated and planned the study, performed microbiology experiments, wrote the draft and refined the manuscript. All authors approved the submitted version of the manuscript.

## Compliance with ethical standards

**Conflict of interest** The authors declare no competing interests.

**Open Access** This article is licensed under a Creative Commons Attribution 4.0 International License, which permits use, sharing, adaptation, distribution and reproduction in any medium or format, as long as you give appropriate credit to the original author(s) and the source, provide a link to the Creative Commons licence, and indicate if changes were made. The images or other third party material in this article are included in the article's Creative Commons licence, unless indicated otherwise in a credit line to the material. If material is not included in the article's Creative Commons licence and your intended use is not permitted by statutory regulation or exceeds the permitted use, you will need to obtain permission directly from the copyright holder. To view a copy of this licence, visit <http://creativecommons.org/licenses/by/4.0/>.

## References

- Alarifi S, Ali D, Verma A et al (2013) Cytotoxicity and genotoxicity of copper oxide nanoparticles in human skin keratinocytes cells. *Int J Toxicol* 32:296–307. <https://doi.org/10.1177/1091581813487563>
- Aruoja V, Pokhrel S, Sihtmäe M et al (2015) Toxicity of 12 metal-based nanoparticles to algae, bacteria and protozoa. *Environ Sci Nano* 2:630–644. <https://doi.org/10.1039/c5en00057b>
- Azizi M, Ghourchian H, Yazdian F et al (2017) Cytotoxic effect of albumin coated copper nanoparticle on human breast cancer cells of MDA-MB 231. *PLoS ONE* 12:1–21. <https://doi.org/10.1371/journal.pone.0188639>
- Bastos CAP, Faria N, Ivask A et al (2018) Ligand-doped copper oxo-hydroxide nanoparticles are effective antimicrobials. *Nanoscale Res Lett* 13:2–8. <https://doi.org/10.1186/s11671-018-2520-7>
- Bondarenko O, Juganson K, Ivask A et al (2013) Toxicity of Ag, CuO and ZnO nanoparticles to selected environmentally relevant test organisms and mammalian cells in vitro: a critical review. *Arch Toxicol* 87:1181–1200. <https://doi.org/10.1007/s00204-013-1079-4>
- Bondarenko OM, Heinlaan M, Sihtmäe M et al (2016) Multilaboratory evaluation of 15 bioassays for (eco)toxicity screening and hazard ranking of engineered nanomaterials: FP7 project NANOVALID. *Nanotoxicology* 10:1229–1242. <https://doi.org/10.1080/17435390.2016.1196251>
- Borkow G, Gabbay J, Dardik R et al (2010) Molecular mechanisms of enhanced wound healing by copper oxide-impregnated dressings. *Wound Repair Regen* 18:266–275. <https://doi.org/10.1111/j.1524-475X.2010.00573.x>
- Brewer GJ (2010) Copper toxicity in the general population. *Clin Neurophysiol* 121:459–460. <https://doi.org/10.1166/jbmb.2011.1121>
- Dobrovolskaia MA, McNeil SE (2007) Immunological properties of engineered nanomaterials. *Nat Nanotechnol* 2:469–478. <https://doi.org/10.1038/nnano.2007.223>
- Douglas SD, Tuluc F (2010) Morphology of monocytes and macrophages. In: Lichtman MA, Kipps TJ, Seligsohn U, et al. (eds) *Williams hematology*, 8th edn. The McGraw-Hill Companies, New York
- Exner M, Bhattacharya S, Christiansen B et al (2017) Antibiotic resistance: what is so special about multidrug-resistant Gram-negative bacteria? *GMS Hyg Infect Control* 12:1–24. <https://doi.org/10.3205/dgkh000290>
- Fink SL, Cookson BT (2005) Apoptosis, pyroptosis, and necrosis: mechanistic description of dead and dying eukaryotic cells. *Infect Immun* 73:1907–1916. <https://doi.org/10.1128/IAI.73.4.1907>
- Gajda Meissner Z, Matyja K, Brown D et al (2019) Importance of surface coating on accumulation dynamics and acute toxicity of copper nanomaterials and dissolved copper to daphnia magna. *Environ Toxicol Chem* 00:1–13. <https://doi.org/10.1002/etc.4617>
- Greulich C, Braun D, Peetsch A et al (2012) The toxic effect of silver ions and silver nanoparticles towards bacteria and human cells occurs in the same concentration range. *RSC Adv* 2:6981–6987. <https://doi.org/10.1039/c2ra20684f>
- Ilves M, Kinaret PAS, Ndika J et al (2019) Surface PEGylation suppresses pulmonary effects of CuO in allergen-induced lung inflammation. *Part Fibre Toxicol* 16:1–21. <https://doi.org/10.1186/s12989-019-0309-1>
- Ivask A, Rõlova T, Kahru A (2009) A suite of recombinant luminescent bacterial strains for the quantification of bioavailable heavy metals and toxicity testing. *BMC Biotechnol* 9:1–15. <https://doi.org/10.1186/1472-6750-9-41>
- Ivask A, Titma T, Visnapuu M et al (2015) Toxicity of 11 metal oxide nanoparticles to three mammalian cell types in vitro. *Curr Top Med Chem* 15:1914–1929. <https://doi.org/10.2174/156802661566150506150109>
- Jachimska B, Pajor A (2012) Physico-chemical characterization of bovine serum albumin in solution and as deposited on surfaces. *Bioelectrochemistry* 87:138–146. <https://doi.org/10.1016/j.bioelechem.2011.09.004>
- Jenkins SI, Weinberg D, Al-Shakli AF et al (2016) “Stealth” nanoparticles evade neural immune cells but also evade major brain cell populations: implications for PEG-based neurotherapeutics. *J Control Release* 224:136–145. <https://doi.org/10.1016/j.jconrel.2016.01.013>

- Juganson K, Ivask A, Blinova I et al (2015) NanoE-Tox: new and in-depth database concerning ecotoxicity of nanomaterials. *Beilstein J Nanotechnol* 6:1788–1804. <https://doi.org/10.3762/bjnano.6.183>
- Käkinen A, Kahru A, Nurmsoo H et al (2016) Solubility-driven toxicity of CuO nanoparticles to Caco2 cells and *Escherichia coli*: effect of sonication energy and test environment. *Toxicol Vitro* 36:172–179. <https://doi.org/10.1016/j.tiv.2016.08.004>
- Karlsson HL, Cronholm P, Gustafsson J, Mo L (2008) Copper oxide nanoparticles are highly toxic a comparison between metal oxide nanoparticles and carbon nanotubes—chemical research in toxicology (ACS Publications). *Chem Res Toxicol* 21:1726–1732. <https://doi.org/10.1021/tx800064j>
- Klaassen CD (ed) (2008) Casarett and Doull's Toxicology: the basic science of poisons, 7th edn. McGraw-Hill, New York
- Kubo A-L, Capjak I, Vrček IV et al (2018) Antimicrobial potency of differently coated 10 and 50 nm silver nanoparticles against clinically relevant bacteria *Escherichia coli* and *Staphylococcus aureus*. *Colloids Surfaces B Biointerfaces*. <https://doi.org/10.1016/j.colsurfb.2018.06.027>
- Li R, Wang X, Ji Z et al (2014) The surface charge and cellular processing of covalently functionalized multiwall carbon nanotubes determine pulmonary toxicity. *ACS Nano* 34:283–293. <https://doi.org/10.1016/j.biomaterials.2012.09.057>
- Líbalová H, Costa PM, Olsson M et al (2018) Toxicity of surface-modified copper oxide nanoparticles in a mouse macrophage cell line: interplay of particles, surface coating and particle dissolution. *Chemosphere* 196:482–493. <https://doi.org/10.1016/j.chemosphere.2017.12.182>
- Loos C, Syrovets T, Musyanovych A et al (2014) Amino-functionalized nanoparticles as inhibitors of mTOR and inducers of cell cycle arrest in leukemia cells. *Biomaterials* 35:1944–1953. <https://doi.org/10.1016/j.biomaterials.2013.11.056>
- Lunov O, Syrovets T, Loos C et al (2011a) Differential uptake of functionalized polystyrene nanoparticles by human macrophages and a monocytic cell line. *ACS Nano* 5:1657–1669. <https://doi.org/10.1021/nn2000756>
- Lunov O, Syrovets T, Loos C et al (2011b) Amino-functionalized polystyrene nanoparticles activate the NLRP3 inflammasome in human macrophages. *ACS Nano* 5:9648–9657. <https://doi.org/10.1021/nn203596e>
- Mantecca P, Kasemets K, Deokar A et al (2017) Airborne nanoparticle release and toxicological risk from metal-oxide-coated textiles: toward a multiscale safe-by-design approach. *Environ Sci Technol* 51:9305–9317. <https://doi.org/10.1021/acs.est.7b02390>
- Montes S, Rivera-mancia S, Diaz-ruiz A et al (2014) Review article copper and copper proteins in Parkinson's disease. *Hindawi Publ* 2014:1–15. <https://doi.org/10.1155/2014/147251>
- Murugan K, Choonara YE, Kumar P et al (2017) Cellular internalisation kinetics and cytotoxic properties of statistically designed and optimised neo-geometric copper nanocrystals. *Mater Sci Eng C* 78:376–388. <https://doi.org/10.1016/j.msec.2017.04.087>
- Nel AE, Mädler L, Velegol D et al (2009) Understanding biophysical interactions at the nano-bio interface. *Nat Mater* 8:543–557. <https://doi.org/10.1038/nmat2442>
- Nguyen VH, Lee BJ (2017) Protein corona: a new approach for nanomedicine design. *Int J Nanomed* 12:3137–3151. <https://doi.org/10.2147/IJN.S129300>
- O'Dell BL (1976) Biochemistry of copper. *Med Clin North Am* 60:687–703. [https://doi.org/10.1016/S0025-7125\(16\)31853-3](https://doi.org/10.1016/S0025-7125(16)31853-3)
- Percival SS (1995) Neutropenia caused by copper deficiency: possible mechanisms of action. *Nutr Rev* 53:59–66. <https://doi.org/10.1111/j.1753-4887.1995.tb01503.x>
- Percival SS (1998) Copper and immunity. *Am J Clin Nutr* 67:1064–1068. <https://doi.org/10.1093/ajcn/67.5.1064S>
- Piret JP, Bondarenko OM, Boyles MSP et al (2017) Pan-European inter-laboratory studies on a panel of in vitro cytotoxicity and pro-inflammation assays for nanoparticles. *Arch Toxicol* 91:2315–2330. <https://doi.org/10.1007/s00204-016-1897-2>
- Rosenberg M, Vija H, Kahru A et al (2018) Rapid in situ assessment of Cu-ion mediated effects and antibacterial efficacy of copper surfaces. *Sci Rep* 8:1–12. <https://doi.org/10.1038/s41598-018-26391-8>
- Sheng Y, Liu C, Yuan Y et al (2009) Long-circulating polymeric nanoparticles bearing a combinatorial coating of PEG and water-soluble chitosan. *Biomaterials* 30:2340–2348. <https://doi.org/10.1016/j.biomaterials.2008.12.070>
- Shi M, Chen Z, Farnaghi S et al (2016) Copper-doped mesoporous silica nanospheres, a promising immunomodulatory agent for inducing osteogenesis. *Acta Biomater* 30:334–344. <https://doi.org/10.1016/j.actbio.2015.11.033>
- Shubin AV, Demidyuk IV, Komissarov AA et al (2016) Cytoplasmic vacuolization in cell death and survival. *Oncotarget*. <https://doi.org/10.18632/oncotarget.10150>
- Tauran Y, Brioude A, Coleman AW et al (2013) Molecular recognition by gold, silver and copper nanoparticles. *World J Biol Chem* 4:35. <https://doi.org/10.4331/wjbc.v4.i3.35>
- Teli MD, Sheikh J (2013) Modified bamboo rayon-copper nanoparticle composites as antibacterial textiles. *Int J Biol Macromol* 61:302–307. <https://doi.org/10.1016/j.ijbiomac.2013.07.015>
- Ude VC, Brown DM, Viale L et al (2017) Impact of copper oxide nanomaterials on differentiated and undifferentiated Caco-2 intestinal epithelial cells; assessment of cytotoxicity, barrier integrity, cytokine production and nanomaterial penetration. *Part Fibre Toxicol* 14:1–16. <https://doi.org/10.1186/s12989-017-0211-7>
- Valodkar M, Jadeja RN, Thounaojam MC et al (2011) Biocompatible synthesis of peptide capped copper nanoparticles and their biological effect on tumor cells. *Mater Chem Phys* 128:83–89. <https://doi.org/10.1016/j.matchemphys.2011.02.039>
- Vanti GL, Masaphy S, Kurjogi M et al (2019) Synthesis and application of chitosan-copper nanoparticles on damping off causing plant pathogenic fungi. *Int J Biol Macromol*. <https://doi.org/10.1016/j.ijbiomac.2019.11.179>
- Wonder E, Simón-Gracia L, Scodeller P et al (2018) Competition of charge-mediated and specific binding by peptide-tagged cationic liposome—DNA nanoparticles in vitro and in vivo. *Biomaterials* 166:52–63. <https://doi.org/10.1016/j.biomaterials.2018.02.052>
- Worthington KLS, Adamcakova-Dodd A, Wongrakpanich A et al (2013) Chitosan coating of copper nanoparticles reduces in vitro toxicity and increases inflammation in the lung. *Nanotechnology* 24:1–19. <https://doi.org/10.1088/0957-4484/24/39/395101>
- Xia T, Kovochich M, Liang M et al (2008) Cationic polystyrene nanosphere toxicity depends on cell-specific endocytic and mitochondrial injury pathways. *ACS Nano* 2:85–96. <https://doi.org/10.1021/nn700256c>

**Publisher's Note** Springer Nature remains neutral with regard to jurisdictional claims in published maps and institutional affiliations.





## Appendix 2

### Publication II

**Vasiliev, G.**, Kubo, A.-L., Vija, H., Kahru, A., Bondar, D., Karpichev, Y., & Bondarenko, O. (2023). Synergistic antibacterial effect of copper and silver nanoparticles and their mechanism of action. *Scientific Reports*, 13(1), 9202. <https://doi.org/10.1038/s41598-023-36460-2>





OPEN

# Synergistic antibacterial effect of copper and silver nanoparticles and their mechanism of action

Grigory Vasiliev<sup>1,2,3</sup>, Anna-Liisa Kubo<sup>1,2</sup>, Heiki Vija<sup>1</sup>, Anne Kahru<sup>1,4</sup>, Denys Bondar<sup>3</sup>, Yevgen Karpichev<sup>3</sup> & Olesja Bondarenko<sup>1,2</sup>✉

Bacterial infections are one of the leading causes of death worldwide. In the case of topical bacterial infections such as wound infections, silver (Ag) has historically been one of the most widely used antibacterials. However, scientific publications have demonstrated the adverse effects of silver on human cells, ecotoxicity and insufficient antibacterial effect for the complete elimination of bacterial infections. The use of Ag in the form of nanoparticles (NPs, 1–100 nm) allows to control the release of antibacterial Ag ions but is still not sufficient to eliminate infection and avoid cytotoxicity. In this study, we tested the potency of differently functionalized copper oxide (CuO) NPs to enhance the antibacterial properties of Ag NPs. The antibacterial effect of the mixture of CuO NPs (CuO, CuO–NH<sub>2</sub> and CuO–COOH NPs) with Ag NPs (uncoated and coated) was studied. CuO and Ag NP combinations were more efficient than Cu or Ag (NPs) alone against a wide range of bacteria, including antibiotic-resistant strains such as gram-negative *Escherichia coli* and *Pseudomonas aeruginosa* as well as gram-positive *Staphylococcus aureus*, *Enterococcus faecalis* and *Streptococcus dysgalactiae*. We showed that positively charged CuO NPs enhanced the antibacterial effect of Ag NPs up to 6 times. Notably, compared to the synergy of CuO and Ag NPs, the synergy of respective metal ions was low, suggesting that NP surface is required for the enhanced antibacterial effect. We also studied the mechanisms of synergy and showed that the production of Cu<sup>+</sup> ions, faster dissolution of Ag<sup>+</sup> from Ag NPs and lower binding of Ag<sup>+</sup> by proteins of the incubation media in the presence of Cu<sup>2+</sup> were the main mechanisms of the synergy. In summary, CuO and Ag NP combinations allowed increasing the antibacterial effect up to 6 times. Thus, using CuO and Ag NP combinations enables to retain excellent antibacterial effects due to Ag and synergy and enhances beneficial effects, since Cu is a vital microelement for human cells. Thus, we suggest using combinations of Ag and CuO NPs in antibacterial materials, such as wound care products, to increase the antibacterial effect of Ag, improve safety and prevent and cure topical bacterial infections.

The development of new antibacterials is one of the top priorities flagged by the World Health Organization and the scientific community<sup>1</sup>. A recent meta-analysis showed that there were 4.95 million deaths associated with antibiotic resistance in 2019 and highlighted the need for urgent action to address antibiotic-resistant bacterial infections<sup>2</sup>. Wound infection is one type of chronic infection that may lead to severe consequences such as limb amputation and, when unmanaged, to death. In 15–27% of cases, bacterial wound infection leads to gangrene that requires amputation of the limb<sup>3</sup> demonstrating that current wound infection management strategies are inefficient and improved approaches are needed.

In the field of traditional antibiotics, the combinatory synergistic concept is currently considered as one of the most promising approaches to treat bacterial infections and avoid resistance<sup>4</sup>. The combination of diverse drugs allows to reduce the dose of the drugs and thus, causes fewer side effects compared to monotherapy<sup>5</sup>.

However, antibiotics are administered systemically and their combinations pose unpredictable pharmacokinetics profiles. Topically applied NP combinations would bypass these drawbacks of systemic antibiotics. Thus, we consider the application of synergistic NPs very promising. We hypothesize that due to the different modes of action on bacteria, Cu and Ag NPs have higher antibacterial efficacy when applied together, whereas Cu

<sup>1</sup>Laboratory of Environmental Toxicology, National Institute of Chemical Physics and Biophysics, Akadeemia tee 23, 12618 Tallinn, Estonia. <sup>2</sup>Nanordica Medical OÜ, Vana-Lõuna tn 39a-7, 10134 Tallinn, Harjumaa, Estonia. <sup>3</sup>Department of Chemistry and Biotechnology, Tallinn University of Technology, Akadeemia tee 15, 12618 Tallinn, Estonia. <sup>4</sup>Estonian Academy of Sciences, Kohtu 6, 10130 Tallinn, Estonia. ✉email: olesja.bondarenko@kbfi.ee

enhances the antibacterial efficacy of Ag NPs—the best metal-based antibacterials known so far. In addition, Cu is a microelement and is beneficial for wound healing, stimulating the migration of fibroblasts, promoting collagen synthesis, being essential for angiogenesis, supporting wound healing<sup>6</sup> and bone regeneration<sup>7</sup>. Thus, Cu and Ag NP combinations could have a superior antibacterial effect, improve wound healing and therefore, be a highly beneficial treatment for infected wounds.

Separately, the antibacterial effects of both CuO and Ag NPs are well-studied. Using the keywords “silver nanoparticle\* bacteria\*” or “copper nanoparticle\* bacteria\*”, the search in PubMed<sup>®</sup> performed on 23th March 2023 retrieved 6,558 and 1,113 responses, respectively.

Antibacterial mechanisms of Ag NPs per se are relatively well understood. When in contact with bacteria, Ag NPs localize on bacterial cell wall and oxidize, leading to the concentrated Ag release at the NP-cell interface<sup>8</sup>. We previously showed that damage to the cell wall of gram-negative bacteria by Ag NPs occurs mainly at the plasma membrane, whereas the outer membrane of the bacterial cell was not a target of NPs<sup>9</sup>.

The molecular mechanisms of CuO NPs are less studied. In 2008, Heinlaan et al. showed that the toxicity of CuO NPs ( $EC_{50} = 79$  mg/l) to bacteria *Vibrio fischeri* but also to crustaceans was due to solubilized Cu ions<sup>10</sup>. Notably, despite its excellent antibacterial effects, toxicity of CuO to human cells is lower compared to toxicity of Ag and Ag NPs. Since Cu is a vital microelement, in some cases CuO NPs facilitate positive effects such as improved angiogenesis and wound healing<sup>6</sup>. Detailed antibacterial mechanisms of CuO NPs were further studied using recombinant *E. coli*<sup>11</sup>. In contrast to Ag NPs that did not cause reactive oxygen species (ROS) under abiotic conditions, CuO NPs, especially positively charged ones, induced significant levels of ROS. The surface charge of NPs can be easily modified through surface functionalization and plays a role in the inactivation of bacteria. Since the cell wall of bacteria is negatively charged, positively charged NPs may adhere better to the bacterial cell walls and inactivate bacteria more efficiently.

We have studied antibacterial NPs since 2008 aiming to understand the toxicity mechanisms of NPs and to increase their efficacy and safety<sup>1,8–10,12–14</sup>. Recent articles and our research demonstrated that the antibacterial effect of NPs can be significantly enhanced if metal-based NPs or respective metals are used in combination. However, almost all previously published work focuses on the combined effects of metal ions and not NPs<sup>15–18</sup>. Among various studied combinations of metals (Ag with Cu, Zn, Co, Cd and Ni), the combination of Ag and Cu had the highest synergistic antibacterial effect against both Gram-negative and Gram-positive bacteria<sup>19</sup>. There is a growing interest in the synergy between Cu and Ag manifested in more published articles in the last years. Most of them described the antibacterial properties of nanoalloys of Cu/Ag<sup>20,21</sup> or Cu/Ag with the addition of some other metals for example tungsten<sup>22</sup>. Furthermore, Jang and al. showed perfect antibacterial anti-biofilm and wound healing properties of Cu/Ag/Graphene Oxide composites in infected wound mouse-model<sup>23</sup>. Remarkably, despite these articles describing antibacterial synergy between Cu and Ag, we did not identify any publications systematically studying the synergistic effect of NP combinations or its mechanisms.

In this study we hypothesized that the synergistic antibacterial mechanism of CuO and Ag NPs is driven by their complementary mechanisms of action: Ag NPs damage bacterial cell walls, facilitating the entrance of CuO NPs into bacteria, where CuO NPs disrupt intracellular molecules. More specifically, we first described the synergistic antibacterial effect between Ag and CuO NPs with different functional groups against various bacteria including multiresistant bacteria. Secondly, we conducted a set of tests to understand the mechanisms of the antibacterial synergy of NPs: measured the outer membrane damage, induction of ROS, bioavailability of Cu and Ag ions and charge transformation of Cu ion.

## Results and discussion

**Characterization of nanoparticles.** The characterization of NPs used in this study is shown in Table 1. CuO NPs (CuO) and CuO functionalized with amino groups (CuO–NH<sub>2</sub>) had positive zeta-potential, CuO functionalized with carboxyl groups (CuO–COOH) had negative zeta-potential. All tested Ag NPs had strong

Metal-based NPs or metal salts	Primary size, nm ± standard deviation	Hydrodynamic diameter (Dh) in MQ water, nm (pdi) ± standard deviation	Dh in RPMI cell culture medium, nm (pdi) ± standard deviation	Zeta-potential in MQ water, mV ± standard deviation	Zeta-potential in RPMI cell culture medium, mV ± standard deviation	Metal content, % ± standard deviation	Dissolution after 24 h in MQ water, % ± standard deviation
CuO	15.9 ± 5.2*	237 ± 31 (0.25)*	204 ± 13 (0.45)*	27.5 ± 1.8*	−10.8 ± 1.4*	76.8 ± 5.7*	103 ± 0.5*
CuO–NH <sub>2</sub>	6.9 ± 2.2*	733 ± 252 (0.24)*	936 ± 229 (0.67)*	25.8 ± 1.3*	−8.9 ± 0.8*	46.2 ± 4.0*	99.3 ± 0.8*
CuO–COOH	9.2 ± 2.5*	1124 ± 128 (0.35)*	303 ± 84 (0.70)*	−12.0 ± 2.2*	−10.2 ± 0.8*	33.6 ± 3.2*	98.9 ± 0.5*
CuSO <sub>4</sub>	NA	NA	NA	NA	NA	37.1 ± 4.5*	102.9 ± 0.3*
cAg	12.5 ± 4**	45.88 ± 0.21 (0.261)	61.2 ± 0.47 (0.24)	−56.6 ± 1.91	−9.76 ± 0.84	83.0 ± 9.8	5.24 ± 0.41
nAg	85.7 ± 29.3***	109.4 ± 1.3 (0.447)	156 ± 3.15 (0.403)	−27.7 ± 1.65	−10.49 ± 0.93	71.8 ± 12.0	1.1 ± 0.32
Ag <sub>2</sub> O	23 ± 16.8	81.265 ± 9.04 (0.604)	81.8 ± 24.21 (0.533)	−50.97 ± 4.15	−10.2 ± 0.2	80.1 ± 11.3	39.7 ± 12.9
AgNO <sub>3</sub>	NA	NA	NA	NA	NA	70.2 ± 7.95	96.7 ± 6.3

**Table 1.** Characterization of nanoparticles (NPs) used in the current study. cAg, Coated silver nanoparticles; nAg, Nanosilver; Ag<sub>2</sub>O, Silver oxide; CuO–NH<sub>2</sub>, CuO coated with amino groups; CuO–COOH, CuO coated with carboxyl groups, RPMI, Roswell Park Memorial Institute medium. \*Characterization of NPs has been done previously<sup>13</sup>. \*\*Characterization of NPs has been done previously<sup>14</sup>. \*\*\*Characterization of NPs has been done previously<sup>8</sup>.

negative zeta-potential ranging from  $-56.6$  mV in the case of coated silver nanoparticles (cAg) to  $-27.7$  mV in the case of nanosilver (nAg). In the RPMI cell culture medium (RPMI CCM) the zeta-potential of NPs was negative for all the NPs ranging from  $-8.9$  mV (CuO-NH<sub>2</sub>) to  $-10.8$  mV (CuO), most likely due to the adsorption of the serum proteins (so called “protein corona”, a dynamic camouflage resulting from the adherence of proteins on the surface of NPs) as suggested previously by Ivask et al.<sup>24</sup>. Thus, we assume that protein adsorption at least partly masked the effect of NP charges in all subsequent experiments. The dissolution among Ag NPs was the highest in the case of Ag<sub>2</sub>O and the lowest in the case of nAg.

**Antibacterial synergy between Cu and Ag compounds.** The synergistic effect was first characterized using RPMI cell culture testing medium because it contains blood serum with growth factors, which makes it similar to transudate that appears during tissue infection. An example of the synergistic antibacterial effect of NPs is shown in Fig. 1. To demonstrate the synergistic effect, we used minimum bactericidal concentration (MBC, the lowest tested concentration yielding no visible bacterial growth on agarised growth medium) as a proxy. While 40 mg/l Ag NPs or 400 mg/l CuO NPs were required to irreversibly inactivate *E. coli*, only 5 mg/l Ag NPs + 25 mg/l CuO NPs were needed when used in combination (Fig. 1).

To quantify and compare the synergistic effect between different NPs and among various bacterial strains, we introduced the term “coefficient of antibacterial synergy”, K(AbS), showing the antibacterial efficiency of NPs combinations (mix) compared to the sum of the MBC values of individual NPs and calculated as follows (Eq. 1):

$$K(\text{AbS}) = 1 / \left( \frac{\text{MBC of antibacteria A in mix}}{\text{MBC of antibacteria A alone}} + \frac{\text{MBC of antibacteria B in mix}}{\text{MBC of antibacteria B alone}} \right) \quad (1)$$

Equation (1) shows the calculation of coefficient of antibacterial synergy (K(AbS)) from minimal bactericidal concentrations (MBC).

Similar synergy calculation has been reported previously for metal mixtures by Vaidya et al.<sup>16</sup>. K(AbS) > 1 marks synergy, K(AbS) = 1 marks additive effect or K(AbS) < 1 marks antagonism.

Figure 1 demonstrates that the MBC of the mixture of cAg and CuO NPs is several times lower than the MBC of the components separately. According to formula of  $K(\text{AbS}) = 1 / \left( \frac{50 \text{ mg/L}}{400 \text{ mg/L}} + \frac{2.5 \text{ mg/L}}{40 \text{ mg/L}} \right) = 1 / (1/8 + 1/16) = 5.33$ . Thus, in this example, the antibacterial effect of the mixture was 5.33 times higher than the sum of the antibacterial effects of the components separately.

Calculations for the mixture of 25 mg/L of CuSO<sub>4</sub> + 5 mg/L of cAg result in the same K(AbS). However, K(AbS) is lower in other variations of CuSO<sub>4</sub>/cAg ratios (for example 200 mg/L of CuSO<sub>4</sub> + 1.5 mg/L of cAg

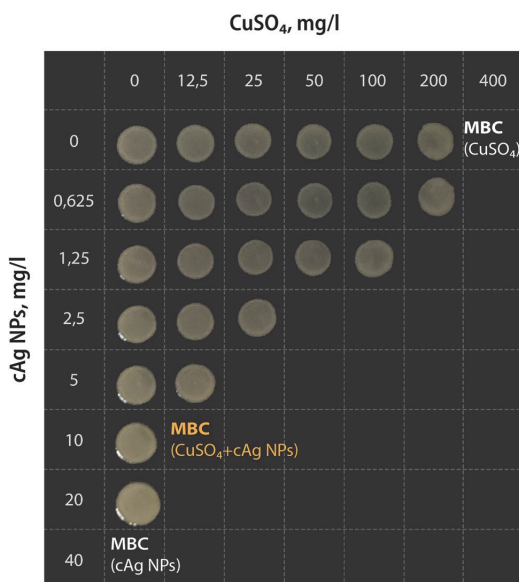


**Figure 1.** The antibacterial synergy between CuSO<sub>4</sub> and cAg. *Escherichia coli* K-12 suspension was incubated with different concentrations of either Ag NPs, CuSO<sub>4</sub> or their combinations in RPMI cell culture medium for 24 h. After incubation 3 µl of the bacteria-NP mixture was pipetted onto agarized broth and minimal bactericidal concentration (MBC, the lowest tested concentration yielding no visible bacterial growth after 24 h incubation at 37 °C in the dark) was determined. The concentrations of cAg and CuSO<sub>4</sub> are shown on the axes. The minimal bactericidal concentration of CuSO<sub>4</sub> and cAg were 400 mg/L and 40 mg/L respectively.

mixture). The difference between K(AbS) depending on Cu/Ag ratio is shown in Supplementary Fig. 1. The highest K(AbS) was mostly observed using the ratio from 1:1 to 12.5:1 Cu/Ag.

**Antibacterial synergy depended on the Cu component.** MBC values of different Cu components alone and in the mixture with cAg in different bacteria are shown in Supplementary Table 1. MBC for different bacteria were similar, excluding *P. aeruginosa*, which was resistant to Cu compounds, despite cAg MBC for *P. aeruginosa* being similar to that of other bacteria.

Calculated K(AbS) for different bacteria is shown in Fig. 2. The evident antibacterial synergistic effect between most of the Cu compounds and Ag NPs was found (Fig. 2, Supplementary Table 1).

Among CuO NPs, the highest K(AbS) with cAg was observed with unfunctionalized CuO and especially CuO-NH<sub>2</sub>, both positively charged. The lowest K(AbS) was observed with negatively charged CuO-COOH, being mostly lower than 2. This suggests that the pristine charge of CuO NPs (reflected in zeta-potential in MQ water) affected antibacterial synergy. Interestingly, the charge of NPs was uniform in cell culture medium due to protein corona (Table 1). This suggests that some pristine surfaces of NPs remained available even after formation of the protein corona in cell culture medium.

The highest K(AbS) was observed for *E. faecalis* and *E. coli* (both K-12 and ESBL). It is interesting to note that *E. coli* ESBL is more resistant to antibiotics compared to *E. coli* K12 and was also more resistant to cAg in this study. However, K(AbS) values were similar in the case of these bacteria. For *E. faecalis*, high K(AbS) was observed for all combinations that may be the result of faster rate of DNA destruction by Cu components compared to Enterobacteria (such as *E. coli*)<sup>25</sup>.

*P. aeruginosa* had the lowest K(AbS) from all the bacteria tested. The reason for that could be the powerful antidrug efflux system and decreased outer membrane permeability<sup>26</sup>.

**Antibacterial synergy depended on the Ag component.** We conducted additional studies with various Ag NPs and AgNO<sub>3</sub> to determine which of them would have stronger antibacterial synergy with the Cu components.

Supplementary Table 2 shows the findings of MBC in *E. coli* K-12 with various Ag and Cu components in the mixture and alone. The calculated K(AbS) are shown in Fig. 3.

When mixed with Cu components, most of Ag NPs showed high K(AbS). In contrast, AgNO<sub>3</sub> did not demonstrate strong antibacterial synergy with Cu components (Fig. 3, Supplementary Table 2). The highest K(AbS) were observed for three mixtures: cAg with CuSO<sub>4</sub> and nAg with CuSO<sub>4</sub>/CuO-NH<sub>2</sub>. The fact that CuSO<sub>4</sub> and CuO-NH<sub>2</sub> were well dissolved (Table 1) and thus, were a source of Cu ions, suggests that Cu ions are required for synergy. The atypical K(AbS) result was in the mix of Ag<sub>2</sub>O and CuSO<sub>4</sub> (no synergy). In contrast to cAg and nAg, Ag<sub>2</sub>O NPs were more oxidized (dissolved). These data strongly indicate that non-oxidized Ag NPs and Cu ions are both required to achieve the strong antibacterial synergistic effect.

**Antibacterial synergy depended on the bacterial medium.** Next, we studied whether the cultivation medium had an effect on antibacterial synergy. MBC of cAg, CuSO<sub>4</sub> and their mixtures in different media

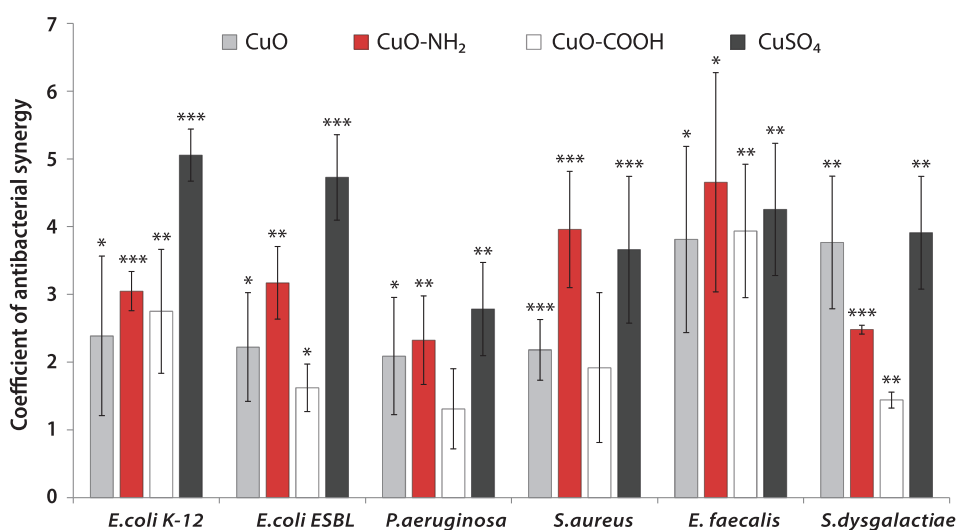


**Figure 2.** Coefficient of antibacterial synergy between cAg and copper components in different bacteria in the RPMI cell culture medium. The mean values with standard deviation are shown. \* $P < 0.05$ ; \*\* $P < 0.01$ ; \*\*\* $P < 0.001$ . cAg, Coated silver nanoparticles; CuO Copper oxide; CuO-NH<sub>2</sub>, Copper oxide coated with amino groups; CuO-COOH, Copper oxide coated with carboxy groups; CuSO<sub>4</sub>, Copper sulphate.

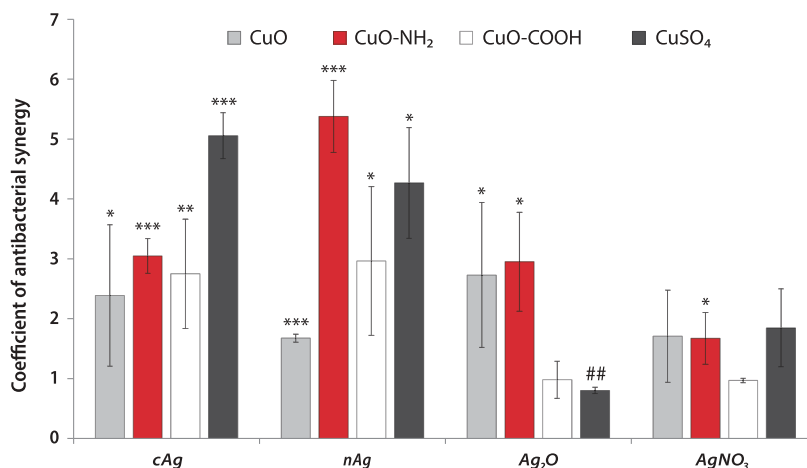


**Figure 3.** Coefficient of antibacterial synergy (K(AbS)) between different Ag and Cu components in RPMI cell culture media with *Escherichia coli* K-12 strain. \* $P < 0.05$ ; \*\* $P < 0.01$ ; \*\*\* $P < 0.001$ ; ## $P < 0.01$  antagonism. Note K(AbS) has been calculated as mean K(AbS) from different experiments, not from mean MBC of components in the mix or alone. The mean values with standard deviation are shown. cAg, Coated silver nanoparticles; nAg, Nanosilver; Ag<sub>2</sub>O, Silver oxide; AgNO<sub>3</sub>, Silver nitrate; CuO, Copper oxide; CuO-NH<sub>2</sub>, Copper oxide coated with amino groups; CuO-COOH, Copper oxide coated with carboxy groups; CuSO<sub>4</sub>, Copper sulphate.

is shown in Supplementary Table 3, and K(AbS) in Fig. 4. In bacterial growth medium with high content of proteins and nutrients, K(AbS) was higher. The highest K(AbS) was in LB medium and the lowest was in MQ (Fig. 4). Importantly, the growth of bacteria was the fastest in LB too (Supplementary Fig. 2). This suggests that synergy is more prominent for cells in the active and dividing phase. Most probably, in the condition of active bacterial growth, the NPs and metal ions released from the NPs have better access to intracellular space for destroying the DNA<sup>27</sup> and damaging proteins. Interestingly, also traditional antibiotics inactivate bacteria less effectively in the non-growing phase, especially *S. aureus*<sup>28</sup>.

### The mechanisms of synergy between CuO and Ag NPs

Several additional tests were performed to understand the mechanisms of antibacterial synergy between Cu and Ag. It was hypothesized that antibacterial synergy is a function of the different modes of action of Cu and Ag. The interaction of beta-lactam antibiotics, which damage the bacterium cell membrane, and aminoglycosides, which inhibit protein synthesis in bacteria, is a well-known example of the classic synergy of antibiotics. The synergy between aminoglycosides and  $\beta$ -lactams has been attributed to  $\beta$ -lactam-mediated membrane damage leading to increased uptake of aminoglycosides<sup>29</sup>.

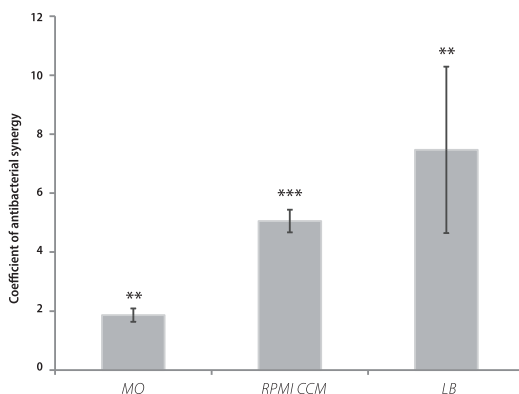


**Figure 4.** Coefficient of antibacterial synergy in different media. Coefficient of antibacterial synergy in the mixture of coated silver nanoparticles and copper sulphate in different growth media against *Escherichia coli* K-12 strain. The mean values with standard deviations are shown. MQ MilliQ water, RPMI.



### The synergy of Cu and Ag components did not depend on bacterial outer membrane damage.

One hypothesis was that one of the components (Cu or Ag NPs) damages the membrane to a larger extent, allowing another component to penetrate into the cell more easily and harm the internal structures. Polymyxin B, which disrupts the outer bacterial membranes of Gram-negative cells<sup>30</sup>, was used as a positive control in this experiment. To verify the hypothesis, the permeability of the outer membrane of two Gram-negative bacteria, *E. coli* K-12 and *Pseudomonas aeruginosa* PAO1, was measured. The results showed that AgNO<sub>3</sub> and cAg damaged the outer membrane of both bacteria (Figs. 5a,b). cAg required more time to damage the membrane compared to AgNO<sub>3</sub>, and *Paeruginosa*'s membrane required more time to be damaged compared to *E. coli*. CuO NPs and CuSO<sub>4</sub> did not cause remarkable membrane damage, especially in *P. aeruginosa*. This data suggests that one of the ways to inactivate cells in the case of Ag compounds is by destroying the outer membranes of the bacteria, whereas Cu compounds act on other cell structures (even high concentrations of Cu that lead to cell death in 24 h do not lead to rapid outer membrane destruction). Membrane destruction by Ag could help Cu to reach these internal cell structures in the case of Ag and Cu mixture. Relying on this data we decided to test this hypothesis by mixing Cu and Ag compounds. A test with a mixture of Cu compounds and cAg was also conducted. cAg damaging action on the membrane was unaffected by the addition of CuSO<sub>4</sub> or Cu-NH<sub>2</sub> (Fig. 5c,d). Tests with the addition of CuO-COOH or CuO to cAg were conducted too, and the additional destructive effect on the membrane was not detected (not shown) as well as with addition of CuSO<sub>4</sub> or Cu-NH<sub>2</sub>. Also, adding of Cu components to Polymyxin B, which rapidly damages the outer membrane, did not enhance the effect of Polymyxin B on the membrane (data not shown). Moreover, the antibacterial synergistic effect between CuSO<sub>4</sub> and Polymyxin B in *E. coli* K-12 in MBC test has not been detected (K(Abs) = 1.054 ± 0.243, data not shown). Thus, we concluded that Ag and Cu act differently on the bacterial outer membrane but their action on the outer membrane is not the main cause of antibacterial synergy.

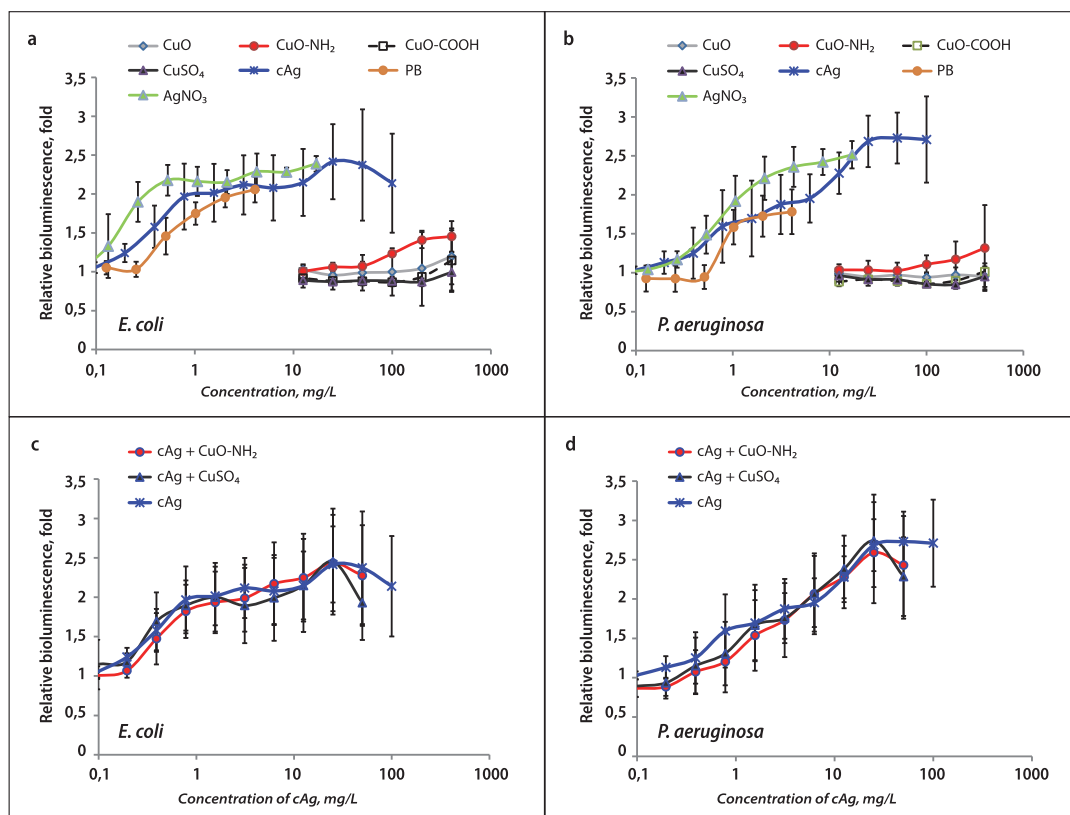


**Figure 5.** Damage of outer bacterial membrane by Ag and Cu compounds or their combination. Increase in fluorescence is indicating the outer membrane damage of *Escherichia coli* (a, c) and *Pseudomonas aeruginosa* (b, d) after 30 min of incubation with the components alone (a, b) and in the mixtures with cAg (c, d). The mean values with standard deviation are shown. cAg, Coated silver nanoparticles; AgNO<sub>3</sub>, Silver nitrate; CuO, Copper oxide; CuO-NH<sub>2</sub>, Copper oxide coated with amino groups; CuO-COOH, Copper oxide coated with carboxy groups; CuSO<sub>4</sub>, Copper sulphate; PB, Polymyxin B.

**The synergy of Cu and Ag components did not depend on reactive oxygen species.** The possibility of Cu ions to redox-cycle between  $\text{Cu}^+/\text{Cu}^{++}$  is known as a Fenton-like reaction, and it can generate reactive oxygen species (ROS) leading to lipid peroxidation, protein oxidation and DNA damage<sup>31</sup>. We next hypothesized that enhanced production of ROS might be the reason of the synergy between Cu and Ag components. Indeed, CuO NPs<sup>13</sup> and Ag NPs<sup>32</sup> were previously shown to induce ROS. We also previously demonstrated that CuO-NH<sub>2</sub> induces more ROS compared to unfunctionalized CuO and CuO-COOH<sup>13</sup>.

ROS generation in this study was determined in both biotic (in presence of bacteria) and abiotic (without bacteria) conditions (Fig. 6). The highest levels of ROS were detected in individual cAg and CuO-NH<sub>2</sub> suspensions (Fig. 6a,b). cAg induced the highest ROS levels in abiotic conditions (Fig. 6a), while CuO-NH<sub>2</sub> in biotic conditions (Fig. 6b). No ROS was detected in the case of CuSO<sub>4</sub> and AgNO<sub>3</sub>.

ROS in the mixture of cAg and Cu components (in a 1:4 ratio) were tested to control the hypothesis that the cAg will produce more ROS after the addition of the CuSO<sub>4</sub> or CuO-NH<sub>2</sub>. Results showed that the addition of CuO-NH<sub>2</sub> or CuSO<sub>4</sub> to cAg did not enhance ROS production in both biotic and abiotic conditions (Fig. 6c,d). Moreover, antagonism has been detected (e.g., lower ROS in cAg + Cu components mixture compared to cAg alone), indicating that ROS was not the cause of antibacterial synergy.

**Silver and copper in a mixture synergistically induced metal efflux genes.** Since the toxicity of metal-based NPs is mostly caused by their ions<sup>10,33</sup>, we decided to measure intracellular Cu and Ag ions. For that, we used bioluminescent biosensor *E. coli* MC1061 pSLcueR/PDNpCopAlux, which produces luciferase in response to intracellular Cu and Ag<sup>34</sup>. In this bacterium, intracellular Ag and Cu ions induce the luminescence of bacteria in a dose-dependent manner.

Since the biosensor bacteria are not selective and detect both Ag and Cu ions, it was not possible to determine intracellular Ag and Cu individually. Therefore, we used the relative values and the coefficient of inductive

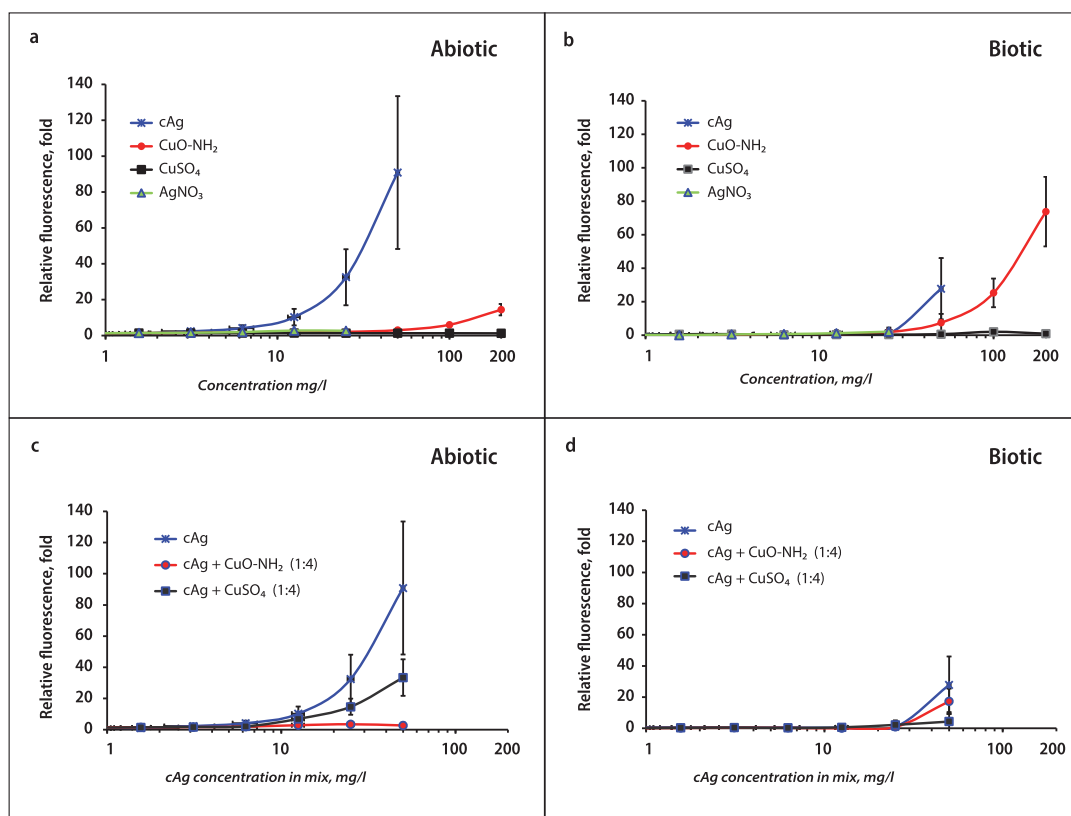


**Figure 6.** Production of reactive oxygen species (ROS) in suspensions. Measurement of induction of ROS in abiotic (a, c) and biotic (b, d) conditions. Measurement of ROS induction was performed after incubation with components alone (a, b) or in the mix of cAg and Cu components in a ratio 1:4 (c, d). cAg, Coated silver nanoparticles; AgNO<sub>3</sub>, Silver nitrate; CuO, Copper oxide; CuO-NH<sub>2</sub>, Copper oxide coated with amino groups; CuSO<sub>4</sub>, Copper sulphate; RFU, Relative fluorescence units.

synergy  $K(\text{InS})$ .  $K(\text{InS})$  was calculated in the same way as the antibacterial synergy coefficient.  $K(\text{InS})$  is the reciprocal of the sum of the ratios of bioluminescence (LC) peak concentrations of components in the mixture to LC peak concentrations alone (Eq. 2).

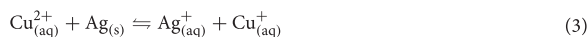
$$K(\text{InS}) = 1 / \left( \frac{\text{LC peak conc of antibacterial A in mix}}{\text{LC peak conc of antibacterial A alone}} + \frac{\text{LC peak conc of antibacterial B in mix}}{\text{LC peak conc of antibacterial B alone}} \right) \quad (2)$$

Equation (2) shows the calculation of coefficient of inductive synergy ( $K(\text{InS})$ ) from bioluminescence (LC) peak concentrations (conc).

At first, the bioluminescence of bacteria with individual Ag and Cu components was measured (Fig. 7a). Afterwards, we mixed Cu components with cAg, and we found a significant shift in the peak of LC to the left (Fig. 7b), but no shift when mixing with  $\text{AgNO}_3$  (Fig. 7c). Peak LC concentrations of components separately and in the mixture are shown in Supplementary Table 4.

The high induction of bioluminescence in response to the intracellular concentration of Cu and Ag ions was observed in the mixtures of Cu components with cAg (Fig. 7b). Lower concentrations of cAg and Cu components in the mixtures were required for response induction. In combination of Cu components with cAg, all mixtures tested showed a high  $K(\text{InS})$ , but not in the mixtures of Cu components and  $\text{AgNO}_3$  (Fig. 8). The fact that  $K(\text{InS})$  was remarkably over 1 in the case of the mixtures of cAg and Cu components revealed that biosensor bacteria sensed higher intracellular concentrations of metal ions in the mixture of cAg and Cu components compared to the sum of the components separately. This was not attributed to the membrane damage caused by cAg and better access of Cu to the inner components of the cells (Fig. 5c,d). It can be assumed that the intracellular concentration of Ag, when combined with  $\text{CuSO}_4$ , was higher due to better dissolution of cAg in the presence of  $\text{Cu}^{2+}$ . Also, the dissolution of  $\text{AgNO}_3$  is very high and cannot be enhanced by Cu ions, which is why we did not observe the synergistic effect between Cu components and  $\text{AgNO}_3$ .

**Better dissolution of Ag NPs in the presence of  $\text{Cu}^{2+}$ .** Next, we investigated Ag NPs dissolution in water and RPMI CCM under two different conditions: with and without the addition of  $\text{CuSO}_4$ . We found a significant difference between the dissolution of Ag NPs with and without  $\text{CuSO}_4$  addition (Fig. 9). In MQ water the difference of nAg and  $\text{Ag}_2\text{O}$  dissolution was more than 4 times and 2 times respectively after  $\text{CuSO}_4$  addition. While in RPMI CCM the difference of nAg dissolution was more than 16 times after  $\text{CuSO}_4$  addition (Fig. 9). We assume that in the mix of nAg and  $\text{CuSO}_4$  in the water there is the effect of improving the dissolution of Ag NPs by the following Eq. 3:



Equation (3) shows the redox reaction between copper and silver components.

In RPMI, the reaction is most probably influenced by organic compounds. For example, the dissolution of  $\text{AgNO}_3$  in serum-containing RPMI CCM might be 100%, but most of the free  $\text{Ag}^+$  ions are complexed by serum proteins<sup>35</sup>. Because Cu ions prevent Ag ions from binding to serum proteins, there was a significant difference in the concentration of free Ag ions in a solution of  $\text{AgNO}_3$  in RPMI CCM with and without  $\text{CuSO}_4$ . Both of these effects are present in a suspension of nAg and  $\text{CuSO}_4$  in RPMI CCM, resulting in a 16-fold increase in the amount of free Ag ions in a  $\text{CuSO}_4$ -containing sample compared to a  $\text{CuSO}_4$ -free sample (Fig. 9). Also, as described previously, already oxidized  $\text{Ag}_2\text{O}$  did not have antibacterial synergy in RPMI CCM with  $\text{CuSO}_4$  and we did not observe better dissolution of  $\text{Ag}_2\text{O}$  in this solvent after the addition of  $\text{CuSO}_4$  (Fig. 9).

**The production of antibacterial  $\text{Cu}^+$  ions in the mixture of Ag NPs and  $\text{Cu}^{2+}$  ions.** As mentioned in the previous section (Eq. 3),  $\text{Cu}^+$  is produced in the mix of Ag NPs and  $\text{Cu}^{2+}$  ions. To prove the presence of  $\text{Cu}^+$  in the mixture, a qualitative chemical reaction was performed as described in the Methods section. In a mixture of components, the qualitative reaction proved the presence of  $\text{Cu}^+$ , but not in nAg suspension,  $\text{AgNO}_3$ , or  $\text{CuSO}_4$  solutions separately. This investigation demonstrated that the equilibrium was established as expected. Also, it has been shown previously that  $\text{Cu}^+$  has a higher antibacterial effect compared to  $\text{Cu}^{2+}$ <sup>36,37</sup>, because of the ability of  $\text{Cu}^+$  to generate OH radicals in the presence of superoxide in a reaction analogous to the Fenton-like reaction<sup>38</sup>. Therefore, the formation of additional  $\text{Cu}^+$  ions in the solution may be among the main factors effecting the antibacterial synergy of the Ag NP/ $\text{Cu}^{2+}$  system.

**Mechanisms of antibacterial synergy of Cu and Ag nanoparticles.** Commonly, synergy occurs when components have a different mechanisms of action. Although the antibacterial synergy between Ag and Cu components (mostly metals and not NPs) has been described before, the mechanisms of synergy have not been studied. Previous publications suggested some mechanisms of antibacterial synergy, whereas authors mainly hypothesized that Ag targets bacterial plasma membrane, while Cu denatures nucleic acids and other internal biomolecules and cell structures<sup>15,16,19,22</sup>. In contrast, in our study, we did not observe a remarkable synergy between Cu components and  $\text{AgNO}_3$  (Fig. 2) or Polymyxin B, which both caused remarkable membrane damage (Fig. 5).

Also, it has been proposed that Cu ions released from CuO alloys inactivate bacteria by boosting ROS production causing DNA damage and lipid peroxidation<sup>16,19,22</sup>. Moreover, Ag NPs anchored on CuO and  $\text{Cu}(\text{OH})_2$  produced ROS in larger amounts compared to CuO<sup>39</sup>, but in this case, ROS production could be enhanced due to  $\text{Cu}(\text{OH})_2$ . We, however, did not observe significant ROS production in  $\text{CuSO}_4$  solution in biotic or abiotic

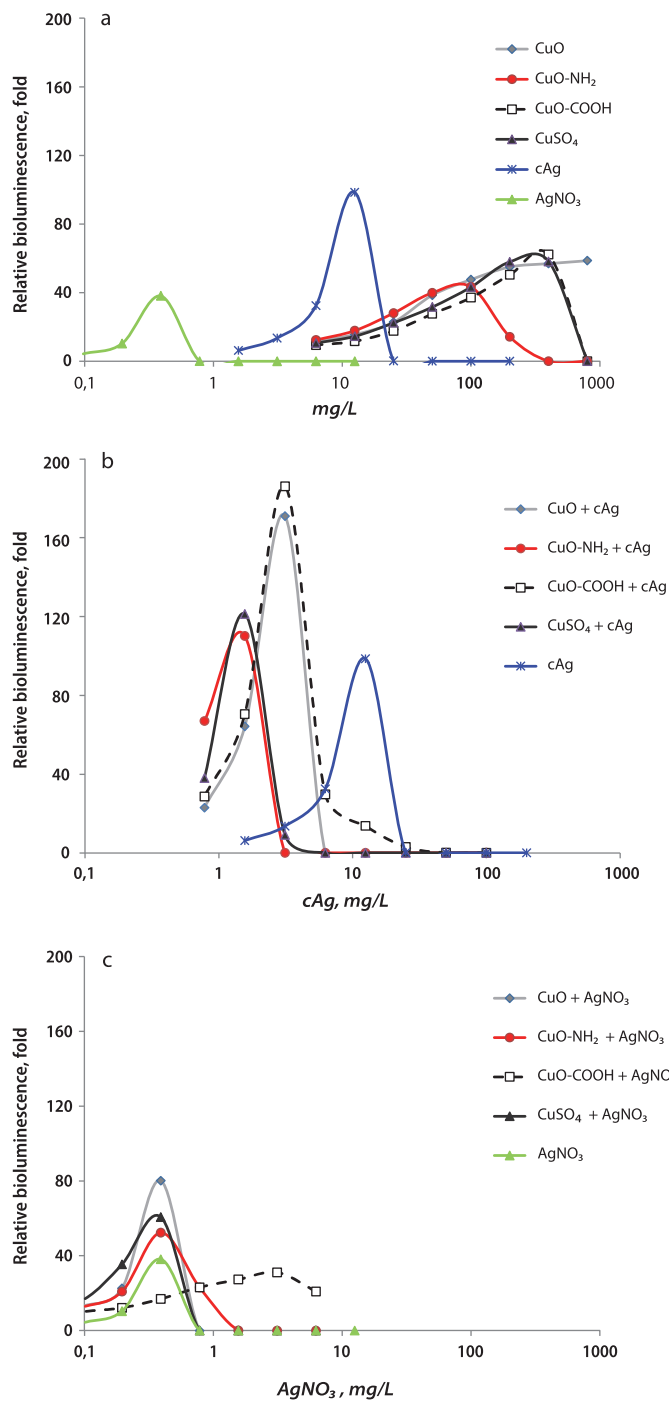


**Figure 7.** Luminescence of biosensor bacteria as reaction to components. Luminescence (LC) of *Escherichia coli* MC1061 pSLcueR/PDNPcopAlux as a reaction to 4 h incubation with components alone (a). The significant shift of peak LC to the left in the mix of copper components with cAg compared to cAg alone (b). No shift of peak LC in the mixture of copper components with AgNO<sub>3</sub> compared to AgNO<sub>3</sub> alone (c). Representative Figures are from 3 independent experiments. cAg, Coated silver nanoparticles; AgNO<sub>3</sub>, Silver nitrate; CuO, Copper oxide; CuO-NH<sub>2</sub>, Copper oxide coated with amino groups; CuO-COOH, Copper oxide coated with carboxy groups; CuSO<sub>4</sub>, Copper sulphate.

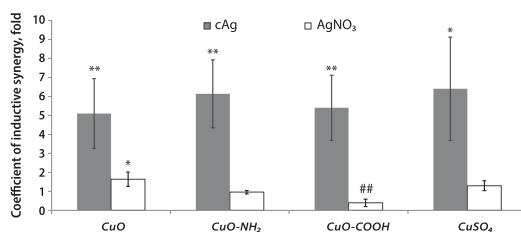


**Figure 8.** Coefficient of inductive synergy in a mixture of Cu and Ag components. Induction of bioluminescence in bacteria was higher in response to the mixture of cAg and Cu components compared to components alone. This enhanced reaction has not been detected in the mixture of AgNO<sub>3</sub> and CuO NPs. \* $P < 0.05$ ; \*\* $P < 0.01$ ; \*\*\* $P < 0.001$ , ##Antagonism  $P < 0.01$ . cAg, Coated silver nanoparticles; AgNO<sub>3</sub>, Silver nitrate; CuO, Copper oxide; CuO-NH<sub>2</sub>, Copper oxide coated with amino groups; CuO-COOH, Copper oxide coated with carboxy groups; CuSO<sub>4</sub>, Copper sulphate.

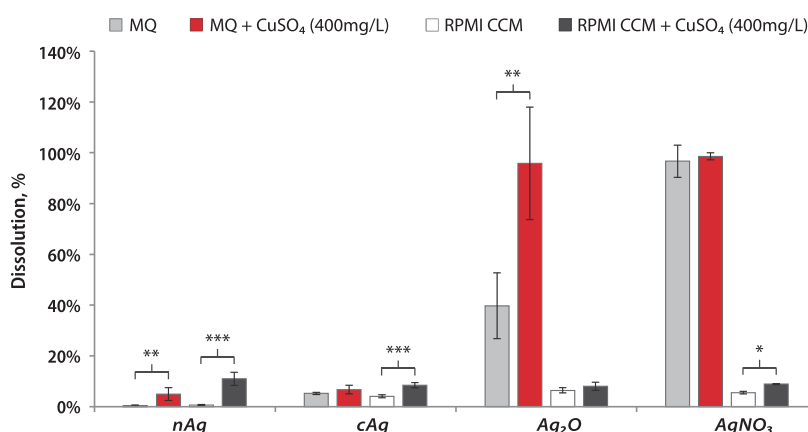


**Figure 9.** Dissolution of silver nanoparticles. Dissolution percentage of silver components (100 mg/L) in water and in RPMI CCM with and without the addition of CuSO<sub>4</sub> (400 mg/L) after 24 h of incubation in a shaker at 37 °C. \* $P < 0.05$ ; \*\* $P < 0.01$ ; \*\*\* $P < 0.001$ . cAg, Coated silver nanoparticles; nAg, Nanosilver; Ag<sub>2</sub>O, Silver oxide; AgNO<sub>3</sub>, Silver nitrate; CuSO<sub>4</sub>, Copper sulphate; RPMI CCM, Roswell Park Memorial Institute cell culture media.

conditions, whereas ROS production by cAg was remarkably higher. On the contrary, the addition of CuSO<sub>4</sub> reduced the amount of ROS production in cAg suspension in biotic and abiotic conditions (Fig. 6).

Jang and al. (2020) showed that the release of Ag<sup>+</sup> ions from NP was significantly higher in the solution with the higher concentration of Cu<sup>2+</sup> ions<sup>23</sup>. Also, the higher release of Ag<sup>+</sup> was related to the higher temperature and longer time of NP incubation<sup>21</sup>. This mechanism of synergy is in line with the results of our study.

Our research has shown that a combination of non-oxidized Ag NPs and Cu ions is essential for the synergistic antibacterial effect. The antibacterial synergy between Ag NPs and Cu components, according to our study, has at least three reasons. First, Cu ions facilitate the oxidation of non-oxidized Ag<sup>0</sup> (Eq. 3) in a redox reaction and, as a result, better dissolution of Ag<sup>+</sup> from Ag NPs in solvents in the presence of Cu<sup>2+</sup> (Fig. 9). Indeed, non-oxidized Ag<sup>0</sup> in NPs is needed for redox reaction with Cu<sup>2+</sup> to produce Ag<sup>+</sup> and Cu<sup>+</sup>. Better dissolution of Ag NPs leads to a higher concentration of Ag<sup>+</sup> in the solvent and intracellularly in bacteria (Fig. 7), causing a stronger antibacterial effect. The second reason is the production of Cu<sup>+</sup> ions in the same redox reaction (Eq. 3). Cu<sup>+</sup> ions are more antibacterial compared to Cu<sup>2+</sup><sup>38</sup>. The third reason is that free Ag ions bind to proteins in the culture medium less effectively in the presence of Cu<sup>2+</sup>, resulting in a larger concentration of free Ag<sup>+</sup> in the solution (Fig. 9). Thus, the release of Cu<sup>2+</sup> ions from CuO NPs is required for the synergistic action. All of the described processes can occur both extracellularly and intracellularly, whereas the latter is more harmful to cell homeostasis. Moreover, other factors, such as zeta-potential and NP surface functionalization might have some minor effects on the antibacterial synergy but in order to prove that, further studies are required.

## Conclusion

Ag and Cu have been used separately as antibacterial agents since ancient times. Our study showed that the antibacterial effect of the NPs mixture containing Ag and Cu components was up to six times higher than the sum of the antibacterial effects of the individual components. The mechanisms of the synergy are: better dissolution of Ag in the presence of Cu ions due to oxidation in the redox reaction, the production of more antibacterial  $\text{Cu}^+$  ions during the same redox reaction and less favorable binding of Ag ions to medium proteins in the presence of Cu ions. The antibacterial synergy between Ag and Cu could be an ideal solution for some medical problems where the elimination of infection is needed and where the antibacterial effect of Ag or Cu alone is not sufficient. For example, the results of the study can be used to develop combinatory nanotechnology to be used in antibacterial wound dressings to treat infected wounds. Since the treatment of some bacterial wound infections is an unsolved problem, combinatory treatment of wounds based on Cu and Ag NPs could reduce wound infection complications (such as infection-related gangrenes and amputations) and increase the quality-adjusted life years (QALY) of patients.

## Methods and materials

**Chemicals.** All the chemicals were at least of analytical grade. Polymyxin B and NaCl were purchased from Sigma-Aldrich Co. (USA);  $\text{AgNO}_3$  from J.T. Baker (USA),  $\text{CuSO}_4$  from Alfa Aesar GmbH & Co. (Germany); 2',7'-dichlorodihydrofluorescein diacetate from Life Technologies (USA); phosphate buffered saline from Biognost (Croatia); tryptone, yeast extract and agar from LabM (UK); RPMI 1640 with glutamine and Sodium Pyruvate from Corning (USA); Fetal Bovine Serum from Gibco (USA).

**Nanoparticles (NPs).** Three types of functionalized and unfunctionalized CuO NPs were obtained from PlasmaChem GmbH (Germany). CuO NPs were synthesized by PlasmaChem by decomposition of  $\text{Cu}_2\text{CO}_3(\text{OH})_2$ , followed by the introduction of the surface groups via treatment with mercaptopropionic acid. Coated Ag NPs (cAg) were obtained from Laboratorios Argenol S. L. (Spain), uncoated Ag NPs (nAg) from Sigma-Aldrich (USA).  $\text{Ag}_2\text{O}$  NPs ( $\text{Ag}_2\text{O}$ ) were synthesized by us as described below.

Commercial NPs were provided as dry powders, and the suspensions were freshly prepared each time before the tests at concentrations of 2000 mg compound/l in endotoxin-free Milli-Q<sup>®</sup> water (MQ). Ten milliliters of CuO NPs suspensions were vortexed and sonicated using probe sonication (Branson 450 Sonifier, USA) for 5 min with an acoustic power of 13 W corresponding to the specific energy of  $3.9 \cdot 10^5 \text{ kJ/m}^{340}$ .

The morphology and primary size of all NPs except  $\text{Ag}_2\text{O}$  were characterized in our previous studies<sup>8,13,41</sup>.

$\text{Ag}_2\text{O}$  NPs characterization by X-ray crystallography and Transmission electron microscopy was performed at the University of Tartu. Scanning transmission electron microscopy (STEM) measurements were made with Cs corrected FEI Titan Themis 200 instrument. Samples were prepared in isopropyl alcohol, sonicated and deposited onto carbon film-covered TEM grids. After evaporation of solvent, the samples were measured with bright field (BF) and high-angle annular dark-field (HAADF) detectors simultaneously.

Hydrodynamic size (Dh), polydispersity index (PDI) and zeta potential (Zeta-potential) of NPs were measured in 100 mg/l suspensions in MQ water or in Roswell Park Memorial Institute (RPMI) cell culture medium with 10% FBS and 1% sodium pyruvate (RPMI CCM) using Malvern Zetasizer (Zetasizer Nano-ZS, Malvern Instruments, UK).

The metal content of the tested compounds was determined using atomic absorption spectroscopy (AAS) (contrAA 800, Analytik Jena Ag). Materials and nanoparticles were incubated in 1 mL of concentrated  $\text{HNO}_3$  (Nitric Acid TraceMetal Grade 67–69%, Seastar Chemicals) for 24 h at 65 °C. After incubation, the suspension was vortexed and diluted 1:1000 in 1%  $\text{HNO}_3$ . The tissue and blood serum were incubated in  $\text{H}_2\text{O}_2$  (Perdrogen 30%, Sigma-Aldrich) and concentrated  $\text{HNO}_3$  at the following ratio 1:1:8 (tissue:  $\text{H}_2\text{O}_2$ :  $\text{HNO}_3$ ) and incubated for 24 h at 65 °C. After incubation, the suspension was diluted 10 times in 1%  $\text{HNO}_3$  and analyzed by AAS. The measurements were done in triplicate in at least two independent experiments.

**Preparation of silver oxide nanoparticles ( $\text{Ag}_2\text{O}$ ).** Analytical reagent grade (anhydrous, with purity over 99.9%) silver nitrate (5 mmol, 0.85 g) was dissolved in 50 mL of DI water and ultrasonicated for 1 min to achieve a homogeneous solution at room temperature.

After the silver nitrate was totally dissolved, sodium hydroxide (10 mmol, 0.39 g) was swiftly added to the reaction mixture at ambient conditions and ultrasonicated for 2 h.

The final solution was cooled down. Then the obtained blackish precipitate was filtered on the Whatman filter paper (Grade 5) and quenched twice with 50 mL of MQ water. The black residue was then dried at 70°C for 12 h providing yields over 60%.

## Cells

**Bacterial cells.** *Escherichia coli* MG1655 K-12 (*E.coli* K-12) (obtained from the *E. coli* genetic stock center, Yale University), *Escherichia coli* ESBL (isolated from the urine of 72 y.o. male patient with chronic prostatitis in West-Tallinn Central Hospital), *Pseudomonas aeruginosa* PAO1 (obtained from Prof. Patrick Plesiat, Besanc, France), *Streptococcus dysgalactiae* DSM 23,147 (obtained from German Collection of Microorganisms and Cell Cultures of Leibniz Institute, Braunschweig, Germany), recombinant bioluminescent *E. coli* MC1061 (pSLcueR/pDNpCOPAlux, constructed in our laboratory previously by Ivask et al.<sup>34</sup>), *Enterococcus faecalis* ATCC 29,212 (obtained from the West-Tallinn Central Hospital) and *Staphylococcus aureus* ATCC 25,923 (obtained from the West-Tallinn Central Hospital) were stored on agarized Luria–Bertani medium (LB, 1% tryptone, 0.5% yeast extract, 0.5% NaCl, 1.5% agar) and before the tests cultivated in 3 mL of RPMI at 37 °C with shaking at 200 rpm overnight. After overnight cultivation, 400  $\mu\text{l}$  of inoculum was mixed with 20 mL of RPMI CCM and incubated

for 4 h and grown to the exponential phase. After the incubation, the optical density of the bacterial suspension at 620 nm ( $OD_{620}$ ) was measured and the suspension at desired  $OD_{620}$  was prepared. In the case of recombinant bacteria, RPMI CCM was supplemented with 100  $\mu\text{g/l}$  ampicillin and 10  $\mu\text{g/l}$  tetracycline to retain the bioluminescence-encoding plasmid.

### Assays

**Evaluation of minimum bactericidal concentration (MBC).** MBC was determined by the lowest concentration that kills 99.9% of the initial bacterial population using the spot test described by Suppi et al.<sup>42</sup>. After overnight cultivation and 4 h incubation to exponential phase, as described before, the bacterial suspension with  $OD_{620}$  0.07 (corresponds to  $2 \times 10^8$  cells/mL<sup>43</sup>) in MQ, RPMI CCM or LB was obtained. 100  $\mu\text{L}$  of bacterial suspension was added to 100  $\mu\text{L}$  components alone or their mix in medium. Bacteria were exposed in RPMI CCM, LB or MQ on 96-well microplates (BD Falcon) at 30 °C for 24 h without shaking in the dark. 3  $\mu\text{L}$  of incubated suspension was pipetted onto agarized LB medium and the viability of bacterial cells (formation of colonies) was visually evaluated after 24 h of incubation. Each experiment was repeated at least three times.

**Measurement of bacterial growth in different media.** Bacteria were prepared for the test as described in the paragraph "Evaluation of the minimum bactericidal concentration (MBC)". Bacterial suspension with  $OD_{620}$  0.03 in MQ, RPMI CCM or LB was incubated for 3 h at 37 °C in a shaker and the bacterial density at  $OD_{620}$  was measured.

**Evaluation of bacterial outer membrane (OM) integrity by 1-NPN assay.** The cell wall permeabilization of *E. coli* and *P. aeruginosa* by  $\text{AgNO}_3$ , cAg, CuO, CuO-COOH, CuO-NH<sub>2</sub>, CuSO<sub>4</sub> and Polymixin B (PB, positive control) was assayed by the cellular uptake of N-Phenyl-naphthalen-1-amine (1-NPN) essentially as described by Helander and Mattila-Sandholm<sup>44</sup>. Differently from a hydrophilic environment, the fluorescence of 1-NPN is significantly enhanced in a hydrophobic environment (e.g., membrane lipid bilayer), rendering it an appropriate dye to probe the outer membrane (OM) integrity of gram-negative bacteria. Briefly, 50  $\mu\text{L}$  of 40  $\mu\text{M}$  1-NPN and 50  $\mu\text{L}$  of the tested compound in 50 mM 3-(N-morpholino)propanesulfonic acid (MOPS) adjusted with tris(hydroxymethyl)aminomethane (TRIS) base to pH 7.2 (MOPS-TRIS buffer) were pipetted into the wells of black microplates. 100  $\mu\text{L}$  of bacterial suspension in 50 mM MOPS-TRIS buffer with  $OD = 0.5$  was dispensed into each well and the fluorescence was measured after 30 min of incubation at RT (Fluoroskan Ascent FL plate luminometer; excitation/emission filters 350/460 nm). The 1-NPN cell uptake factor was calculated and presented as a ratio between the intensity of fluorescence values of the bacterial suspension incubated with and without test compounds. At least three independent experiments were performed in technical duplicates.

**CopA gene induction of luminescent bacteria.** Induction of luminescence in bacteria by intracellular Ag and Cu ions was performed using recombinant biosensor bacteria *Escherichia coli* MC1061 (pSLcueR/pDN-PcopAlux). The response of recombinant *E. coli* to intracellular Ag and Cu ions is mediated via CueR activator protein and its regulated *copA* promoter that is fused to the bioluminescence encoding genes<sup>34</sup>. Therefore, in the sub-toxic region, the presence of intracellular Ag and Cu ions leads to the increase of bioluminescence of these recombinant bacteria in a dose-dependent manner.

The preparation of test bacteria and the procedure of the biosensor assay were analogous to the bacterial growth inhibition assay with one exception: the growth medium of bioluminescent Ag-biosensor *E. coli* MC1061 (pSLcueR/pDN-PcopAlux) was supplemented with 100  $\mu\text{g/l}$  ampicillin and 10  $\mu\text{g/l}$  tetracycline during overnight cultivation to maintain the recombinant plasmids. Orion II plate luminometer (Berthold Detection Systems) was used for the bioluminescence (BL) measurement. 100  $\mu\text{L}$  of bacterial suspension with  $OD_{620}$  0.1 was exposed to components or their mix in RPMI CCM (sample) or RPMI CCM (background) at 30 °C for 4 h. Dose-response curves of the Ag and Cu biosensor were obtained by plotting the applied concentrations of Cu and Ag against the bioluminescence of Ag/Cu-biosensor (as fold induction) in respective samples. The concentration with the highest bioluminescence value from each component has been marked as the peak of LC. Fold induction was calculated as follows:

$$\text{Induction}(\text{fold}) = \frac{BL_{\text{sample}}}{BL_{\text{background}}}$$

where  $BL_{\text{sample}}$  is the bioluminescence of Ag/Cu-biosensor in the sample and  $BL_{\text{background}}$  is the background bioluminescence considering darkening of luminescence due to NPs.

**Quantification of reactive oxygen species (ROS).** Since presence of cells may influence generation and neutralization of ROS, ROS was quantified in both, biotic (in the presence of cells) and abiotic (without cells) conditions.

To study cellular (biotic) ROS production, fresh stock of 2',7'-dichlorodihydrofluorescein diacetate ( $\text{H}_2\text{DCFDA}$ ) was dissolved in ethanol to a concentration of 0.6 mg/mL and subsequently diluted in 0.1 M sodium phosphate buffer. 100  $\mu\text{L}$  of component in MQ water was pipetted into the wells. Then, 100  $\mu\text{L}$  of bacterial culture (*E. coli* K-12 at  $OD_{620} = 0.1$ ) in MQ water was added. The test plates were incubated at 30 °C for 4 h. After incubation 100  $\mu\text{L}$  of the mixture was aliquoted into black non-transparent 96 well plates, and  $\text{H}_2\text{DCFDA}$  was added to the cells at a final concentration of 1.5  $\mu\text{g/mL}$ . After 30 min of incubation, the fluorescence was measured using a microplate reader (excitation/emission at 485/527 nm). In the assay,  $\text{H}_2\text{DCFDA}$  diffuses through the cell

membrane and is processed by intracellular esterases to a non-fluorescent dichlorofluorescein (DCFH). DCFH is then converted to the highly fluorescent 2',7'-dichlorofluorescein (DCF) due to the presence of intracellular ROS.

To study ROS in abiotic conditions, the acetate group of H<sub>2</sub>DCFDA was cleaved by 0.01 M NaOH at RT for 30 min. The dye was diluted with 0.1 M Na-phosphate buffer to a concentration of 24 µg/mL and then added to each well in the black nontransparent 96 well plates, to yield a final dye concentration of 12 µg/mL. The results were divided by the blank and presented as relative light units (RFUs).

**Determination of dissolution of the components.** For the dissolution analysis, 100 mg/l cAg, Ag<sub>2</sub>O, nAg, AgNO<sub>3</sub>, CuSO<sub>4</sub> (a recovery control) were incubated in MQ water or in RPMI CCM at 37 °C for 24 h and afterwards centrifuged at 320,000 × g for 30 min (Beckman Coulter ultracentrifuge). After centrifugation, the supernatants were collected and the silver concentration analyzed by AAS (contraA 800, Analytik Jena Ag). The percentage of NP dissolution was calculated according to the silver concentration in the supernatant after centrifugation, 100 mg/l was taken as 100%. The measurements were done in triplicate in at least two independent experiments.

**Detection of Cu<sup>+</sup> in the suspension.** The detection of Cu<sup>+</sup> was conducted using the iodometric method<sup>45</sup>. The Cu<sup>2+</sup> was masked by a complex formation with potassium oxalate; then, the Cu<sup>+</sup> was oxidized to Cu<sup>2+</sup> by potassium iodate in the presence of 2 M hydrochloric acid using the 1% starch solution as an indicator of the presence of iodine, which appears when the reaction is completed.

**Statistical analysis.** P values using Student's t-test, standard deviations and mean values were calculated in Microsoft Excel.

### Data availability

The data used and/or analyzed during the current study is available from the corresponding author on reasonable request.

Received: 27 January 2023; Accepted: 4 June 2023

Published online: 06 June 2023

### References

1. Theuretzbacher, U., Outtersson, K., Engel, A. & Karlén, A. The global preclinical antibacterial pipeline. *Nat. Rev. Microbiol.* **18**, 275–285 (2020).
2. Murray, C. J. *et al.* Global burden of bacterial antimicrobial resistance in 2019: A systematic analysis. *Lancet* **399**, 629–655 (2022).
3. Armstrong, D. G. & Lipsky, B. A. Singh. Pdf Ulcer. Pdf. **293**, 217–228 (2005).
4. Theuretzbacher, U. Dual-mechanism antibiotics. *Nat. Microbiol.* **5**, 984–985 (2020).
5. León-Buitimea, A., Garza-Cárdenas, C. R., Garza-Cervantes, J. A., Lerma-Escalera, J. A. & Morones-Ramírez, J. R. The demand for new antibiotics: Antimicrobial peptides, nanoparticles, and combinatorial therapies as future strategies in antibacterial agent design. *Front. Microbiol.* **11**, 1–10 (2020).
6. Kornblatt, A. P., Nicoletti, V. G. & Travaglia, A. The neglected role of copper ions in wound healing. *J. Inorg. Biochem.* **161**, 1–8 (2016).
7. Bari, A. *et al.* Copper-containing mesoporous bioactive glass nanoparticles as multifunctional agent for bone regeneration. *Acta Biomater.* **55**, 493–504 (2017).
8. Kurvet, I., Kahru, A., Bondarenko, O., Ivask, A. & Ka, A. Particle-cell contact enhances antibacterial activity of silver nanoparticles. *PLoS ONE* **8**, e64060 (2013).
9. Bondarenko, O. M. *et al.* Plasma membrane is the target of rapid antibacterial action of silver nanoparticles in *Escherichia coli* and *Pseudomonas aeruginosa*. *Int. J. Nanomed.* **13**, 6779–6790 (2018).
10. Heinlaan, M., Ivask, A., Blinova, I., Dubourguier, H. C. & Kahru, A. Toxicity of nanosized and bulk ZnO, CuO and TiO<sub>2</sub> to bacteria *Vibrio fischeri* and crustaceans *Daphnia magna* and *Thamnocephalus platyurus*. *Chemosphere* **71**, 1308–1316 (2008).
11. Bondarenko, O., Ivask, A., Käkinen, A. & Kahru, A. Sub-toxic effects of CuO nanoparticles on bacteria: Kinetics, role of Cu ions and possible mechanisms of action. *Environ. Pollut.* **169**, 81–89 (2012).
12. Bondarenko, O. *et al.* Nanotoxicology and nanomedicine: The Yin and Yang of nano-bio interactions for the new decade. *Nano Today* <https://doi.org/10.1016/j.nantod.2021.101184> (2021).
13. Kubo, A.-L. *et al.* Surface carboxylation or PEGylation decreases CuO nanoparticles' cytotoxicity to human cells in vitro without compromising their antibacterial properties. *Arch. Toxicol.* **94**, 1561–1573 (2020).
14. Kubo, A. L. *et al.* Antimicrobial potency of differently coated 10 and 50 nm silver nanoparticles against clinically relevant bacteria *Escherichia coli* and *Staphylococcus aureus*. *Colloids Surf. B* **170**, 401–410 (2018).
15. Fisher, K., Pope, M. & Phillips, C. Combined effect of copper and silver against *Pseudomonas aeruginosa*. *J. Hosp. Infect.* **73**, 180–182 (2009).
16. Vaidya, M. Y., McBain, A. J., Butler, J. A., Banks, C. E. & Whitehead, K. A. Antimicrobial efficacy and synergy of metal ions against *Enterococcus faecium*, *Klebsiella pneumoniae* and *Acinetobacter baumannii* in planktonic and biofilm phenotypes. *Sci. Rep.* **7**, 5911 (2017).
17. Yahya, M. T., Kutz, S. M., Landeen, L. K. & Gerba, C. P. Swimming pool disinfection: An evaluation of the efficacy of copper: Silver ions. *J. Environ. Health* **51**, 282–285 (1989).
18. Landeen, L. K., Yahya, M. T. & Gerba, C. P. Efficacy of Copper and silver ions and reduced levels of free chlorine in inactivation of *Legionella pneumophila*. *Appl. Environ. Microbiol.* **55**, 3045–3050 (1989).
19. Garza-Cervantes, J. A. *et al.* Synergistic antimicrobial effects of silver/transition-metal combinatorial treatments. *Sci. Rep.* **7**, 903 (2017).
20. Tao, Y., Zhou, F., Wang, K., Yang, D. & Sacher, E. AgCu NP formation by the Ag NP catalysis of Cu ions at room temperature and their antibacterial efficacy: A kinetic study. *Molecules* **27**, 6951 (2022).
21. Zhou, F., Zhu, Y., Yang, L., Yang, D. Q. & Sacher, E. Ag NP catalysis of Cu ions in the preparation of AgCu NPs and the mechanism of their enhanced antibacterial efficacy. *Colloids Surf. A Physicochem. Eng. Asp.* **632**, 127831 (2022).
22. Bankier, C. *et al.* Synergistic antibacterial effects of metallic nanoparticle combinations. *Sci. Rep.* **9**, 16074 (2019).



23. Jang, J. *et al.* Development of antibiofilm nanocomposites: Ag/Cu bimetallic nanoparticles synthesized on the surface of graphene oxide nanosheets. *ACS Appl. Mater. Interfaces* **12**, 35826–35834 (2020).
24. Ivask, A. *et al.* Toxicity of 11 metal oxide nanoparticles to three mammalian cell types in vitro. *Curr. Top. Med. Chem.* **15**, 1914–1929 (2015).
25. Warnes, S. L., Caves, V. & Keevil, C. W. Mechanism of copper surface toxicity in *Escherichia coli* O157:H7 and *Salmonella* involves immediate membrane depolarization followed by slower rate of DNA destruction which differs from that observed for Gram-positive bacteria. *Environ. Microbiol.* **14**, 1730–1743 (2012).
26. Li, X.-Z., Zhang, L. & Poole, K. Interplay between the MexA-MexB-OprM multidrug efflux system and the outer membrane barrier in the multiple antibiotic resistance of *Pseudomonas aeruginosa*. *J. Antimicrob. Chemother.* **45**, 433–436 (2000).
27. Warnes, S. L., Green, S. M., Michels, H. T. & Keevil, C. W. Biocidal efficacy of copper alloys against pathogenic enterococci involves degradation of genomic and plasmid DNAs. *Appl. Environ. Microbiol.* **76**, 5390–5401 (2010).
28. Eng, R. H. K., Padberg, F. T., Smith, S. M., Tan, E. N. & Cherubin, C. E. Bactericidal effects of antibiotics on slowly growing and nongrowing bacteria. *Antimicrob. Agents Chemother.* **35**, 1824–1828 (1991).
29. Kohanski, M. A., Dwyer, D. J. & Collins, J. J. How antibiotics kill bacteria: From targets to networks. *Nat. Rev. Microbiol.* **8**, 423–435 (2010).
30. Moubareck, C. A. Polymyxins and bacterial membranes: A review of antibacterial activity and mechanisms of resistance. *Membranes* **10**, 1–30. <https://doi.org/10.3390/membranes10080181> (2020).
31. Dupont, C. L., Grass, G. & Rensing, C. Copper toxicity and the origin of bacterial resistance—New insights and applications. *Metallics* **3**, 1109 (2011).
32. Choi, O. & Hu, Z. Size dependent and reactive oxygen species related nanosilver toxicity to nitrifying bacteria. *Environ. Sci. Technol.* **42**, 4583–4588 (2008).
33. Bondarenko, O. *et al.* Toxicity of Ag, CuO and ZnO nanoparticles to selected environmentally relevant test organisms and mammalian cells in vitro: A critical review. *Arch. Toxicol.* **87**, 1181–1200 (2013).
34. Ivask, A., Rõlova, T. & Kahru, A. A suite of recombinant luminescent bacterial strains for the quantification of bioavailable heavy metals and toxicity testing. *BMC Biotechnol.* **9**, 1–15 (2009).
35. Gnanadhas, D. P., Ben Thomas, M., Thomas, R., Raichur, A. M. & Chakravorty, D. Interaction of silver nanoparticles with serum proteins affects their antimicrobial activity in vivo. *Antimicrob. Agents Chemother.* **57**, 4945–4955 (2013).
36. Popov, S. *et al.* Factors enhancing the antibacterial effect of monovalent copper ions. *Curr. Microbiol.* **77**, 361–368 (2020).
37. Saphier, M., Silberstein, E., Shotland, Y., Popov, S. & Saphier, O. Prevalence of monovalent copper over divalent in killing *Escherichia coli* and *Staphylococcus aureus*. *Curr. Microbiol.* **75**, 426–430 (2018).
38. Rapisarda, V. A., Montelongo, L. R., Farias, R. N. & Massa, E. M. Characterization of an NADH-linked cupric reductase activity from the *Escherichia coli* respiratory chain. *Arch. Biochem. Biophys.* **370**, 143–150 (1999).
39. Muppudathi, M. & Perumal, P. Ag@CuO@Cu(OH)<sub>2</sub>: A synergistic catalyst for H<sub>2</sub>O<sub>2</sub> detection with peroxidase-mimic activity without interference of O<sub>2</sub>. *ChemistrySelect* **6**, 10253–10257 (2021).
40. Käkkinen, A., Kahru, A., Nurmsoo, H., Kubo, A.-L. & Bondarenko, O. M. Solubility-driven toxicity of CuO nanoparticles to CaCO<sub>3</sub> cells and *Escherichia coli*: Effect of sonication energy and test environment. *Toxicol. In Vitro* **36**, 172–179 (2016).
41. Blinova, I. *et al.* Toxicity of two types of silver nanoparticles to aquatic crustaceans *Daphnia magna* and *Thamnocephalus platyurus*. *Environ. Sci. Pollut. Res.* **20**, 3456–3463 (2013).
42. Suppi, S. *et al.* A novel method for comparison of biocidal properties of nanomaterials to bacteria, yeasts and algae. *J. Hazard. Mater.* **286**, 75–84 (2015).
43. Silvestro, L. *et al.* Antibacterial and antimembrane activities of cecropin A in *Escherichia coli*. *Antimicrob. Agents Chemother.* **44**, 602–607 (2000).
44. Helander, I. M. Fluorometric assessment of Gram-negative bacterial permeabilization. 213–219 (2000).
45. Jabber, M. S. A. & Stephen, W. I. The titrimetric determination of copper(I), copper(II) and copper metal in admixture. *Fresenius' Zeitschrift für Analytische Chemie* **311**, 259–264 (1982).

## Acknowledgements

We thank Dr. Villem Aruoja (National Institute of Chemical Physics and Biophysics, Estonia) for English corrections of the manuscript.

## Author contributions

Conceptualization, G.V., O.B.; Data curation, G.V. and A.-L.K.; Formal analysis, G.V.; Investigation, G.V., A.-L.K. and O.B.; Methodology, G.V., A.-L.K., O.B., H.V. and D.B.; Project administration, O.B., A.K., Y.K.; Resources, A.K., Y.K. and O.B.; Validation, O.B.; Visualization, G.V.; Writing draft, G.V. and O.B.; Review of manuscript, G.V., A.-L.K., O.B., H.V., D.B., Y.K., A.K. All authors have read and agreed to the published version of the manuscript.

## Funding

EIC Accelerator Grant No. 190199469 (NANOWOUND) from the European Commission (Grigory Vasiliev, Anna-Liisa Kubo, Olesja Bondarenko). GOVSG16 Grant from Estonian Research Council (Grigory Vasiliev, Anna-Liisa Kubo, Olesja Bondarenko). Arengufond\_OB Grant from Development Fund of National Institute of Chemical Physics and Biophysics (Grigory Vasiliev, Anna-Liisa Kubo, Olesja Bondarenko). PRG749 Grant from Estonian Research Council (Anne Kahru). Grant COVSG5 from Estonian Research Agency (Denys Bondar, Yevgen Karpichev). The study was partially supported by the European Regional Development Fund Project “Emerging orders in quantum and nanomaterials” (TK134).

## Competing interests

A.-L.K., G.V., O.B. are co-founders of Nanordica Medical developing nanoparticle-based antibacterial products. A.K., D.B., H.V. and Y.K. declare no competing interests.

## Additional information

**Supplementary Information** The online version contains supplementary material available at <https://doi.org/10.1038/s41598-023-36460-2>.

**Correspondence** and requests for materials should be addressed to O.B.

**Reprints and permissions information** is available at [www.nature.com/reprints](http://www.nature.com/reprints).

**Publisher's note** Springer Nature remains neutral with regard to jurisdictional claims in published maps and institutional affiliations.



**Open Access** This article is licensed under a Creative Commons Attribution 4.0 International License, which permits use, sharing, adaptation, distribution and reproduction in any medium or format, as long as you give appropriate credit to the original author(s) and the source, provide a link to the Creative Commons licence, and indicate if changes were made. The images or other third party material in this article are included in the article's Creative Commons licence, unless indicated otherwise in a credit line to the material. If material is not included in the article's Creative Commons licence and your intended use is not permitted by statutory regulation or exceeds the permitted use, you will need to obtain permission directly from the copyright holder. To view a copy of this licence, visit <http://creativecommons.org/licenses/by/4.0/>.

© The Author(s) 2023



## Appendix 3







### Publication III

Kubo, A. L., Rausalu, K., Savest, N., Žusinaite, E., **Vasiliev, G.**, Viirsalu, M., Plamus, T., Krumme, A., Merits, A., & Bondarenko, O. (2022). Antibacterial and Antiviral Effects of Ag, Cu and Zn Metals, Respective Nanoparticles and Filter Materials Thereof against Coronavirus SARS-CoV-2 and Influenza A Virus. *Pharmaceutics*, 14(12). <https://doi.org/10.3390/pharmaceutics14122549>



## Article

# Antibacterial and Antiviral Effects of Ag, Cu and Zn Metals, Respective Nanoparticles and Filter Materials Thereof against Coronavirus SARS-CoV-2 and Influenza A Virus

Anna-Liisa Kubo <sup>1,2,†</sup>, Kai Rausalu <sup>3,†</sup>, Natalja Savest <sup>4</sup>, Eva Žusinaite <sup>3</sup>, Grigory Vasiliev <sup>1,2</sup>, Mihkel Viirsalu <sup>4</sup>, Tiia Plamus <sup>4</sup>, Andres Krumme <sup>4,\*</sup>, Andres Merits <sup>3,\*</sup> and Olesja Bondarenko <sup>1,2,\*</sup>

<sup>1</sup> Laboratory of Environmental Toxicology, National Institute of Chemical Physics and Biophysics, Akadeemia tee 23, 12618 Tallinn, Estonia

<sup>2</sup> Nanordica Medical OÜ, Vana-Lõuna 39a-7, 10134 Tallinn, Estonia

<sup>3</sup> Institute of Technology, University of Tartu, Nooruse 1, 50411 Tartu, Estonia

<sup>4</sup> Laboratory of Polymers and Textile Technology, Department of Materials and Environmental Technology, Tallinn University of Technology, Ehitajate tee 5, 19086 Tallinn, Estonia

\* Correspondence: andres.krumme@taltech.ee (A.K.); andres.merits@ut.ee (A.M.); olesja.bondarenko@kbfi.ee (O.B.)

† These authors contributed equally to this work.



**Citation:** Kubo, A.-L.; Rausalu, K.; Savest, N.; Žusinaite, E.; Vasiliev, G.; Viirsalu, M.; Plamus, T.; Krumme, A.; Merits, A.; Bondarenko, O.

Antibacterial and Antiviral Effects of Ag, Cu and Zn Metals, Respective Nanoparticles and Filter Materials Thereof against Coronavirus SARS-CoV-2 and Influenza A Virus. *Pharmaceutics* **2022**, *14*, 2549.

<https://doi.org/10.3390/pharmaceutics14122549>

Academic Editor: Maria Nowakowska

Received: 26 October 2022

Accepted: 15 November 2022

Published: 22 November 2022

**Publisher's Note:** MDPI stays neutral with regard to jurisdictional claims in published maps and institutional affiliations.



**Copyright:** © 2022 by the authors. Licensee MDPI, Basel, Switzerland. This article is an open access article distributed under the terms and conditions of the Creative Commons Attribution (CC BY) license (<https://creativecommons.org/licenses/by/4.0/>).

**Abstract:** Due to the high prevalence of infectious diseases and their concurrent outbreaks, there is a high interest in developing novel materials with antimicrobial properties. Antibacterial and antiviral properties of a range of metal-based nanoparticles (NPs) are a promising means to fight airborne diseases caused by viruses and bacteria. The aim of this study was to test antimicrobial metals and metal-based nanoparticles efficacy against three viruses, namely influenza A virus (H1N1; A/WSN/1933) and coronaviruses TGEV and SARS-CoV-2; and two bacteria, *Escherichia coli* and *Staphylococcus aureus*. The efficacy of ZnO, CuO, and Ag NPs and their respective metal salts, i.e., ZnSO<sub>4</sub>, CuSO<sub>4</sub>, and AgNO<sub>3</sub>, was evaluated in suspensions, and the compounds with the highest antiviral efficacy were chosen for incorporation into fibers of cellulose acetate (CA), using electrospinning to produce filter materials for face masks. Among the tested compounds, CuSO<sub>4</sub> demonstrated the highest efficacy against influenza A virus and SARS-CoV-2 (1 h IC<sub>50</sub> 1.395 mg/L and 0.45 mg/L, respectively), followed by Zn salt and Ag salt. Therefore, Cu compounds were selected for incorporation into CA fibers to produce antiviral and antibacterial filter materials for face masks. CA fibers comprising CuSO<sub>4</sub> decreased SARS-CoV-2 titer by 0.38 logarithms and influenza A virus titer by 1.08 logarithms after 5 min of contact; after 1 h of contact, SARS-CoV-2 virus was completely inactivated. Developed CuO- and CuSO<sub>4</sub>-based filter materials also efficiently inactivated the bacteria *Escherichia coli* and *Staphylococcus aureus*. The metal NPs and respective metal salts were potent antibacterial and antiviral compounds that were successfully incorporated into the filter materials of face masks. New antibacterial and antiviral materials developed and characterized in this study are crucial in the context of the ongoing SARS-CoV-2 pandemic and beyond.

**Keywords:** coronavirus; silver; zinc oxide; copper oxide; toxicity; face masks; electrospinning

## 1. Introduction

The recent emergence of severe acute respiratory syndrome coronavirus 2 (SARS-CoV-2), the causative agent of COVID-19, has tremendous worldwide socioeconomic impacts. The genome of SARS-CoV-2 shares about 80% identity with that of SARS-CoV-1, a coronavirus causing SARS disease. SARS-CoV-2 is a positive-strand enveloped RNA virus, with the size of the virion ca. 125 nm in diameter. The spike glycoprotein S on the surface of the virion determines the attachment and the entry of the virus to the host cells [1–3]. The binding affinity of the SARS-CoV-2 S protein to its cellular receptor hACE2 is higher as compared to that of S protein of the SARS-CoV-1 [4], making SARS-CoV-2 extremely

transmittable [5–8]. To prevent virus transmission, it is suggested by the World Health Organization (WHO) to wear masks for avoiding the nosocomial transmission of the virus. Moreover, according to the WHO and the Centers for Disease Control and Prevention, wearing of masks is a relevant measure to reduce the spread of the coronavirus [9–11].

SARS-CoV-2 is an enveloped virus, similar to the Zika virus (ZIKV), Ebola virus (EBOV), SARS-CoV-1, and MERS-CoV [12], bearing a lipid envelope derived from the host cell membranes. Traditionally, antiviral agents and disinfectants are used to reduce the spread and inactivate these viruses [13]. To tackle the viral pandemics similar to COVID-19 through the implementation of materials comprising metals is a promising means [14–18]. Metals such as silver, copper, and zinc are well-known antimicrobials against a wide array of bacteria [19,20] and viruses, including human influenza A virus and SARS-CoV-2 [21–28]. The use of nanoparticles (NPs; size range, 1–100 nm) instead of metal salts enables control over metal ion release, prevents the rapid inactivation of metal ions, and enhances the antimicrobial effect of metal ions [19,29]. In particular, metal-based NPs are well-known for their antibacterial and antiviral properties, showing a significant response even at low concentrations, due to their high surface-to-volume ratio [19,30–32]. In the recent article by Bahrami et al., the authors reviewed the effects of a wide range of metal-based NPs on SARS-CoV-2 and showed that Ag NPs inhibited virus entry, reduced oxidative stress, and inhibited viral RNA synthesis. Cu NPs, on the other hand, damaged the virus membrane, destroyed the RNA, and interfered with functional proteins [21].

The outstanding virucidal efficacy of metal-based NPs makes them excellent materials to be applied on common surfaces toward impairing infection spread. Antimicrobial surface-coating materials comprising copper, silver, and zinc have shown good virucidal efficacy in controlling the transmission of viruses such as influenza A virus, human immunodeficiency virus type 1 (HIV-1), dengue virus type 2 (DENV-2), and human herpesvirus 1 (HHV-1) [14,33]. Considerable loss of human coronavirus HuCoV-229E infectivity was observed on copper-containing surfaces after 30 min of contact [34]. Surfaces treated with copper are already used in hospitals for the prevention of the spread of microbial contaminations and potentially viral transmissions [35].

Recently, many organic compounds of polymers, including biopolymers, have shown potential as antibacterial and antiviral agents to impair the spread of infectious diseases [36]. These polymer matrices are excellent as carriers of metal NPs and metals. Metals can be incorporated in the materials permanently, and these metal–polymer composites are efficient antimicrobials. Polymers and fiber materials thereof are used as components of fabrics and textiles and filter materials. Traditionally, the incorporation of the metal additives in the polymer matrices is achieved by the coating of the metals on the surface of the fibers or impregnation in the blend of polymer fibers [37]. Mostly, these materials are synthetic. For example, common surgical masks consist of plastic-based polymers such as polypropylene, polyurethane, polyacrylonitrile, polystyrene, polycarbonate, polyethylene, or polyester [38]. However, bio-based polymers are preferred for the future developments of the new biodegradable materials.

In this study, we tested the antibacterial and antiviral properties of the salts of Cu, Ag, and Zn; and respective NPs to develop new effective antimicrobial biomaterials thereof. To test the antibacterial properties of the compounds and materials, *E. coli* and *S. aureus* were selected, and for the antiviral properties, influenza A virus and coronaviruses transmissible gastroenteritis virus (TGEV) and SARS-CoV-2 were selected. The metal-based components with the best antimicrobial properties were incorporated into biopolymer CA, which is a natural environmentally friendly bio-based polymer. As the main results of the study, we provided valuable data on toxicity of studied metals and NPs to different bacteria and viruses and developed novel antimicrobial CuSO<sub>4</sub>-based filter material that inactivates SARS-CoV-2 within minutes of exposure.

## 2. Materials and Methods

### 2.1. Materials and Chemicals

CuO-NH<sub>2</sub> and CuO-COOH were obtained from PlasmaChem GmbH (Germany). Ag NPs (nAg) were obtained from Sigma-Aldrich. CuO and CuSO<sub>4</sub> were purchased as powders from Sigma-Aldrich and Alfa Aesar, respectively. AgNO<sub>3</sub> was obtained from J.T.Baker, and ZnSO<sub>4</sub> and ZnO from Sigma-Aldrich.

Cellulose acetate (CA) in granules with an average molecular mass of 30,000 g/mol was purchased from Aldrich Chemistry. Acetonitrile and dimethyl acetamide (DMA<sub>c</sub>) were from Sigma-Aldrich. Thymol (laboratory reagent grade), which was used as an additive to increase the porosity of electrospun filter materials, was obtained from Fisher Chemistry, and HNO<sub>3</sub> was from Seastar Chemicals.

### 2.2. Viruses and Cells

The human influenza A virus, strain A/WSN/1933 (H1N1), was kindly provided by Prof. Denis Kaynov (Norwegian University of Science and Technology, NTNU, Trondheim, Norway). Transmissible gastroenteritis virus (TGEV) was a kind gift from Prof. Luis Enjuanes (Centro Nacional de Biotecnología-Consejo Superior de Investigaciones Científicas, CNB-CSIC, Madrid, Spain). SARS-CoV-2 Estonian isolate 3049 was propagated from a nasopharyngeal swab of RT-qPCR-positive patient's sample. MDCK-2 (Madin-Darby canine kidney, the American Type Culture Collection code CCL-34) cells were used for propagation and titration of influenza virus; Vero-E6 (African green monkey, ((ATCC)) code CRL-1586) cells were used for propagation and titration of SARS-CoV-2, and ST cells (a kind gift from Prof. Luis Enjuanes' laboratory) were used for propagation and titration of TGEV. All cells were grown in DMEM medium (Corning) containing 10% heat-inactivated fetal bovine serum (FBS, PAN Biotech), in the presence of 100 units/mL penicillin and 100 µg/mL streptomycin (Sigma).

Influenza A virus was grown in MDCK-2 cells. The virus growth medium (VGM) was DMEM, containing 0.2% bovine serum albumin (BSA, Sigma), 100 units/mL penicillin, 100 µg/mL streptomycin, and 1 µg/mL TPCK-treated (N-tosyl-L-phenylalanine chloromethyl ketone) trypsin (Sigma). TGEV was grown in ST cells in VGM, which was DMEM that contained 0.2% BSA, 100 units/mL penicillin, and 100 µg/mL streptomycin. SARS-CoV-2 was propagated in Vero-E6 cells in a VGM (DMEM complemented with 0.2% BSA and penicillin/streptomycin).

### 2.3. Dispersion Analysis for Polymer Solvent Systems with Metal Nanoparticles

CA was used as a polymer matrix for electrospinning solution preparation. Two solvents, acetonitrile and DMA<sub>c</sub> were used to prepare solvent dispersions. NP and metal additives were used for CA polymer solutions to enhance the antibacterial and antiviral properties of the filter materials produced by electrospinning. CA polymer filter materials were electrospun in acetone–DMA<sub>c</sub> solvent systems at 2:1 and 3:1 ratios. The solvent systems with metal compounds were characterized for dispersion by using dynamic light scattering (DLS) for evaluating the profile for size distribution for the particles and CA polymers in solution and provide additional information about the compatibility and quality of the NP polymer–solvent systems (Supplementary Table S1).

### 2.4. Electrospinning of Filter Materials

CA polymer solutions were prepared in an acetonitrile–DMA<sub>c</sub> mixture in a mass mixing ratio of 2:1. The concentration of CA in the solvent mixture was 17 wt.%. To obtain a homogeneous solution, the added polymer was dissolved in the solvent mixture by mechanical mixing with the magnetic stirrer, at room temperature, for 24 h. The additives of CuO and CuSO<sub>4</sub> in total mass concentration of 12.5 wt.% and 18.75 wt.% were added, achieving 7.5% and 10% Cu concentrations in polymer, respectively, and the solutions were stirred again for 24 h to achieve the homogeneity. To avoid precipitation of CuSO<sub>4</sub> salt in



CA solution, the ultrasonication treatment was applied for another 30 min using probe sonication (Branson Sonifier 450).

The electrospinning process was performed by using an in-house built-laboratory-scale horizontal electrospinning setup with cylindrical rotating collector covered with the non-woven fiber material with a 25 g/m<sup>2</sup> density. The operating parameters for electrospinning are summarized in Supplementary Table S2. In brief, the electrospinning solution containing CA polymer in acetonitrile–DMA<sub>c</sub> mixture in mass mixing ratio 2:1 was placed in a 2 mL syringe with a needle diameter of 0.4–0.6 mm. The solution was electrospun at 10 kV, with the distance of 15 cm between the collector and the needle. The pumping rate was from 0.4 up to 0.9 mL/h depending on the solution viscosity. The electrospinning was performed at room temperature and at an air humidity of 60%. The humidity of the isolated electrospinning box was controlled by using a portable humidity device, Air-O-Swiss.

#### 2.4.1. Analysis of Morphology of Electrospun Filter Material

The morphology of the filter materials was determined by high-resolution scanning electron microscope (SEM) Zeiss Ultra 55. For high-resolution imaging, in-lens secondary electron detection at an accelerating voltage (AV) of 4 kV was used. To study the chemical composition of samples, the back-scattered electron detector was used at 15 kV AV. Scanning transmission electron microscope (STEM) images were acquired by an FEI Titan Themis 200 microscope equipped with the Super X detector system for an energy-dispersive X-ray spectroscopy (EDX). For STEM measurements, biopolymer material was cut with scissors to fit in a 3 mm-diameter sample holder. Fibers were fixed by placing them between two Au grids.

#### 2.4.2. Air Permeability Testing of Electrospun Filter Materials

Air permeability testing of the materials was conducted according to the Medical Masks standard EVS-EN 14683:2019 (Estonian Centre for Standardisation and Accreditation). Before measuring, the filter mats were conditioned according to the Standard (Estonian Centre for Standardisation and Accreditation). The air permeability measurements were performed by using the measuring device FX 3340 MinAir (Textest Instruments). All measurements were performed on the sample area of 5.0 cm<sup>2</sup> with 0.272 m/s air speed. The results are presented as the arithmetic average of 5 measurements with the standard deviation.

#### 2.4.3. Testing of Aerosol Filtration Efficiency of Electrospun Filter Materials

Aerosol filtration efficiency was measured according to the standards [39], using the aerosol generator TSI model 3076, the aerosol analyzer Scanning Mobility Particle Sizer (SMPS) TSI model 3082 + Condensation Particle Counter (CPC) TSI model 3775, the dryer TSI filtered air supply 3074B, silica gel dryer TSI 3062, and the differential monometer CHY 886U. Polydisperse aerosol with a particle range of 11.8–429.4 nm was used for testing, covering a particle size of 300 nm, which N95 masks are certified to filtrate for [39].

#### 2.4.4. Hydrophobicity/Hydrophilicity Determining

The hydrophobicity/hydrophilicity of the filter materials was estimated by measuring the contact angle, using the Sessile drop method [40] with the device DataPhysics OCA 20 and SCA 20 software (DataPhysics Instruments GmbH, Filderstadt, Germany). Distilled water was used as a liquid agent to create the drop on the measured surface of the material. All measurements were performed at room temperature and the air humidity at 40%.

#### 2.4.5. Quantification of Metal Content and the Released Metal Content of the Fiber Materials

For the quantification of the metal content, the fiber materials were cut 2 × 2 cm<sup>2</sup> and incubated in 1 mL of HNO<sub>3</sub> (Nitric Acid TraceMetal Grade 67–69%, Seastar Chemicals) for 24 h at 65 °C. After incubation, the suspension was vortexed and diluted 1:1000 in 1% HNO<sub>3</sub>. The concentrations of Cu and Ag in diluted suspensions were analyzed by Atomic absorption spectroscopy (AAS) (contrAA 800, Analytik Jena Ag, Analytik Jena GmbH, Jena, Germany).

For the quantification of released metal content, the  $2 \times 2 \text{ cm}^2$  of filter material was added into 3 mL of DI water for 5 or 20 min and incubated at  $36 \text{ }^\circ\text{C}$  on a shaker. After incubation, the supernatant was dissolved (1:9) in  $\text{HNO}_3$  (Nitric Acid TraceMetal Grade 67–69%, Seastar Chemicals) for 10 min, at room temperature, and vortexed, followed by the dilution of the solutions 100 times in 1%  $\text{HNO}_3$  and analysis by AAS (contraAA 800, Analytik Jena Ag).

### 2.5. Cytotoxicity Assay

The cytotoxic effects of CuO, ZnO and Ag NPs and corresponding salts were studied by using the WST-1 assay. WST-1 reagent (Roche) was used according to the manufacturers' protocol. The cells (MDCK-2, Vero-E6, or ST) were grown to approximately 70% confluency on 96-well plates. The growth medium was removed, and metal NPs or salts at specified concentrations were diluted in the growth medium at  $100 \text{ }\mu\text{L}/\text{well}$ . Then, 48 h later, WST-1 reagent was added ( $10 \text{ }\mu\text{L}/\text{well}$ ), the cells were incubated for 3 h, and the optical density (OD) at 450 nm was determined by a Tecan Sunrise spectrophotometer. Data analysis was carried out by averaging the OD reads of triplicate wells, subtracting blank (wells without cells), and comparing the derived values with the 0-controls (cells treated with growth medium without NPs). The controls' viability was considered to be 100%, and cell viability  $<80\%$  was considered to be an indication of the cytotoxicity of the used materials.

### 2.6. Antibacterial Assay

*Escherichia coli* MG1655 strain was obtained from the genetic stock center (Yale University), and *Staphylococcus aureus* 6538 strain was obtained from the ATCC. Before the tests, the bacteria were cultivated in 3 mL of RPMI, at  $37 \text{ }^\circ\text{C}$ , with shaking at 200 rpm, overnight. Then  $400 \text{ }\mu\text{L}$  of overnight cultures was mixed with 20 mL of LB broth and incubated for 4 h to reach the exponential growth phase. After the incubation, the OD at 620 nm (OD<sub>620</sub>) was measured, and bacterial suspension at absorbance 0.1 (measured at OD 620) was prepared. A total of  $500 \text{ }\mu\text{L}$  of suspension was spread on the square Petri dish ( $10 \text{ cm} \times 10 \text{ cm}$ ) with LB agar. On the freshly inoculated LB agar, the filter materials were placed, followed by incubation for 24 h at  $37 \text{ }^\circ\text{C}$ ; the antibacterial effect of the materials was then evaluated by visual inspection.

### 2.7. Assessment of Antiviral Activity of Nanomaterials and Corresponding Salts in Suspensions

Virus stocks in cell culture medium were diluted 10 times in water; virus titers were  $6.65 \times 10^4$  pfu/mL for influenza A virus,  $8.35 \times 10^6$  pfu/mL for TGEV, and  $2.5 \times 10^5$  pfu/mL for SARS-CoV-2. The CuO-COOH, CuO-NH<sub>2</sub>, CuO, ZnO, and Ag nanomaterial suspensions and corresponding salts' (CuSO<sub>4</sub>, AgNO<sub>3</sub>, and ZnSO<sub>4</sub>) dilutions were prepared in distilled water. Viruses and nanomaterials at specified concentrations were mixed 1:1 and incubated for 1 h, at room temperature. After incubation, the viruses were titrated by plaque assays. For this, the 10-fold dilution series in VGM was prepared from the virus–nanomaterial mixtures, starting from  $10^{-1}$  to  $10^{-4}$  dilutions.

In the case of the influenza A virus and TGEV, 100% confluent cells on 12-well plates were washed with phosphate buffered saline (PBS) and infected with  $150 \text{ }\mu\text{L}$  dilution per well in duplicate for 1 h at  $37 \text{ }^\circ\text{C}$  and 5% CO<sub>2</sub> in a humidified atmosphere, gently rocking the plates every 15 min. Then infection inoculum was removed and replaced with VGM containing 1% carboxymethylcellulose (CMC); in the case of the influenza A virus, the mixture was supplemented with TPCK-trypsin at a final concentration of  $1 \text{ }\mu\text{g}/\text{mL}$ . At 96 h post-infection, the plates were stained with crystal violet, washed, and dried; the plaques were then visually counted, and the virus titers were calculated.

For SARS-CoV-2, 100% confluent Vero E6 cells grown on the 96-well plates were infected with  $25 \text{ }\mu\text{L}$  dilution per well in duplicate for 1 h at  $37 \text{ }^\circ\text{C}$  and 5% CO<sub>2</sub>, and then they were layered with 1% CMC in VGM and incubated for 48 h at  $37 \text{ }^\circ\text{C}$  and 5% CO<sub>2</sub> in a humidified atmosphere. The plates were fixed with ice-cold 80% acetone in PBS for 1 h at  $-20 \text{ }^\circ\text{C}$  and air-dried for at least 1 h. The plates were blocked with the Thermo

Scientific blocking buffer (Ref. No. 37587) and then stained with rabbit monoclonal anti-SARS-CoV-2 nucleocapsid antibody (Icosagen Ltd., R1-166-100, Tartu, Estonia) and secondary anti-rabbit IRDye800-conjugated antibody (LI-COR). The stained plates were read at 800 nm, using LI-COR Odyssey machine; the immuno-stained plaques were counted in the wells with visually distinguished single plaques, and the virus titers were calculated by taking into account the volume of viral inoculum. The data were further analyzed with GraphPad Prism 9.0 software (San Diego, CA, USA) to calculate the half maximal inhibitory concentration (IC<sub>50</sub>) for each virus and nanomaterial combination.

### 2.8. Deactivation of Viruses by Fiber Materials

The electrospun fiber materials were cut into 2 × 2 cm pieces and weighed to ensure that the weight difference of pieces was less than 10%. The autoclaved material pieces were placed onto 12-well plates. Then 30 µL of TGEV (2.5 × 10<sup>5</sup> pfu-s) or influenza A virus (1.8 × 10<sup>4</sup> pfu-s) was pipetted onto material, and 470 µL DMEM (without additives) was added. The sample was collected immediately (5 min time point), or the material piece was incubated with virus for 1 h at 28 °C, 5% CO<sub>2</sub>, in a humidified atmosphere. The samples were collected from the well by pipet. Then a material piece was placed in a 1.5 mL tube; centrifuged for 3 min at 13,400 × g; and the liquid samples were combined, mixed, and titrated by plaque assay.

To evaluate the antiviral activity of materials against SARS-CoV-2, the materials were cut into 2 × 2 cm pieces and placed into 50 mL falcon tubes. Then 30 µL of SARS-CoV-2 virus stock was added. For the 0 h time point, the sample was processed immediately, and for the 1 h time point, the samples were incubated at 28 °C by adding 470 µL of PBS, followed by brief vortexing and centrifugation at 3200 × g for 3 min at room temperature. Supernatants were collected to the tubes, and 10-fold dilutions were prepared in VGM (final volume of 200 µL). For the plaque assay, the Vero E6 cells seeded on a 96-well plate on the previous day were incubated with 100 µL diluted sample/well for 1 h at 37 °C in a humidified 5% CO<sub>2</sub> atmosphere. After incubation, the cells were overlaid with VGM/1% CMC solution and incubated for 48 h at 37 °C in a humidified 5% CO<sub>2</sub> atmosphere. The cells were fixed with ice-cold 80% acetone/PBS at −20 °C for 1 h, followed by an immunoplaque assay with anti-SARS-CoV2-N 82C3 (Icosagen Ltd., R1-166-100), as described above.

### 2.9. Statistical Analysis

IC<sub>50</sub> was calculated by using GraphPad Prism 9.0 software, and *p*-values were calculated in Excel, using Student's *t*-test.

## 3. Results

### 3.1. Antiviral Efficacy of Nanoparticles in Suspensions

The physicochemical properties of NPs were characterized by our group before [41,42] and are summarized in Supplementary Table S3. The antiviral properties of metal NPs and corresponding salts were investigated by a plaque assay first in suspensions against influenza A virus and coronaviruses TGEV and SARS-CoV-2. TGEV was used as a model for coronavirus susceptibility evaluation—as a safer Biosafety Level 2 (BSL2) model for a coronavirus. Metal salts were used as controls to the NPs tested. The absence of cytotoxicity of tested compounds was confirmed on cell lines *in vitro* since the infection of cells by virus in suspension with tested compounds was an integral part of the plaque assay. The testing of metal compounds' antiviral efficacies in suspensions was performed at the 1-hour time point, as we were aiming to generate and test materials with high efficacies.

The testing in suspensions showed that the most potent metal salt against all viruses, *i.e.*, A/WSN/1933 (H1N1), SARS-CoV-2, and TGEV, was CuSO<sub>4</sub> (IC<sub>50</sub> 1.40, 0.45, and 4.44 mg/L, respectively) (Table 1), indicating the superiority of copper and, more precisely, copper ions in the antiviral testing setup. Please refer to the dose response curves in Supplementary Figures S1–S3. Thus, CuO, CuO-NH<sub>2</sub>, or CuO-COOH were less effective against tested viruses than CuSO<sub>4</sub> (with the exception of CuO-COOH that has IC<sub>50</sub> value

0.57 mg/L for A/WSN/1933 (H1N1)) (Table 1). This might be due to the fact that carboxylation has additional antiviral efficacy, as COOH groups readily bind to viral RNA [43].

**Table 1.** Antiviral efficacy of metal salts and metal nanoparticles against influenza A virus, SARS-CoV-2, and TGEV in water suspensions.

Substance	IC50 (mg/L)		
	Influenza A Virus	SARS-CoV-2	TGEV
CuSO <sub>4</sub>	1.40	0.45	4.44
CuO	49.25	>100	383.4
CuO-NH <sub>2</sub>	1.88	149.1	8.8
CuO-COOH	0.57	79.68	13.75
ZnSO <sub>4</sub>	3.39	35.65	ND
ZnO	134.8	ND	ND
AgNO <sub>3</sub>	>100	NA	>100
Ag NP	>1000	NA	NA

NA—not applicable: since Ag NPs and AgNO<sub>3</sub> were toxic to VeroE6 cells used for tests with SARS-CoV-2 already at 10 mg/L. ND—not determined.

Silver is a well-known antibacterial and a promising agent in the fight against coronavirus, whereas, in our study, the AgNO<sub>3</sub> salt was not effective even in the highest concentration tested (100 mg/L) and did not reduce the titers of A/WSN/1933 (H1N1) and TGEV enough to calculate IC50. The other metal in the study, Zn salt, ZnSO<sub>4</sub>, was less effective against the tested influenza and coronavirus compared to CuSO<sub>4</sub> (Table 1). Hence, we selected copper compounds as a salt CuSO<sub>4</sub> and CuO NPs for incorporation into filter materials.

### 3.2. Development and Characterization of Filter Materials

#### 3.2.1. Compatibility of NPs with Solvent Systems for Preparation of the Filter Materials

Next, CuSO<sub>4</sub> and CuO NPs were incorporated into 17% CA polymer to produce filter materials. First, the compatibility of CA polymers in dispersions of acetone–DMAc (Ac–DMAc) solvent systems with NPs and metals was tested. The NH<sub>2</sub> and COOH functionalized and unfunctionalized CuO NPs in suspensions and CuSO<sub>4</sub> were evaluated by DLS in solvent systems compatible with CA for 24-h and 1-week time points (Supplementary Table S1). The functionalized NPs CuO-NH<sub>2</sub> and CuO-COOH formed aggregates in solvents, as exemplified by the high polydispersity index (PDI) values (0.7–1) and, thus, were not suitable for electrospinning. Hence, surface-functionalized NPs were not used to produce fiber materials, whereas the unfunctionalized CuO NPs, and especially CuSO<sub>4</sub> salt, demonstrated excellent compatibility to be incorporated into CA filter materials and were used for generating the fiber materials.

#### 3.2.2. Development of Filter Materials

Filter materials were produced by using electrospinning techniques and CA as a polymer carrier for CuSO<sub>4</sub> and CuO NPs (Table 2). Moreover, thymol was used for the electrospinning of filter materials to raise the porosity and hydrophilicity of the nanofibers, as previously described [44]. We hypothesize that by increasing porosity, thymol will improve metal release and, thus, antimicrobial properties of filter materials, and by raising the hydrophilicity, we will obtain better release of the metal ions to inactivate the virus efficiently. The developed filter materials were named as follows: CA (CA without antimicrobial components); CA\_7.5%CuSO<sub>4</sub> (CA with 7.5% CuSO<sub>4</sub>); CA\_10%CuO (CA with 10% CuO); CA\_thymol (CA with 10% thymol); and CA\_thymol\_7.5%CuSO<sub>4</sub> (CA with 10% thymol and 7.5% CuSO<sub>4</sub>). All shown percentages were calculated based on Cu content.

**Table 2.** Characteristics of electrospun filter materials.

Samples	Mat Thickness	SEM Diameter	Air Permeability	Aerosol Filtration Efficiency, %	Aerosol Filtration Efficiency, %	Hydrophobic/Hydrophilic Measuring	Contact Angle Measuring
	mm	nm	Pa/cm <sup>2</sup>	whole range 11.8–429.4 nm	300 nm		°
CA	0.051	750	125.0	99.3	99.6	hydrophobic	104
CA_7.5% CuSO <sub>4</sub>	0.062	972	54.1	84.3	85.5	hydrophobic	107
CA_10% CuO	0.163	759	47.4	78.4	81.6	hydrophobic	99
CA_thymol	0.036	545	45.4	ND *	ND	hydrophilic	82
CA_thymol_7.5% CuSO <sub>4</sub>	ND	431	55.9	ND	ND	hydrophilic	86

\* ND—not determined, CA—cellulose acetate.

The maximum nominal concentration of Cu from CuSO<sub>4</sub> and CuO that we were able to incorporate into CA was up to 8% (Table 3). Namely, when 7.5% of Cu from CuSO<sub>4</sub> was added to CA polymer solutions (sample designated CA\_7.5%CuSO<sub>4</sub>), the measured concentration of Cu in the final filter material was 4.68%. Thymol remarkably improved the incorporation of CuSO<sub>4</sub> into CA; with the addition of 7.5% of Cu from CuSO<sub>4</sub> to CA with thymol, the measured concentration of Cu in this filter material was very close to nominal, 7.38%. The filter materials were characterized for fiber morphologies, material thickness, hydrophilicity/hydrophobicity, and air-filtration parameters (Table 2). Thymol improved the hydrophilicity of the materials and the release of Cu 1.7 times compared to CA fibers without thymol (Tables 2 and 3).

**Table 3.** The metal content and release of copper ions from CA filter materials.

Fiber Material	Cu Content, %	Released Cu Content, 1 h, %
CA	0	ND
CA_7.5%CuSO <sub>4</sub>	4.68 ± 1.1	46
CA_10%CuO	8.01 ± 0.39	0
CA_thymol	0	ND
CA_thymol_7.5%CuSO <sub>4</sub>	7.38 ± 0.61	78

ND—not determined.

### 3.2.3. Morphology of Filter Materials

Scanning electron microscopy (SEM) was used to assess the morphology of fibers of filter materials (Figures 1 and 2 and Supplementary Figure S4). According to SEM, all fibers had random orientation (Figures 1 and 2). The average diameter of the fibers was 600 nm, giving one of the biggest advantages of nanoscale: through the addition of a small quantity of metals or NPs to maximize specific functionalities on a high scale. We confirmed by EDX that filter materials with CuSO<sub>4</sub> and CuO contained a high concentration of Cu (Figure 1D,F), whereas CA alone contained only traces of Cu (Figure 1B). In addition, CuO NPs were clearly visible in the case of CA with CuO NPs (Figure 1E). The addition of thymol in the CA materials did not increase the porosity of material, but it altered the surface structure of the fibers, giving more specific surface area for the material and virus interaction to take place (Figure 2).

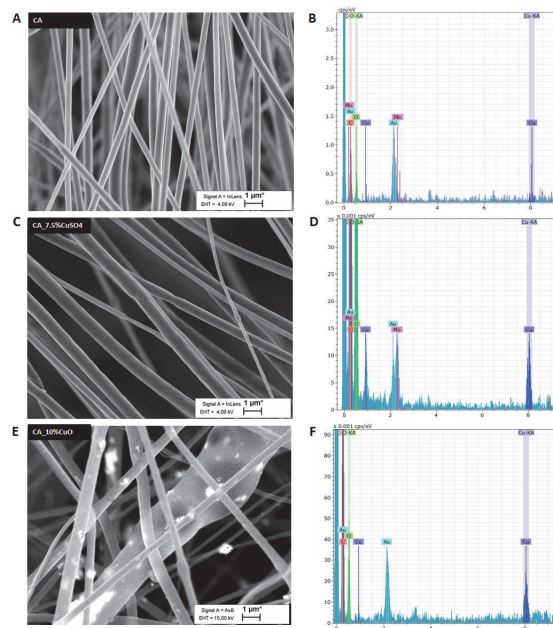


**Figure 1.** Morphological characteristics by SEM imaging for electrospun CA filter mats (panels A,C,E) and EDX analysis of the mats (panels B,D,F). Please refer to the different scales on the y-axis.

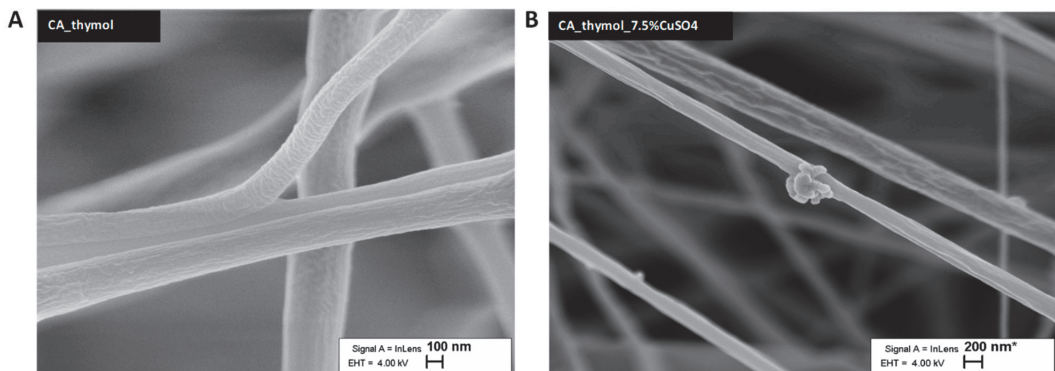


**Figure 2.** Morphological characteristics by SEM imaging for electrospun CA filter mats comprising thymol (A) and  $\text{CuSO}_4$  (B) as additives, showing the texture change on the surface.

### 3.2.4. Thickness, Hydrophilicity, and Air Filtration Parameters of Filter Materials

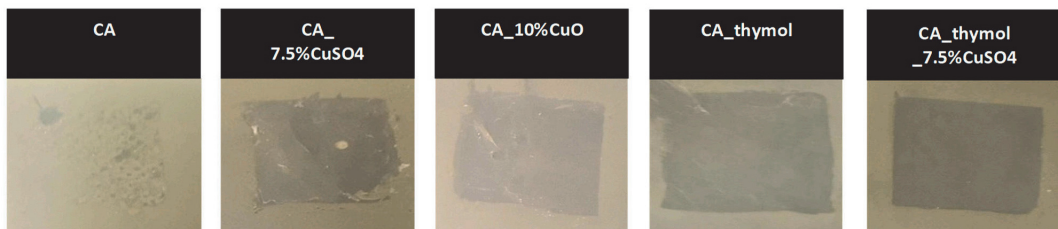
The filtration performances were measured by determining the penetration of 1% NaCl aerosol particles, using an Aerosol generator TSI model 3076. The air permeability and the particle filtration efficiency were associated with the mat thickness having higher air permeability and filtration efficiency for mats with ca. 0.05 mm thickness. The thickness of the produced mats was very similar, being in the range of 0.04–0.06 mm with the exception of  $\text{CA}_{10\%}\text{CuO}$  (0.163 mm). The small variation of this parameter can be explained with non-uniform distribution of additives in the electrospun material as the handmade electrospun device with rotating drum collector was used. In this study, the aim was to use electrospinning technique for producing protective material with nanosize fibers comprising different additives. The choice of the electrospinning parameters depended on the solution properties, viscosity, and the distribution/mixing/compatibility of the used

additives in the polymer solutions. Thus, the changing of the flow rate enabled us to adjust to these parameters (Supplementary Table S2). Compared to the materials of CA without Cu compounds, the air permeability of Cu-containing CA materials decreased around 2.5 times but was still acceptable [45]. Thus, the materials had acceptable performance parameters and were used in further tests (Table 2).

### 3.3. Antibacterial Efficacy of Filter Materials Comprising Copper NPs and Copper Salt

In the next step, the antibacterial activity of developed filter materials was studied against *E. coli* and *S. aureus*. The antibacterial activity of the materials against bacteria was assessed on agar diffusion assay and is visualized in Figure 3. As expected, CA alone (control) did not inhibit the growth of bacteria. All other filter materials had excellent antibacterial activity against both *E. coli* and *S. aureus*. Interestingly, CA with thymol had an antibacterial effect even without the incorporation of Cu compounds. The best antibacterial effect (the largest bacteria-free zone) was observed in the case of CA with CuSO<sub>4</sub> and CA with thymol and CuSO<sub>4</sub>.

#### *Escherichia coli* K12



#### *Staphylococcus aureus* (ATCC 25923)

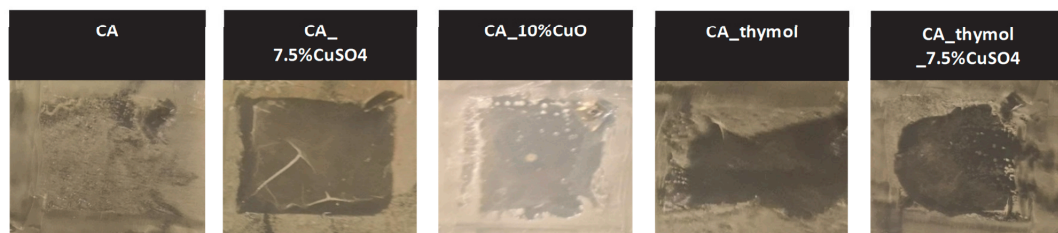


**Figure 3.** Antibacterial activity of filter materials against bacteria *Escherichia coli* and *Staphylococcus aureus*. The filter materials were removed for the images to demonstrate the bacteria-free area under the materials.

### 3.4. Antiviral Efficacy of Fiber Materials Comprising Antimicrobial Metals

Previously, the antiviral efficacy was measured for nanoparticles in suspensions (Table 1). The antiviral activity of the produced filter materials against A/WSN/1933 (H1N1), SARS-CoV-2, and TGEV viruses was studied by incubating virus stock with the material and determination of the effect on virus titer by plaque assay. The best virucidal effect (virucidal effect is expressed as reduction of viral titers after 5 min and 1 h of exposure) was observed in the case of CA with CuSO<sub>4</sub> and CA with thymol and CuSO<sub>4</sub> (Figure 4). Materials comprising CuSO<sub>4</sub> reduced influenza A virus titers 1.1–1.8 log already after 5 min of exposure and 1.6–1.8 log after 1 h of exposure (Figure 4A). From three tested viruses, the virucidal effect of all filter materials on TGEV was the lowest: 5-minute exposure resulted in no significant virus titer reduction, and mild 0.2 log reduction was observed after 1-hour exposure for CA

material with  $\text{CuSO}_4$ ; and no effect was observed when thymol was the additive for the same material (Figure 4C). From the tested viruses, the best virucidal effect of filter materials was observed for SARS-CoV-2: CA fibers with 7.5% Cu from  $\text{CuSO}_4$  completely eliminated infectivity of SARS-CoV-2 after 1 h of contact exposure, and CA\_thymol\_7.5% $\text{CuSO}_4$  material reduced the titer by 1.14 logs (Figure 4B). Interestingly, different from filter materials comprising  $\text{CuSO}_4$ , the materials of CA with 10% CuO were not effective against any of the tested viruses (Figure 4). The addition of thymol alone to the CA material, however, reduced A/WSN/1933 (H1N1) titer approximately 0.7 logs compared to the CA control material without additives, but the difference was not statistically significant (Figure 4A). Thymol's antiviral effect was limited to the influenza virus in our experiments, as the CA\_thymol material did not reduce the titers of coronaviruses, indicating the importance of hydrophobicity in the antiviral efficacy [46]. We suggest that the influenza virus is more susceptible to released Cu ions, and SARS-CoV-2 is more susceptible to the hydrophobic interactions of the material. To summarize, similar to the antibacterial properties, filter materials with  $\text{CuSO}_4$  demonstrated the best antiviral properties (Figure 4), and, additionally, material hydrophilicity and hydrophobicity played a role.

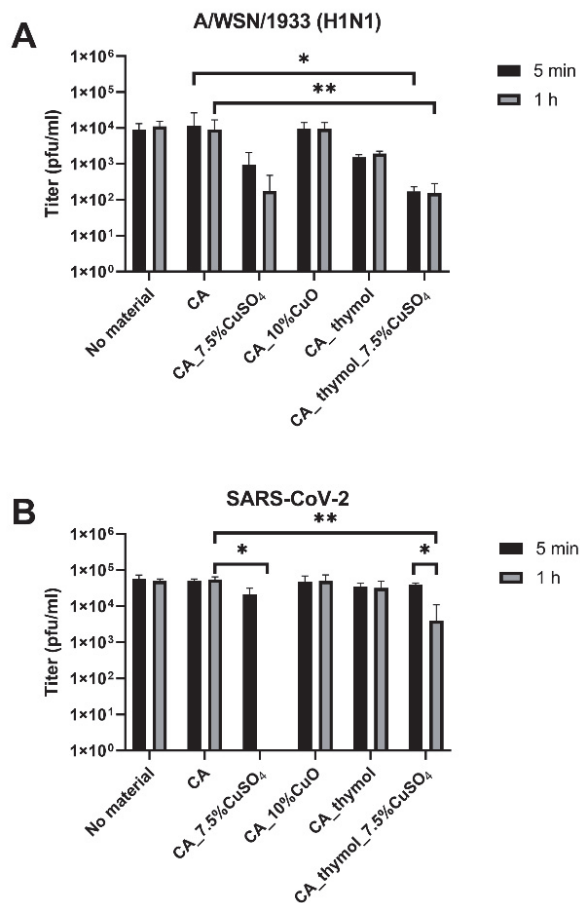
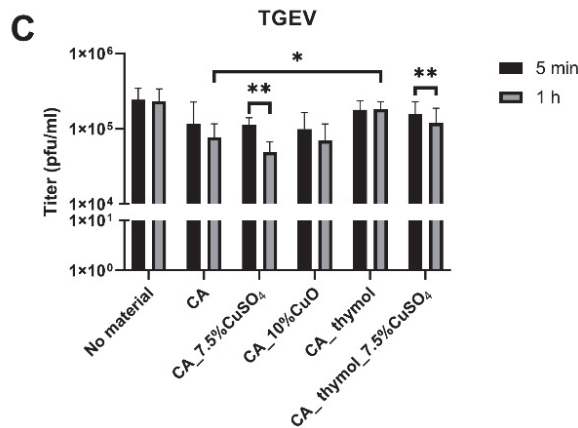


Figure 4. Cont.





**Figure 4.** Antiviral properties of CA without additives (control), 7.5% CuSO<sub>4</sub> and 10% CuO in CA against influenza A/WSN/1933 (H1N1) virus (A), SARS-CoV-2 (B), and transmissible gastroenteritis coronavirus TGEV (C). Statistical significance is represented as follows: \*  $p < 0.05$ ; \*\*  $p < 0.01$ .

#### 4. Discussion

Influenza A virus is a respiratory virus that has caused several historic outbreaks, such as the Spanish flu in 1918, the 1977 Russian flu pandemic, and the 2009 swine flu pandemic. SARS-CoV-2 has caused over 600 million human infections and at least 6.5 million deaths in less than 3 years. The rapid spread of these viruses serves as evidence of the highly effective spread that occurs mostly (or at least partly) by the droplet-transmission ways [47,48]. Hence, the development of antiviral filter materials and face masks could be an option to suspend the transmission of these viruses, their variants, and other airborne pathogens. The use of antiviral and antimicrobial masks from environmentally friendly materials will significantly reduce the adverse environmental impact and the risk of contamination during their handling and disposal, as this is an important concern during the pandemic [49]. These masks could aid to protect the public health in community settings and in various healthcare settings. For example, the face masks based on these filter materials may be used in hospitals even beyond the pandemic caused by SARS-CoV-2 in order to prevent hospital-acquired infections. The bacteria *Escherichia coli* and *Staphylococcus aureus* are the major causes of hospital-acquired infections [50]. The pathogenic strains of *E. coli* have been associated with pneumonia and the pathogenic strains of *S. aureus* with pneumonia and meningitis. Due to the differential membrane structures of *E. coli* and *S. aureus*, they represent the Gram-negative and the Gram-positive bacteria, respectively. Thus, we used these two bacteria as models to study the antibacterial properties of the developed filter materials. To investigate the antiviral properties of the developed materials, we used two respiratory viruses: influenza A/WSN/1933 (H1N1) virus and SARS-CoV-2 and TGEV, a coronavirus mostly transmitted by oral route.

It has been reported that, depending on the surfaces, the human coronaviruses can remain infectious for up to 9 days [51], and influenza A virus can for up to 2 days [52], whereas survival is longest on the most common surfaces, such as wooden, stainless steel, and plastic. One way is to tackle the transmission of pathogens by impairing the infectious properties of these viruses and bacteria by new antimicrobial materials. The virucidal properties of fiber materials comprising metals have been investigated in previous studies. For example, Hodek et al. showed that protective hybrid coating prepared via sol-gel method and applied on glass slides or into the wells of polymethyl methacrylate plates containing silver, copper, and zinc cations effectively inactivated HIV and other enveloped viruses [33,53]. That brought us to the current study to test Ag, Zn, and Cu compounds as potential antivirals against SARS-CoV-2, TGEV, and other enveloped viruses first in suspensions and to use the most promising of them to incorporate into polymers to produce

filter materials for face masks. These filter materials were intended to inactivate respiratory viruses, as well as common bacterial pathogens causing hospital acquired infections.

In our study, the metals were first tested in the suspensions. Somewhat surprisingly, Ag, the most widely used antibacterial metal, was not efficient to inhibit viruses used in our tests that showed (in suspensions) IC<sub>50</sub> values >100 mg/L for AgNO<sub>3</sub> against A/WSN/1933 (H1N1) and TGEV, and >1000 mg/L for Ag NP-s against influenza A virus. The reason could be that the antibacterial activity of Ag and Cu is strongly attributed to the release of ions and their effect on cellular components and processes. In this regard, virus particles having no metabolic activities are drastically different from bacteria. Ag ions interfere with metabolic processes such as energy generation and cell proliferation, which are important for bacteria but not for virus particles. In contrast, Cu ions have been reported to damage the virus capsid and envelope [54]. Indeed, Cu compounds were effective against influenza A virus from 0.57 to 49.25 mg/L, depending on the compound and functionalization of the NPs, and they showed the lowest IC<sub>50</sub> for CuO-COOH (Table 1). Of the tested Cu compounds, CuSO<sub>4</sub> was the most efficient against SARS-CoV-2 (IC<sub>50</sub> 0.45 mg/L) and, to a lesser extent, against TGEV (IC<sub>50</sub> 4.44 mg/L). In our experiments influenza virus was more sensitive to CuO NPs with or without NH<sub>2</sub> or COOH modifications than coronaviruses. The high sensitivity of this virus to these compounds is most probably due to the rapid release of Cu ions from CuO-COOH [41] and COOH properties to effectively bind RNA of SARS-CoV-2 [55], thus impairing the propagation of the virus. The CuO-NH<sub>2</sub> actively releases the Cu ions and generates more ROS damaging the virus compared to unfunctionalized CuO [41]. Zn compounds were less effective than Cu compounds against A/WSN/1933 (H1N1), having IC<sub>50</sub> values from 3.39 to 134.8 mg/L after 1 h of contact. Zn is also generally less potent metal against bacteria as compared to Cu and Ag [19,56], and its modest antiviral activity in the current study is in concurrence with the previous report where ZnO had 50% activity against influenza A virus at 75 mg/L concentration after 4 h of exposure [57].

Our findings confirmed the excellent antiviral properties of copper and are in agreement with those of multiple studies [23,34,36,58–63]. This might be due to copper's capability to generate reactive oxygen species (ROS) in a moist environment, which oxidizes the capsid proteins of viruses [64]. Cu destroys the replication abilities by interacting with the hereditary material and propagation abilities of SARS-CoV and disturbs the host and virus interaction and, thus, internalization of the viral particles of influenza and other respiratory viruses [65]. Fujimori et al. investigated the antiviral activity of copper iodide (CuI) nanoparticles of 160 nm in size against swine influenza virus, whereas CuI nanoparticles inactivated the virus in a dose-dependent manner, and the total inactivation was observed after 1 h of contact for 100 mg/L concentration [23]. The antiviral activity of CuI nanoparticles was mainly attributed to the release of one-valent copper ions, which lead to the generation of ROS that caused the oxidation of viral proteins and the damage of the viral RNA. Thus, there is a high potential of copper to be used as an antiviral agent in face masks to impair the airborne disease transmission of influenza and coronaviruses in hospitals and in household settings [62].

For enhanced effects and targeted applications, CuSO<sub>4</sub> and CuO NPs were incorporated into polymers to develop functional antimicrobial materials. Compared to traditional biocides, antimicrobial polymers have advantages such as enhanced antimicrobial activity, prolonged release of active substances, and the avoidance of resistance [66,67]. Based on the literature data and on our tests of different metals and NPs in suspensions (Table 1), we selected Cu compounds for incorporation into CA, a modified natural polymer that is biodegradable and therefore has environmentally friendly properties. As a fiber, it is used in textiles for its low price, softness, comfort, ease for modifications, and ability to provide controlled release of incorporated compounds [68,69]. Therefore, we developed CA filter materials comprising CuO and CuSO<sub>4</sub> and tested them for antibacterial and antiviral activities. CuO was chosen as an additive to the polymer because of the tested Cu compounds the COOH- and NH<sub>2</sub>-functionalized CuO NPs had excellent antiviral properties in suspension.

To produce face masks with copper, COOH- NH<sub>2</sub>-functionalized and unfunctionalized CuO NPs and CuSO<sub>4</sub> were first tested for their compatibility with CA polymer and solvent systems. Acetone and DMAc were selected as solvents, since DMAc is readily adjustable to electrospinning with a wide range of polymers for filtering purposes and acetone is added to the solvent system to facilitate fiber formation and filter material synthesis in electrospinning. However, both CuO NPs with surface functionalization demonstrated incompatibility with the selected solvent system by forming large aggregates, as reflected in large hydrodynamic size and high polydispersity indexes (Supplementary Table S1).

Hence, CA filter materials with CuSO<sub>4</sub> and CuO NPs were produced, with or without thymol demonstrating good air permeability and particle filtration properties (Table 2). All materials with Cu compounds posed high antibacterial activity against *E. coli* and *S. aureus*, with the CuSO<sub>4</sub>-based material having the highest efficacy (Figure 4). While CuO NP-based filter materials did not exhibit antiviral properties, CuSO<sub>4</sub>-based filter materials showed some efficacy against A/WSN/1933 (H1N1) (titer reduced ca. 1.7 log) and differing efficacy against coronaviruses after 1 h of contact. The high efficacy of CuSO<sub>4</sub>-containing materials against bacteria and viruses was due to the high release of Cu from the materials containing CuSO<sub>4</sub> (46–78% after 1 h), whereas no release of the ions was detected for fibers containing CuO (Table 3). Since tests with SARS-CoV-2 were very demanding and necessitated BSL-3 conditions and infrastructure, we also attempted to use coronavirus TGEV as a model coronavirus to screen compounds and filter materials before tests with SARS-CoV-2. Antiviral properties of CuSO<sub>4</sub>-based filter materials against TGEV were low: less than 1 log reduction in titer after 1-h exposure. In contrast, the SARS-CoV-2 titer decreased to the point of being not detectable after exposure to CA\_7.5%CuSO<sub>4</sub> material and approximately 1.1 log after 1 h of exposure to CA\_thymol\_7.5%CuSO<sub>4</sub> material (Figure 4). Our data indicate that, as a surrogate model for SARS-CoV-2, TGEV is inferior to no-related influenza A virus that uses the same entry route as SARS-CoV-2. We assume the difference in SARS-CoV-2 and TGEV susceptibility to CuSO<sub>4</sub> containing materials is because TGEV similarly to other viruses that spread in fecal–oral way is in general less susceptible to antivirals, since it is adapted to the harsh conditions of gastrointestinal tract [70].

To improve the antiviral efficacy of the material, thymol was added to CA. Thymol is considered to be an excellent additive as it possesses inherent antibacterial activity as shown by others [71] and in our study (Figure 3). Moreover, thymol facilitates material hydrophilicity that in general enhances antiviral activity [72–75] and porosity that increases the active surface area [44]. Thus, we used the thymol to increase hydrophilicity, hypothesizing that it will increase the release of antiviral Cu ions.

Indeed, in our study addition of thymol increased the hydrophilicity of filter materials (Table 2) but did not improve their antiviral and antibacterial properties (Figures 3 and 4). Surprisingly, in case of SARS-CoV-2, thymol even reduced the antiviral properties of CA with CuSO<sub>4</sub> 1.14 log after 1 h of contact (Figure 4B). From the literature, it is known that hydrophobic properties of materials enable a better contact with the lipid parts of viruses and bacteria, whereas the hydrophilic properties facilitate a better release of metal ions from the fibers [72,75]. Indeed, in our study, the addition of thymol increased the release of Cu ions (Table 3) but did not improve antiviral properties. Based on these data, we assume that, in addition to Cu release from filter materials, the major factor determining antiviral properties is hydrophobicity. We suggest that hydrophobicity of the material determined antiviral efficacy against SARS-CoV-2 (hydrophobic material without thymol was more effective) and is consistent with the previous literature [18]. Presumably, the effect of hydrophobicity/hydrophilicity is different for different viruses, depending on the properties of their envelope [33,53]. SARS-CoV-2 has a hydrophobic lipid envelope, and we assume that hydrophobic filter materials enabled better virus–material contact, enhancing antiviral properties of material.

The successful antiviral efficacy of materials comprising copper compounds that was demonstrated in this study is consistent with the previous literature. For example, masks containing ca. 2% weight/weight (*w/w*) copper particles spunbond in polypropylene fabric

in fiber layers showed antiviral properties: a 2.88 log and 3.13 log additional reduction of infectivity of human influenza A virus were observed after 30 min of exposure as compared to the control masks without copper nanoparticles [58]. To the best of our knowledge, biopolymer-based CuSO<sub>4</sub>-containing CA filter materials developed in this study are unique and have not been reported in the literature. The CA filter material containing 7.5% CuSO<sub>4</sub> had excellent antibacterial properties (Figure 3), completely inactivated SARS-CoV-2 (Figure 4B), and caused 1.6 log reduction of A/WSN/1933 (H1N1) virus titers (Figure 4A) after 1 h of exposure, providing broad-spectrum protection from air-borne pathogens. These properties are similar and consistent with previously described analogous materials. Self-sterilizing photoactive nanomask composed of biopolymer Shellac showed ca. 2–3 log decreased viability of *E. coli* after 1 h of exposure and loss of infectivity of virus-like particles after 5 min of exposure [76]. The mask fibers containing licorice root in the composition of biocompatible polymers [77] and face masks containing copper [78] or quaternary ions [79] have also been demonstrated to possess antiviral efficacies against SARS-CoV-2 virus. In the study of Jung et al., the authors coated the filter layer of commercially available face masks from synthetic polypropylene with a thin film of copper and demonstrated that SARS-CoV-2 titer was reduced by more than 75% after 1 h of exposure to this mask [78].

In summary, the incorporation of CuSO<sub>4</sub> into filter materials is a promising mean to obtain materials that prevent spread of enveloped viruses, such as influenza viruses; coronaviruses, including SARS-CoV-2; and bacteria such as *E. coli* and *S. aureus*.

## 5. Conclusions

Here we presented valuable data on virucidal effects of Zn, Cu, and Ag salts and respective NPs to three viruses, TGEV, influenza A virus, and SARS-CoV-2. Out of the tested compounds, the CuSO<sub>4</sub> and CuO NPs had the best antiviral properties and compatibility with the electrospinning technique, followed by Zn and Ag, and thus, they were selected to develop novel filter materials as an intervention to mitigate the spread of pathogens such as viruses A/WSN/1933 (H1N1), SARS-CoV-2, and TGEV and the bacteria *E. coli* and *S. aureus*. As a main result of the study, novel filter materials based on biopolymer cellulose acetate and incorporating CuSO<sub>4</sub> or CuO NPs were developed. CuSO<sub>4</sub>-based filter materials were the most effective against SARS-CoV-2 and reduced virus titers already after 5 min of exposure and completely inactivated the virus after 1 h of exposure. Our data on antiviral and antibacterial properties of metals, metal-based NPs, and filter material thereof will help to govern the future development of advanced antibacterial and antiviral materials and surfaces.

**Supplementary Materials:** The following supporting information can be downloaded at: <https://www.mdpi.com/article/10.3390/pharmaceutics14122549/s1>. Table S1: Dynamic light scattering (DLS) for evaluation of nanoparticles in suspensions for producing filter materials. Table S2: Operating parameters for electrospinning of the filter materials. Table S3: Physicochemical properties characterization of nanoparticles in suspensions. Figure S1: Antiviral properties of metal compounds against A/WSN/1933 (H1N1) virus in water suspensions. Note the differences in units (concentration of CuO and ZnO is shown in mg/l). Figure S2: Antiviral properties of metal compounds against TGEV virus in water suspensions. Note the differences in units. Figure S3: Antiviral properties of metal compounds against SARS-CoV-2 virus (Estonian strain 3049) in water suspensions. Figure S4: Scanning electron micrograph of CA fibers. References [41,80] are cited in the supplementary materials.

**Author Contributions:** Conceptualization, A.-L.K.; Data curation, K.R. and E.Ž.; Formal analysis, K.R.; Funding acquisition, O.B.; Investigation, A.-L.K., E.Ž., G.V., T.P., A.K. and O.B.; Methodology, K.R., N.S., E.Ž., G.V., M.V., T.P. and A.M.; Project administration, O.B.; Resources, A.K. and A.M.; Supervision, A.K., A.M. and O.B.; Validation, O.B.; Visualization, A.-L.K. and K.R.; Writing—original draft, A.-L.K. and K.R. All authors have read and agreed to the published version of the manuscript.

**Funding:** This work was supported by the grant COVSG16 from the Estonian Research Council, the Development Grant Arengufond\_OB from the National Institute of Chemical Physics and Biophysics (Estonia), and by the European Regional Development Fund project “Emerging orders in quantum and nanomaterials” (TK134).

**Institutional Review Board Statement:** Not applicable.

**Informed Consent Statement:** Not applicable.

**Data Availability Statement:** Not applicable.

**Acknowledgments:** We acknowledge Aile Tamm and Mihkel Rähn for scanning transmission electron microscopy measurements at the University of Tartu, Institute of Physics; Angela Ivask and Merilin Rosenberg (University of Tartu, Estonia) for fruitful discussions and Araik Karapetjan and Ruslan Nenahhov (AS Esfil Tehno, Estonia) for technical advices during development of filter materials.

**Conflicts of Interest:** The authors declare no conflict of interest.

## References

- Menachery, V.D.; Yount, B.L.; Debbink, K.; Agnihothram, S.; Gralinski, L.E.; Plante, J.A.; Graham, R.L.; Scobey, T.; Ge, X.Y.; Donaldson, E.F.; et al. A SARS-like Cluster of Circulating Bat Coronaviruses Shows Potential for Human Emergence. *Nat. Med.* **2015**, *21*, 1508–1513. [[CrossRef](#)] [[PubMed](#)]
- Xia, X. Domains and Functions of Spike Protein in SARS-CoV-2 in the Context of Vaccine Design. *Viruses* **2021**, *13*, 109. [[CrossRef](#)] [[PubMed](#)]
- Sternberg, A.; Naujokat, C. Structural Features of Coronavirus SARS-CoV-2 Spike Protein: Targets for Vaccination. *Life Sci.* **2020**, *257*, 118056. [[CrossRef](#)] [[PubMed](#)]
- Wan, Y.; Shang, J.; Graham, R.; Baric, R.S.; Li, F. Receptor Recognition by the Novel Coronavirus from Wuhan: An Analysis Based on Decade-Long Structural Studies of SARS Coronavirus. *J. Virol.* **2020**, *94*, e00127–20. [[CrossRef](#)] [[PubMed](#)]
- Li, R.; Pei, S.; Chen, B.; Song, Y.; Zhang, T.; Yang, W.; Shaman, J. Substantial Undocumented Infection Facilitates the Rapid Dissemination of Novel Coronavirus (SARS-CoV-2). *Science* **2020**, *368*, 489–493. [[CrossRef](#)]
- Ochani, R.K.; Yasmin, F.; Jatoi, N.N. Epidemic Amidst the Coronavirus Disease-19 Pandemic. *J. Glob. Health* **2021**, *11*, 03056. [[CrossRef](#)]
- Hasöksüz, M.; Kiliç, S.; Saraç, F. Coronaviruses and SARS-CoV-2. *Turkish J. Med. Sci.* **2020**, *50*, 549–556. [[CrossRef](#)]
- Khan, M.; Syed, F.A.; Hamad, Z.A.; Muhammad, N.T.; Saif, S.; Khan, M.; Khan, S.T. Epidemiology and Progress So Far. *Moléculas* **2021**, *26*, 39. [[CrossRef](#)]
- WHO. Mask Use in the Context of COVID-19. Available online: <https://extranet.who.int/iris/restricted/handle/10665/331789> (accessed on 3 May 2022).
- CDC. Coronavirus Disease 2019 Recommendation Regarding the Use of Cloth Face Coverings, Especially in Areas of Significant. Available online: <https://stacks.cdc.gov/view/cdc/86440> (accessed on 3 May 2022).
- Gholamreza, F.; Nadaraja, A.V.; Milani, A.S.; Golovin, K. Enhanced Protection Face Masks Do Not Adversely Impact Thermophysiological Comfort. *PLoS ONE* **2022**, *17*, e0265126. [[CrossRef](#)]
- Neuman, B.W.; Adair, B.D.; Yoshioka, C.; Quispe, J.D.; Orca, G.; Kuhn, P.; Milligan, R.A.; Yeager, M.; Buchmeier, M.J. Supramolecular Architecture of Severe Acute Respiratory Syndrome Coronavirus Revealed by Electron Cryomicroscopy. *J. Virol.* **2006**, *80*, 7918–7928. [[CrossRef](#)]
- Siddharta, A.; Pfaender, S.; Vielle, N.J.; Dijkman, R.; Friesland, M.; Becker, B.; Yang, J.; Engelmann, M.; Todt, D.; Windisch, M.P.; et al. Virucidal Activity of World Health Organization-Recommended Formulations Against Enveloped Viruses, Including Zika, Ebola, and Emerging Coronaviruses. *J. Infect. Dis.* **2017**, *215*, 902–906. [[CrossRef](#)]
- Rai, M.; Deshmukh, S.D.; Ingle, A.P.; Gupta, I.R.; Galdiero, M.; Galdiero, S. Metal Nanoparticles: The Protective Nanoshield against Virus Infection. *Crit. Rev. Microbiol.* **2016**, *42*, 46–56. [[CrossRef](#)] [[PubMed](#)]
- Jarach, N.; Dodiuk, H.; Kenig, S. Polymers in the Medical Antiviral Front-Line. *Polymers* **2020**, *12*, 1727. [[CrossRef](#)] [[PubMed](#)]
- Chakravarty, M.; Vora, A. Nanotechnology-Based Antiviral Therapeutics. *Drug Deliv. Transl. Res.* **2021**, *11*, 748–787. [[CrossRef](#)] [[PubMed](#)]
- Nasri, N.; Rusli, A.; Teramoto, N.; Jaafar, M.; Ishak, K.M.K.; Shafiq, M.D.; Hamid, Z.A.A. Past and Current Progress in the Development of Antiviral/ Antimicrobial Polymer Coating towards COVID-19 Prevention: A Review. *Polymers* **2021**, *13*, 4234. [[CrossRef](#)]
- Chua, M.H.; Cheng, W.; Goh, S.S.; Kong, J.; Li, B.; Lim, J.Y.C.; Mao, L.; Wang, S.; Xue, K.; Yang, L.; et al. Face Masks in the New COVID-19 Normal: Materials, Testing, and Perspectives. *Research* **2020**, *2020*, 1–40. [[CrossRef](#)] [[PubMed](#)]
- Bondarenko, O.; Juganson, K.; Ivask, A.; Kasemets, K.; Mortimer, M.; Kahru, A. Toxicity of Ag, CuO and ZnO Nanoparticles to Selected Environmentally Relevant Test Organisms and Mammalian Cells in Vitro: A Critical Review. *Arch. Toxicol.* **2013**, *87*, 1181–1200. [[CrossRef](#)]

20. Ivask, A.; Juganson, K.; Bondarenko, O.; Mortimer, M.; Aruoja, V.; Kasemets, K.; Blinova, I.; Heinlaan, M.; Slaveykova, V.; Kahru, A. Mechanisms of Toxic Action of Ag, ZnO and CuO Nanoparticles to Selected Ecotoxicological Test Organisms and Mammalian Cells in Vitro: A Comparative Review. *Nanotoxicology* **2014**, *8*, 57–71. [CrossRef]
21. Bahrami, A.; Arabestani, M.R.; Taheri, M.; Farmany, A.; Norozzadeh, F.; Hosseini, S.M.; Nozari, H.; Nouri, F. Exploring the Role of Heavy Metals and Their Derivatives on the Pathophysiology of COVID-19. *Biol. Trace Elem. Res.* **2022**, *200*, 2639–2650. [CrossRef]
22. Jeremiah, S.S.; Miyakawa, K.; Morita, T.; Yamaoka, Y.; Akihida, R. Potent Antiviral Effect of Silver Nanoparticles on SARS-CoV-2. *Biochem. Biophys. Res. Commun.* **2020**, *533*, 195–200. [CrossRef]
23. Fujimori, Y.; Sato, T.; Hayata, T.; Nagao, T.; Nakayam, M.; Nakayam, T.; Sugamat, R.; Suzuki, K. Novel Antiviral Characteristics of Nanosized Copper(i) Iodide Particles Showing Inactivation Activity against 2009 Pandemic H1N1 Influenza Virus. *Appl. Environ. Microbiol.* **2011**, *78*, 951–955. [CrossRef] [PubMed]
24. Xiang, D.X.; Chen, Q.; Pang, L.; Zheng, C. long Inhibitory Effects of Silver Nanoparticles on H1N1 Influenza A Virus in Vitro. *J. Virol. Methods* **2011**, *178*, 137–142. [CrossRef] [PubMed]
25. Maduray, K.; Parboosing, R. Metal Nanoparticles: A Promising Treatment for Viral and Arboviral Infections. *Biol. Trace Elem. Res.* **2020**, *199*, 3159–3176. [CrossRef] [PubMed]
26. De Toledo, G.G.; Toledo, V.H.; Lanfredi, A.J.C.; Escote, M.; Champi, A.; DA SILVA, M.C.C.; Nantes-Cardoso, I.L. Promising Nanostructured Materials against Enveloped Virus. *An. Acad. Bras. Cienc.* **2020**, *92*, 1–22. [CrossRef] [PubMed]
27. Aallaei, M.; Molaakbari, E.; Mostafavi, P.; Salarizadeh, N.; Malaksah, R.E.; Afzali, D. Investigation of Cu Metal Nanoparticles with Different Morphologies to Inhibit SARS-CoV-2 Main Protease and Spike Glycoprotein Using Molecular Docking and Dynamics Simulation. *J. Mol. Struct.* **2022**, *1253*, 132301. [CrossRef] [PubMed]
28. Rani, I.; Goyal, A.; Bhatnagar, M.; Manhas, S.; Goel, P.; Pal, A.; Prasad, R. Potential Molecular Mechanisms of Zinc- and Copper-Mediated Antiviral Activity on COVID-19. *Nutr. Res.* **2021**, *92*, 109–128. [CrossRef]
29. Karlsson, H.; Toprak, M.S.; Fadeel, B. Toxicity of Metal and Metal Oxide Nanoparticles. In *Handbook on the Toxicology of Metals*; Elsevier: Amsterdam, The Netherlands, 2015; pp. 75–112. ISBN 9780444594532.
30. Cronholm, P.; Karlsson, H.L.; Hedberg, J.; Lowe, T.A.; Winnberg, L.; Elihn, K.; Wallinder, I.O.; Möller, L. Intracellular Uptake and Toxicity of Ag and CuO Nanoparticles: A Comparison between Nanoparticles and Their Corresponding Metal Ions. *Small* **2013**, *9*, 970–982. [CrossRef]
31. Kubo, A.L.; Capjak, I.; Vrček, I.V.; Bondarenko, O.M.; Kurvet, I.; Vija, H.; Ivask, A.; Kasemets, K.; Kahru, A. Antimicrobial Potency of Differently Coated 10 and 50 nm Silver Nanoparticles against Clinically Relevant Bacteria Escherichia Coli and Staphylococcus Aureus. *Colloids Surf. B Biointerfaces* **2018**, *170*, 401–410. [CrossRef]
32. Gupta, A.; Mumtaz, S.; Li, C.; Hussain, I.; Vincent, M.R. Combatting Antibiotic-Resistant Bacteria Using Nanomaterials. *Chem. Soc. Rev.* **2020**, *48*, 415–427. [CrossRef]
33. Hodek, J.; Zajícová, V.; Lovetinská-Šlamborová, I.; Stibor, I.; Müllerová, J.; Weber, J. Protective Hybrid Coating Containing Silver, Copper and Zinc Cations Effective against Human Immunodeficiency Virus and Other Enveloped Viruses. *BMC Microbiol.* **2016**, *16*, 56. [CrossRef]
34. Warnes, S.L.; Little, Z.R.; Keevil, C.W. Human Coronavirus 229E Remains Infectious on Common Touch Surface Materials. *MBio* **2015**, *6*, e01697-15. [CrossRef] [PubMed]
35. Michels, H.T.; Keevil, C.W.; Salgado, C.D.; Schmidt, M.G. From Laboratory Research to a Clinical Trial: Copper Alloy Surfaces Kill Bacteria and Reduce Hospital-Acquired Infections. *Health Environ. Res. Des. J.* **2015**, *9*, 64–79. [CrossRef] [PubMed]
36. Balasubramaniam, B.; Prateek; Ranjan, S.; Saraf, M.; Kar, P.; Singh, S.P.; Thakur, V.K.; Singh, A.; Gupta, R.K. Antibacterial and Antiviral Functional Materials: Chemistry and Biological Activity toward Tackling COVID-19-like Pandemics. *ACS Pharmacol. Transl. Sci.* **2021**, *4*, 8–54. [CrossRef] [PubMed]
37. Palza, H. Antimicrobial Polymers with Metal Nanoparticles. *Int. J. Mol. Sci.* **2015**, *16*, 2099–2116. [CrossRef]
38. Aragaw, T.A. Surgical Face Masks as a Potential Source for Microplastic Pollution in the COVID-19 Scenario. *Mar. Pollut. Bull.* **2020**, *159*, 111517. [CrossRef]
39. The University of British Columbia What Size Particle Is Important to Transmission of COVID-19? Available online: <https://www.aerosol.mech.ubc.ca/what-size-particle-is-important-to-transmission> (accessed on 22 June 2022).
40. Mills, K. 4—Measurement and Estimation of Physical Properties of Metals at High Temperatures. *Fundam. Metall.* **2005**, 109–177. [CrossRef]
41. Kubo, A.L.; Vasiliev, G.; Vija, H.; Krishtal, J.; Tõugu, V.; Visnapuu, M.; Kisand, V.; Kahru, A.; Bondarenko, O.M. Surface Carboxylation or PEGylation Decreases CuO Nanoparticles' Cytotoxicity to Human Cells in Vitro without Compromising Their Antibacterial Properties. *Arch. Toxicol.* **2020**, *94*, 1561–1573. [CrossRef]
42. Ivask, A.; Bondarenko, O.; Jepihhina, N.; Kahru, A. Profiling of the Reactive Oxygen Species-Related Ecotoxicity of CuO, ZnO, TiO<sub>2</sub>, Silver and Fullerene Nanoparticles Using a Set of Recombinant Luminescent Escherichia Coli Strains: Differentiating the Impact of Particles and Solubilised Metals. *Anal. Bioanal. Chem.* **2010**, *398*, 701–716. [CrossRef]
43. Zhao, Z.; Cui, H.; Song, W.; Ru, X.; Zhou, W.; Yu, X. A Simple Magnetic Nanoparticles-Based Viral RNA Extraction Method for Efficient Detection of SARS-CoV-2. *bioRxiv* **2020**, 518055. [CrossRef]
44. Chen, Y.; Qiu, Y.; Chen, W.; Wei, Q. Electrospun Thymol-Loaded Porous Cellulose Acetate Fibers with Potential Biomedical Applications. *Mater. Sci. Eng. C* **2020**, *109*, 110536. [CrossRef]

45. Pu, Y.; Zheng, J.; Chen, F.; Long, Y.; Wu, H.; Li, Q.; Yu, S.; Wang, X.; Ning, X. Preparation of Polypropylene Micro and Nanofibers by Electrostatic-Assisted Melt Blown and Their Application. *Polymers* **2018**, *10*, 959. [[CrossRef](#)] [[PubMed](#)]
46. Lishchynskiy, O.; Shymborska, Y.; Stetsyshyn, Y.; Raczkowska, J.; Skirtach, A.G.; Peretiatchko, T.; Budkowski, A. Passive Antifouling and Active Self-Disinfecting Antiviral Surfaces. *Chem. Eng. J.* **2022**, *446*, 137048. [[CrossRef](#)] [[PubMed](#)]
47. Gandhi, M.; Beyrer, C.; Goosby, E. Masks Do More Than Protect Others During COVID-19: Reducing the Inoculum of SARS-CoV-2 to Protect the Wearer. *J. Gen. Intern. Med.* **2020**, *35*, 3063–3066. [[CrossRef](#)] [[PubMed](#)]
48. Roberts, K.L.; Shelton, H.; Stilwell, P.; Barclay, W.S. Transmission of a 2009 H1N1 Pandemic Influenza Virus Occurs before Fever Is Detected, in the Ferret Model. *PLoS ONE* **2012**, *7*, e43303. [[CrossRef](#)]
49. Selvaranjan, K.; Navaratnam, S.; Rajeev, P.; Ravintherakumaran, N. Environmental Challenges Induced by Extensive Use of Face Masks during COVID-19: A Review and Potential Solutions. *Environ. Chall.* **2021**, *3*, 100039. [[CrossRef](#)]
50. Suetens, C.; Hopkins, S.; Kolman, J.; Högberg, L.D. *European Centre for Disease Prevention and Control. Point Prevalence Survey of Healthcare-Associated Infections and Antimicrobial Use in European Acute Care Hospitals*; ECDC: Stockholm, Sweden, 2013.
51. Kampf, G.; Todt, D.; Pfaender, S.; Steinmann, E. Persistence of Coronaviruses on Inanimate Surfaces and Their Inactivation with Biocidal Agents. *J. Hosp. Infect.* **2020**, *104*, 246–251. [[CrossRef](#)] [[PubMed](#)]
52. Oxford, J.; Berezin, E.N.; Courvalin, P.; Dwyer, D.E.; Exner, M.; Jana, L.A.; Kaku, M.; Lee, C.; Letlape, K.; Low, D.E.; et al. The Survival of Influenza A(H1N1)Pdm09 Virus on 4 Household Surfaces. *Am. J. Infect. Control.* **2014**, *42*, 423–425. [[CrossRef](#)]
53. Merkl, P.; Long, S.; McInerney, G.M.; Sotiriou, G.A. Antiviral Activity of Silver, Copper Oxide and Zinc Oxide Nanoparticle Coatings against SARS-CoV-2. *Nanomaterials* **2021**, *11*, 1312. [[CrossRef](#)]
54. Meister, T.L.; Fortmann, J.; Breisch, M.; Sengstock, C.; Steinmann, E.; Köller, M.; Pfaender, S.; Ludwig, A. Nanoscale Copper and Silver Thin Film Systems Display Differences in Antiviral and Antibacterial Properties. *Sci. Rep.* **2022**, *12*, 1–10. [[CrossRef](#)]
55. Balkrishna, A.; Arya, V.; Rohela, A.; Kumar, A.; Verma, R.; Kumar, D.; Nepovimova, E.; Kuca, K.; Thakur, N.; et al. Nanotechnology Interventions in the Management of COVID-19: Prevention, Diagnosis and Virus-Like Particle Vaccines. *Vaccines* **2021**, *9*, 1129. [[CrossRef](#)]
56. Lemire, J.A.; Harrison, J.J.; Turner, R.J. Antimicrobial Activity of Metals: Mechanisms, Molecular Targets and Applications. *Nat. Rev. Microbiol.* **2013**, *11*, 371–384. [[CrossRef](#)]
57. Ghaffari, H.; Tavakoli, A.; Moradi, A.; Tabarraei, A.; Bokharaei-Salim, F.; Zahmatkeshan, M.; Farahmand, M.; Javanmard, D.; Kiani, S.J.; Esghaei, M.; et al. Inhibition of H1N1 Influenza Virus Infection by Zinc Oxide Nanoparticles: Another Emerging Application of Nanomedicine. *J. Biomed. Sci.* **2019**, *26*, 70. [[CrossRef](#)] [[PubMed](#)]
58. Borkow, G.; Zhou, S.S.; Page, T.; Gabbay, J. A Novel Anti-Influenza Copper Oxide Containing Respiratory Face Mask. *PLoS ONE* **2010**, *5*, e11295. [[CrossRef](#)] [[PubMed](#)]
59. Imai, K.; Ogawa, H.; Bui, V.N.; Inoue, H.; Fukuda, J.; Ohba, M.; Yamamoto, Y.; Nakamura, K. Inactivation of High and Low Pathogenic Avian Influenza Virus H5 Subtypes by Copper Ions Incorporated in Zeolite-Textile Materials. *Antivir. Res.* **2012**, *93*, 225–233. [[CrossRef](#)] [[PubMed](#)]
60. Ito, A.; Tsuneki, A.; Yoshida, Y.; Ryoike, K.; Kaidoh, T.; Kageyama, S. In Vitro Inhibition of Cytopathic Effect of Influenza Virus and Human Immunodeficiency Virus by Bamboo Leaf Extract Solution and Sodium Copper Chlorophyllin. *Yonago Acta Med.* **2016**, *59*, 61–65.
61. Minoshima, M.; Lu, Y.; Kimura, T.; Nakano, R.; Ishiguro, H.; Kubota, Y.; Hashimoto, K.; Sunada, K. Comparison of the Antiviral Effect of Solid-State Copper and Silver Compounds. *J. Hazard. Mater.* **2016**, *312*, 1–7. [[CrossRef](#)]
62. Cortes, A.A.; Zuñiga, J.M. The Use of Copper to Help Prevent Transmission of SARS-Coronavirus and Influenza Viruses. A General Review. *Diagn. Microbiol. Infect. Dis.* **2020**, *98*, 115176. [[CrossRef](#)]
63. Zerbib, S.; Vallet, L.; Muggeo, A.; De Champs, C.; Lefebvre, A.; Jolly, D.; Kanagaratnam, L. Copper for the Prevention of Outbreaks of Healthcare-Associated Infections in a Long-Term Care Facility for Elders. *J. Post Acute Long Term Care Med.* **2020**, *21*, 68–71.e1. [[CrossRef](#)]
64. Shionoiri, N.; Sato, T.; Fujimori, Y.; Nakayama, T.; Nemoto, M.; Matsunaga, T.; Tanaka, T. Investigation of the Antiviral Properties of Copper Iodide Nanoparticles against Feline Calicivirus. *J. Biosci. Bioeng.* **2012**, *113*, 580–586. [[CrossRef](#)]
65. Govind, V.; Bharadwaj, S.; Sai Ganesh, M.R.; Vishnu, J.; Shankar, K.V.; Shankar, B.; Rajesh, R. Antiviral Properties of Copper and Its Alloys to Inactivate COVID-19 Virus: A Review. *BioMetals* **2021**, *34*, 1217–1235. [[CrossRef](#)]
66. Konai, M.M.; Bhattacharjee, B.; Ghosh, S.; Haldar, J. Recent Progress in Polymer Research to Tackle Infections and Antimicrobial Resistance. *Biomacromolecules* **2018**, *19*, 1888–1917. [[CrossRef](#)]
67. Kamaruzzaman, N.F.; Tan, L.P.; Hamdan, R.H.; Choong, S.S.; Wong, W.K.; Gibson, A.J.; Chivu, A.; De Fatima Pina, M. Antimicrobial Polymers: The Potential Replacement of Existing Antibiotics? *Int. J. Mol. Sci.* **2019**, *20*, 2747. [[CrossRef](#)]
68. Fischer, S.; Thümmler, K.; Volkert, B.; Hettrich, K.; Schmidt, I.; Fischer, K. Properties and Applications of Cellulose Acetate. *Macromol. Symp.* **2008**, *262*, 89–96. [[CrossRef](#)]
69. Cheng, H.N.; Dowd, M.K.; Selling, G.W.; Biswas, A. Synthesis of Cellulose Acetate from Cotton Byproducts. *Carbohydr. Polym.* **2010**, *80*, 449–452. [[CrossRef](#)]
70. Hansen, G.H.; Delmas, B.; Besnardeau, L.; Vogel, L.K.; Laude, H.; Sjöström, H.; Norén, O. The Coronavirus Transmissible Gastroenteritis Virus Causes Infection after Receptor-Mediated Endocytosis and Acid-Dependent Fusion with an Intracellular Compartment. *J. Virol.* **1998**, *72*, 527–534. [[CrossRef](#)] [[PubMed](#)]

71. Marchese, A.; Orhan, I.E.; Daglia, M.; Barbieri, R.; Di Lorenzo, A.; Nabavi, S.F.; Gortzi, O.; Izadi, M.; Nabavi, S.M. Antibacterial and Antifungal Activities of Thymol: A Brief Review of the Literature. *Food Chem.* **2016**, *210*, 402–414. [[CrossRef](#)]
72. Kuroda, K.; Caputo, G.A.; DeGrado, W.F. The Role of Hydrophobicity in the Antimicrobial and Hemolytic Activities of Poly-methacrylate Derivatives. *Chem. A Eur. J.* **2009**, *15*, 1123–1133. [[CrossRef](#)]
73. Ahmed, F.; Ayoub Arbab, A.; Jatoi, A.W.; Khatri, M.; Memon, N.; Khatri, Z.; Kim, I.S. Ultrasonic-Assisted Deacetylation of Cellulose Acetate Nanofibers: A Rapid Method to Produce Cellulose Nanofibers. *Ultrason. Sonochem.* **2017**, *36*, 319–325. [[CrossRef](#)]
74. Mikaeili, F.; Gouma, P.I. Super Water-Repellent Cellulose Acetate Mats. *Sci. Rep.* **2018**, *8*, 12472. [[CrossRef](#)]
75. Pham, P.; Oliver, S.; Wong, E.H.H.; Boyer, C. Effect of Hydrophilic Groups on the Bioactivity of Antimicrobial Polymers. *Polym. Chem.* **2021**, *12*, 5689–5703. [[CrossRef](#)]
76. Kumar, S.; Karmacharya, M.; Joshi, S.R.; Gulenko, O.; Park, J.; Kim, G.H.; Cho, Y.K. Photoactive Antiviral Face Mask with Self-Sterilization and Reusability. *Nano Lett.* **2021**, *21*, 337–343. [[CrossRef](#)] [[PubMed](#)]
77. Chowdhury, M.A.; Shuvho, M.B.A.; Shahid, A.; Haque, M.M.; Kashem, A.M.; Shiung, L.S.; Ong, H.C.; Uddin, A.; Mofijur, M. Prospect of Biobased Antiviral Face Mask to Limit the Coronavirus Outbreak. *Environ. Res.* **2021**, *192*, 110294. [[CrossRef](#)]
78. Jung, S.; Byeon, E.Y.; Kim, D.G.; Lee, D.G.; Ryoo, S.; Lee, S.; Shin, C.W.; Jang, H.W.; Yang, J.Y.; Kim, H.J.; et al. Copper-Coated Polypropylene Filter Face Mask with SARS-CoV-2 Antiviral Ability. *Polymers* **2021**, *13*, 1367. [[CrossRef](#)] [[PubMed](#)]
79. Selwyn, G.S.; Ye, C.; Bradfute, S.B. Anti-SARS-CoV-2 Activity of Surgical Masks Infused with Quaternary Ammonium Salts. *Viruses* **2021**, *13*, 960. [[CrossRef](#)] [[PubMed](#)]
80. Blinova, I.; Niskanen, J.; Kajankari, P.; Kanarbik, L.; Käkinen, A.; Tenhu, H.; Kahru, A. Toxicity of two types of silver nanoparticles to aquatic crustaceans *Daphnia magna* and *Thamnocephalus platyurus*. *Environ. Sci. Pollut. Res.* **2013**, *20*, 3456–3463. [[CrossRef](#)] [[PubMed](#)]



## Curriculum vitae

### Personal data

Name: Grigory Vasiliev  
Date of birth: 22.12.1987  
Place of birth: Tartu, Estonia  
Citizenship: Estonian

### Contact data

E-mail: grigory.vasiliev9@gmail.com

### Education

2018–2023 Tallinn University of Technology, PhD  
2013–2017 University of Tartu, Residency in Infectious Diseases  
2007–2013 University of Tartu, Faculty of Medicine, Degree in Medicine (MD)  
1995–2007 Narva Humanitaarhümnaasium, High School Certificate

### Language competence

Russian mother tongue  
Estonian fluent  
English fluent  
Spanish basic

### Professional employment

2021–... Specialist in Infectious Diseases in West-Tallinn Hospital  
2020–2021 Medical doctor in COVID-19 Department in Narva Hospital  
2020–2021 Medical doctor in Unit of Emergency Medicine in North Estonia Medical Centre  
2018–2020 Specialist in Infectious Diseases in West-Tallinn Hospital  
2013–2017 Residency in Infectious Diseases  
2013–2014 Working in Unit of Emergency Medicine

### Additional training and awards

International practice for medical students in Orthopaedic department in Spain, Oviedo (1 month), 2010.

The American Austrian Foundation's Open Medical Institute Salzburg Medical Seminar in Infectious Diseases (1 week). Diploma for excellent presentation, 2017.

Training "Antimicrobial Coatings" (5 day), Amsterdam, 2019.

"Introduction to CRISPR-Cas9 Genome Editing – Design to Analysis", Darmstadt, (4 days), 2019.

ENOVA Training School "Immunoactive carbohydrates and adjuvants: antibacterial vaccines, from research to clinical trials", Florence (3 days), 2019.

12th International Congress "Biomaterials and Nano-biomaterials: Recent Advances Safety – Toxicology and Ecology Issues" (6 days) Heraklion, Greece Diploma "Best Young Presentation Recognition", 2021.

GCP – Good Clinical Practice (1 day), Tartu University, Estonia, 2021.

Internship for CRISPR technologies in Sydney University (4 months), 2022.

## Elulookirjeldus

### Isikuandmed

Nimi: Grigory Vasiliev  
Sünniaeg: 22.12.1987  
Sünnikoht: Tartu, Eesti  
Kodakondsus: eesti

### Kontaktandmed

E-post: grigory.vasiliev9@gmail.com

### Hariduskäik

2018–2023 Tallinna Tehnikaülikool, PhD  
2013–2017 Tartu Ülikool, nakkushaiguste residentuur  
2007–2013 Tartu Ülikool, Arstiteaduskond, Meditsiinkraad (MD)  
2005–2007 Narva Humanitaarhümnaasium, keskkooli tunnistus

### Keelteoskus

vene emakeel  
eesti kõrgtase  
inglise kõrgtase  
hispaania algtase

### Teenistuskäik

2021–... Lääne-Tallinna haigla, nakkushaiguste arst  
2019–... Nanordica Medical OÜ  
2020–2021 Narva haigla COVID-19, osakonna arst  
2020–2021 Põhja-Eesti Regionaalhaigla, erakorralise meditsiini osakonna arst  
2018–2020 Lääne-Tallinna haigla, nakkushaiguste arst  
2013–2017 Nakkushaiguste residentuur  
2013–2014 Ida-Tallinna Keskhaigla, erakorralise meditsiini osakonna arst

### Täiendusõpe ja auhinnad

Rahvusvaheline praktika meditsiiniüliõpilastele ortopeediaosakonnas, Oviedo (1 kuu), 2010.

Ameerika-Austria Fondi Avatud Meditsiininstituudi Salzburgi Meditsiiniline Seminar Nakkushaiguste alal (1 nädal), diplom "Excellent presentation", Salzburg, 2017.

5-päevane koolitus "Antimicrobial Coatings", Amsterdam, 2019.

Koolitus "Introduction to CRISPR-Cas9 Genome Editing – Design to Analysis" Darmstadt, (4 päeva), 2019.

ENOVA koolitus "Training School Immunoactive carbohydrates and adjuvants: antibacterial vaccines, from research to clinical trials", Firenze (3 päeva), 2019.

Rahvusvaheline kongress "Biomaterials and Nano-biomaterials: Recent Advances Safety – Toxicology and Ecology Issues" (6 päeva), diplom "Best Young Presentation Recognition", Heraklion, 2021.

GCP – Hea Kliinilise Tava koolitus (1 päev), Eesti, 2021.

Praktika CRISPR-tehnoloogia alal Sydney Ülikoolis, Sydney (4 kuud), 2022.

ISSN 2585-6901 (PDF)  
ISBN 978-9916-80-011-9 (PDF)